SEMI-ANNUAL STATUS REPORT ON NASA GRANT NAG 1-1087 "IDENTIFICATION OF AERODYNAMIC MODELS FOR MANEUVERING AIRCRAFT"

KU-FRL-872-4

C. Edward Lan and C. C. Hu

Flight Research Laboratory
The University of Kansas Center for Research, Inc.
Lawrence, Kansas 66045-2969

March 11, 1992

In the previous semi-annual report, a Fourier analysis method for unsteady aerodynamic modeling was presented in the AIAA paper No.91-2867 (Ref.1, a copy of the version that was accepted by the AIAA Journal being attached.). The results from a set of test data for a 70-deg. delta wing reported in Ref.2 as well as two other sets of test data for two-dimensional airfoil sections reported in Ref.3 had been used to verify this method of modeling responses of harmonic motions at different reduced frequencies. In addition, some other cases for a 70-deg. delta wing's harmonic ramp motions also were calculated by indicial formulation in the past work.

During this reporting period (9/1/91-2/29/92), two more sets of test data obtained at the NASA Langley Research Center have been used to show the generality of the Fourier analysis method and validate the indicial formulation of time integration. They are discussed below.

1. Fourier Functional Analysis

In the present method, the aerodynamic response can be written as

$$
\begin{aligned}
C_L \cong\ & C_{ave} \\
& + E_{11}\dot{\alpha} + E_{21}\ddot{\alpha} + C_1 * (H_{11}\alpha + H_{21}\dot{\alpha}) * (1 - PD_1) \\
& + E_{12}\dot{\alpha}_2 + E_{22}\ddot{\alpha}_2 + C_2 * (H_{12}\alpha^2 + H_{22}\alpha\dot{\alpha} + H_{32}\dot{\alpha}^2) \\
& \qquad * (1 - PD_2) \\
& + E_{13}\dot{\alpha}_3 + E_{23}\ddot{\alpha}_3 + C_3 * (H_{13}\alpha^3 + H_{23}\alpha^2\dot{\alpha} + H_{33}\alpha\dot{\alpha}^2 + H_{43}\dot{\alpha}^3) \\
& \qquad * (1 - PD_3) \\
& \qquad + \ldots
\end{aligned}
\tag{1}
$$

From the past experience of analyzing five sets of experimental data, it was found that the final values of E_{ij} and H_{ij} could change significantly by using different initial values for E_{ij} and H_{ij} as well as different reference values for C_j. This was mainly because that the gradient method for finding the best E_{ij} and H_{ij} was unable to locate the global minimum. Furthermore, the denominator of the Padé approximant must have negative roots only so that in time domain the corresponding exponential terms will die out at large time. This requirement can be regarded as a constraint in the optimization process.

To remedy these two problems and also make the present method more general and user-friendly in analyzing any given set of test data, another optimization loop has been added outside the existing loops for the purpose of choosing proper initial values for E_{ij} and H_{ij} and the best C_j automatically.

Other task to improve the accuracy of the present method is to include the static test data as additional dynamic stall data at a very low reduced frequency, such as k=1.0E-6. The main purpose of this implementation is to avoid possible poor extrapolations at low k in the integration of indicial integral.

Two sets of harmonic motions test data ,one for a 70-deg. delta wing and the other for a F-18 model , were analyzed by the updated version of the present method. The results are presented in Figs.1 and Figs.2 respectively. Five Fourier terms are used in this analysis. All results were done by the same set of build-in initial data for E_{ij},H_{ij} and C_j without any try-and-error effort by users. The results show that the updated version of the present method is able to capture all hysteresis effects. Comparing with the up-stroke data , most of the down-stroke data are modeled with less accuracy. The reason is that the trend of the hysteresis behavior on down-strokes is not as consistent as those on up-

strokes (see Figs.7). This may imply that a higher order Padé approximant could be needed to model responses which have more complicated hysteresis effects. It is noted that the mismatched part of F-18 C_m response at k=0.0075 is due to the even more inconsistent trend of the hysteresis behavior occurring in the region of high angles of attack.

2. The validity of indicial formulation of time integration

As indicated in Ref.1, an indicial formulation for any arbitrary motion is written as

$$C_L(t') = C_{L_{indicial}}[t'-\tau,\ \alpha(\tau),\ \dot{\alpha}(\tau)]_{\tau=0} + C_{ave} + \sum_{j=1}^{m} (E_{1j}\dot{\alpha}_j + E_{2j}\ddot{\alpha}_j)$$
$$+ \sum_{j=1}^{m} \int_0^{t'} \frac{d\ (a.f.)_j}{d\alpha} * (1 - a_{1j}e^{-a_{3j}(t'-\tau)} - a_{2j}e^{-a_{4j}(t'-\tau)}) \frac{d\alpha(\tau)}{d\tau}\, d\tau \qquad (2)$$
$$+ \frac{\ell}{V_\infty} \sum_{j=1}^{m} \int_0^{t'} \frac{d\ (a.f.)_j}{d\ \dot{\alpha}} * (1 - a_{1j}e^{-a_{3j}(t'-\tau)} - a_{2j}e^{-a_{4j}(t'-\tau)}) \frac{d\dot{\alpha}(\tau)}{d\tau}\, d\tau$$

To show the validity of the above formulation, three types of motion have been analyzed.

(1) Harmonic motion and harmonic ramp motion:

The first type of motion is used to compared with Fourier modeling results; meanwhile, the second one is used to show the agreement with the static value at the time when the motion stops.

As it was known in the past study, discontinuity could happen in the calculation of time integral if the given motion has a sudden change in $\dot{\alpha}$. This can be easily solved by slightly increasing the amplitude of original model (α_0; see Eq. 3a), such as by 2.5 degrees. In the following calculations, the amplitude of harmonic model which originally

was 30. degree has been set to be 30.5 degree for harmonic ramp motions and 32.5 degree for constant rate pitching motions respectively. It should be emphasized that this does not change the actual instantaneous values of α and $\dot{\alpha}$ in the indicial time integration. It merely changes the values of equivalent frequency (k) and phase angle (ϕ).

The results of harmonic motions and harmonic ramp motions are plotted in Figs. 3 for the delta wing and Figs. 4 for the F-18 model respectively. In the harmonic ramp motions, all responses eventually approach the static values corresponding to the angle of attack when the motion stops.

(2)Constant rate pitching motion:

This is used to compare with test data at the same pitch rate.

Two special treatments about this type of motion should be mentioned. First of all, an arbitrary motion has to be represented locally by a cosine function in order to utilize the results of harmonic modeling. At a certain time of arbitrary motion, α and $\dot{\alpha}$ can be described by the cosine and sine functions as

$$\alpha_1 = \alpha_m + \alpha_o \cos(kt' + \phi) = \alpha_m + \alpha \tag{3a}$$

$$\dot{\alpha} = -\alpha_o k \sin(kt' + \phi) \tag{3b}$$

By knowing the harmonic model's mean angle of attack(α_m) and amplitude(α_0), an equivalent reduced frequency k and an equivalent phase angle ϕ at that given time t' can be solved by Newton's method. Near the two ends of a harmonic model's α range, for example 2.5 deg. or 62.5 deg. in the present test model, the equivalent k tends to be high because of large $\dot{\alpha}$ and/or α. From the experience with constant rate pitching motions, it was found that an unreasonably extrapolated high value of k at a starting point would lead to an unacceptable result in simulation. So, one of the variables, α_m and α_0, must be treated as an unknown, instead of k, when the extrapolated k-value is greater than a given allowable value k_{max}. Through a series of tests, the mean angle of attack α_m was chosen as the other unknown in case the extrapolated k-value exceeds a given allowable k_{max}.

Secondly, as the constant-rate pitch-down motions start at a high α, the time integration should start from a static value by setting $t' \rightarrow \infty$ to the first term of Eq. (2).

The results of the constant rate pitching motions are presented in Figs.5 for the delta wing and Figs.6 for the F-18 model respectively. As expected, all results for pitch-up motions are well predicted except in the region near the starting point, in particular for C_D. The reason for this is again the equivalent frequency being too high. Investigation is underway to find an improved solution. On the other hand, some of the results for pitch-down motions are not as good as those for pitch-up motions. The discrepancies in predicting pitch-down motions can be attributed to the poor numerical modeling of harmonic motions on down-strokes,especially at low and moderate reduced frequencies. The latter is, in turn, caused by the non-smooth variation of the response from one

frequency to the other, as can be seen from Figure 7.

3. Work Underway

Additional investigation is underway to compare the computed response with data when the mean angle of attack and amplitude are significantly different from those used in building up the model.

4. References

(1) Chin, S. and Lan, C. E., "Fourier Functional Analysis for Unsteady Aerodynamic Modeling." AIAA Paper 91-2867.

(2) Soltani, M.R.; Bragg, M.B.; and Brandon, J.M., "Experimental Measurements on an Oscillating 70-Degree Delta Wing in Subsonic Flow." AIAA Paper 88-2576.

(3) McAlister, K.W.; Pucci, S.L.; McCroskey, W.J.; and Carr,L.W.,"An Experimental Study of Dynamic Stall on Advanced Airfoil Sections. Volume 2:Pressure and Force Data." NASA TM-84245, Sept. 1982

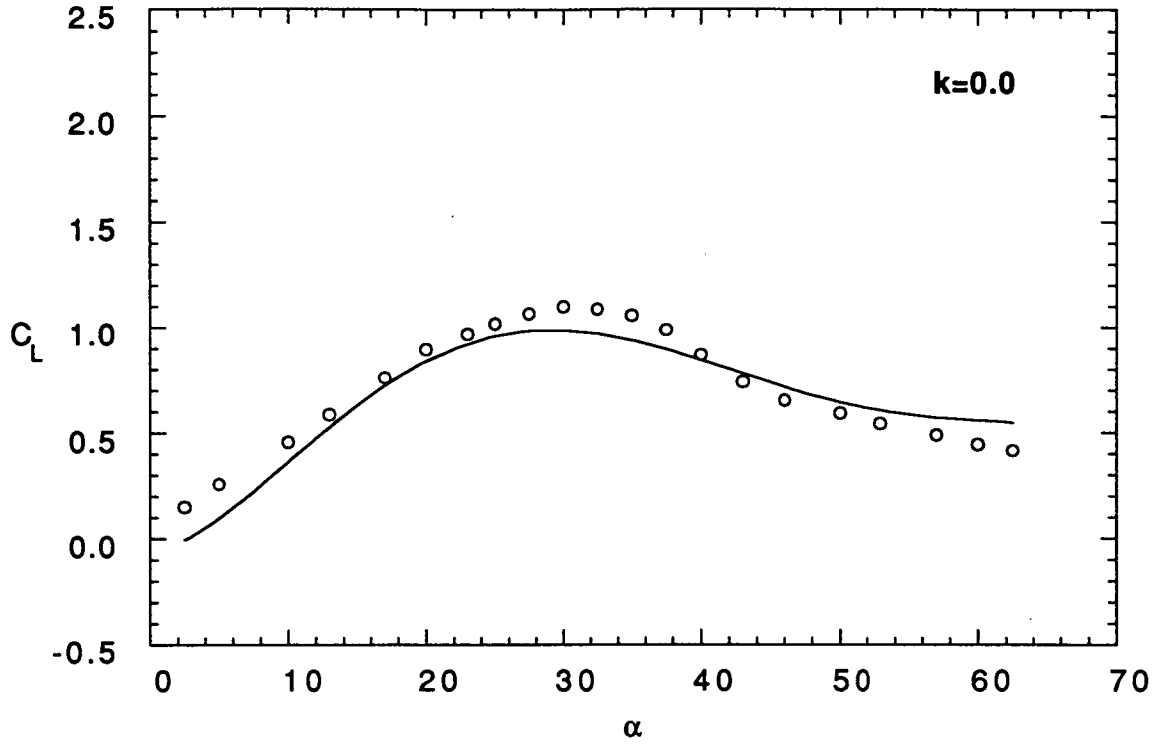

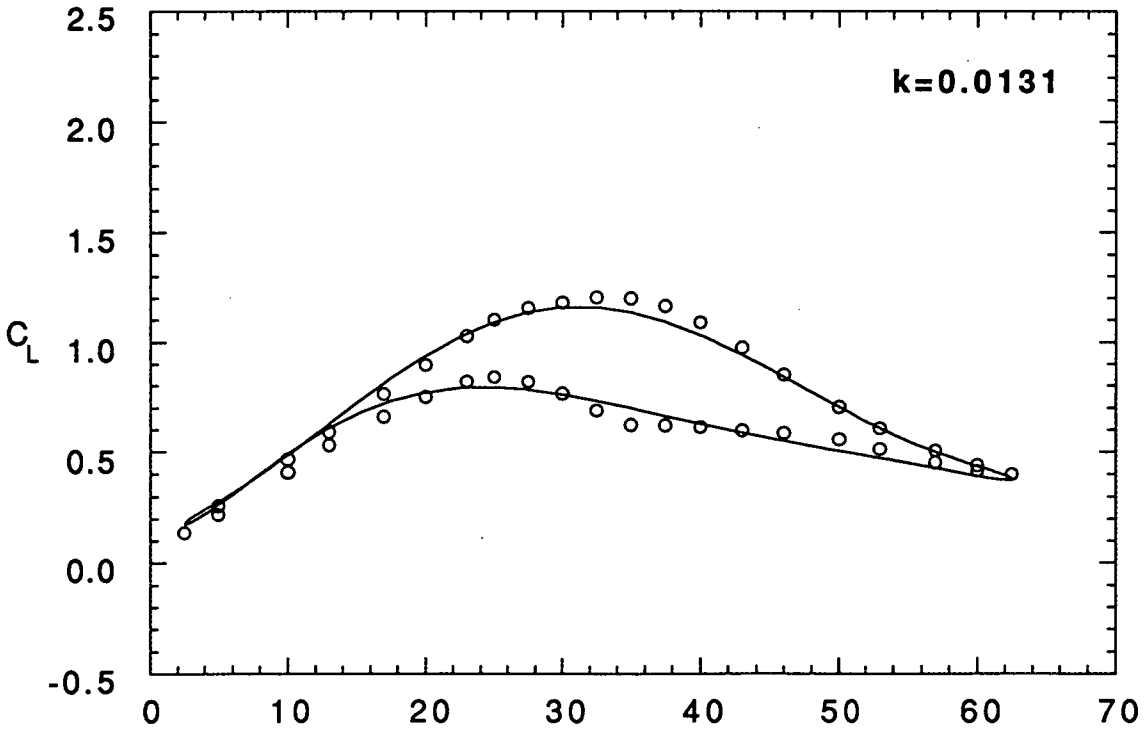

(a)Lift Data

Figure 1 Analysis of 70-deg. Delta Wing Dynamic Stall Data

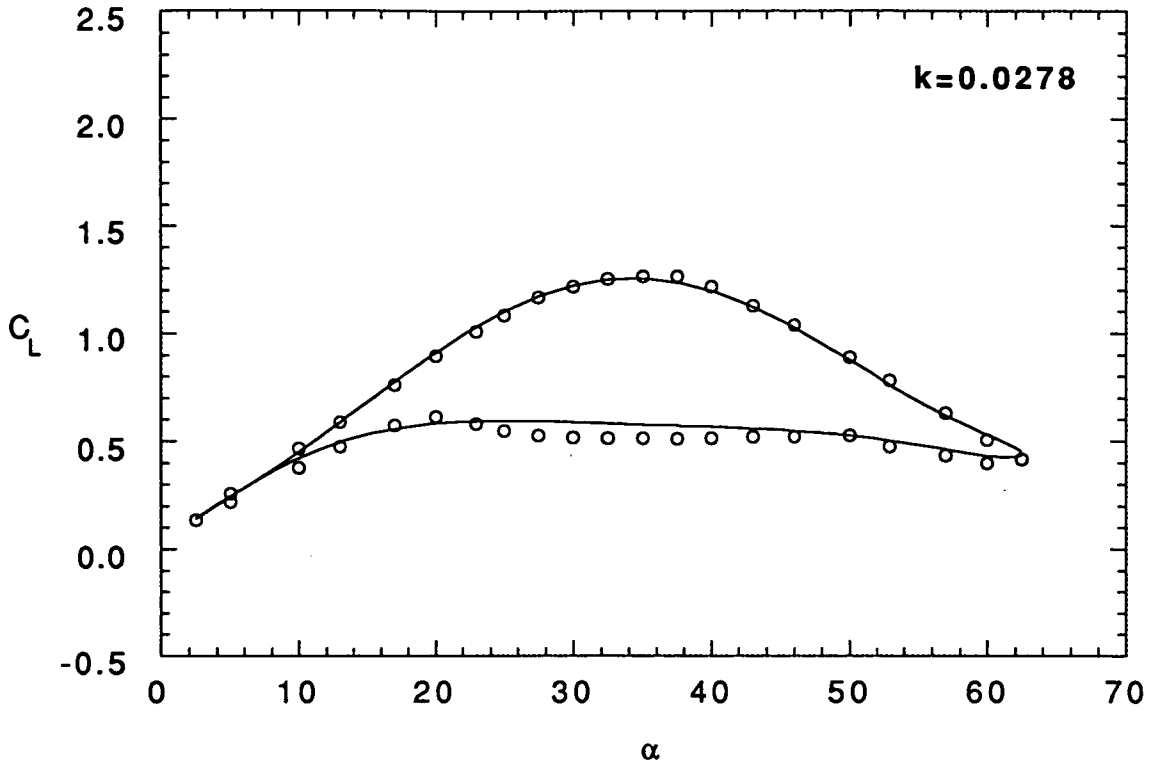

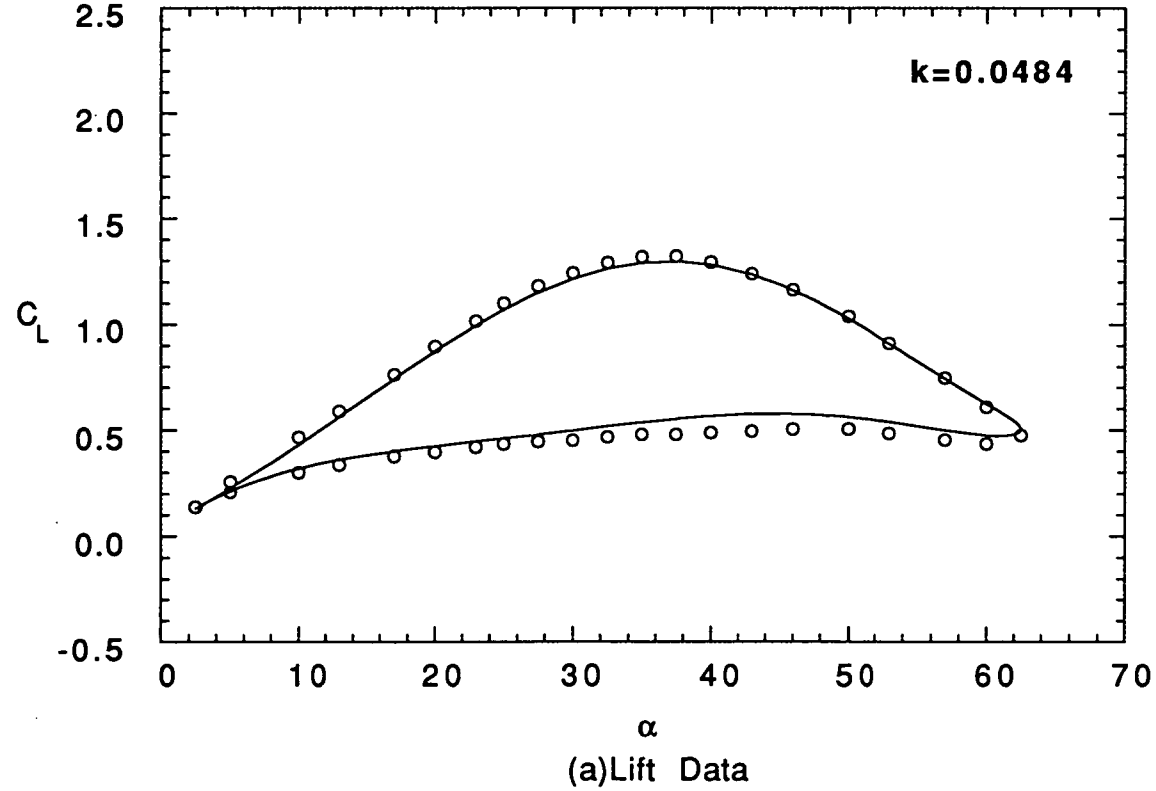

(a)Lift Data

Figure 1 Continued

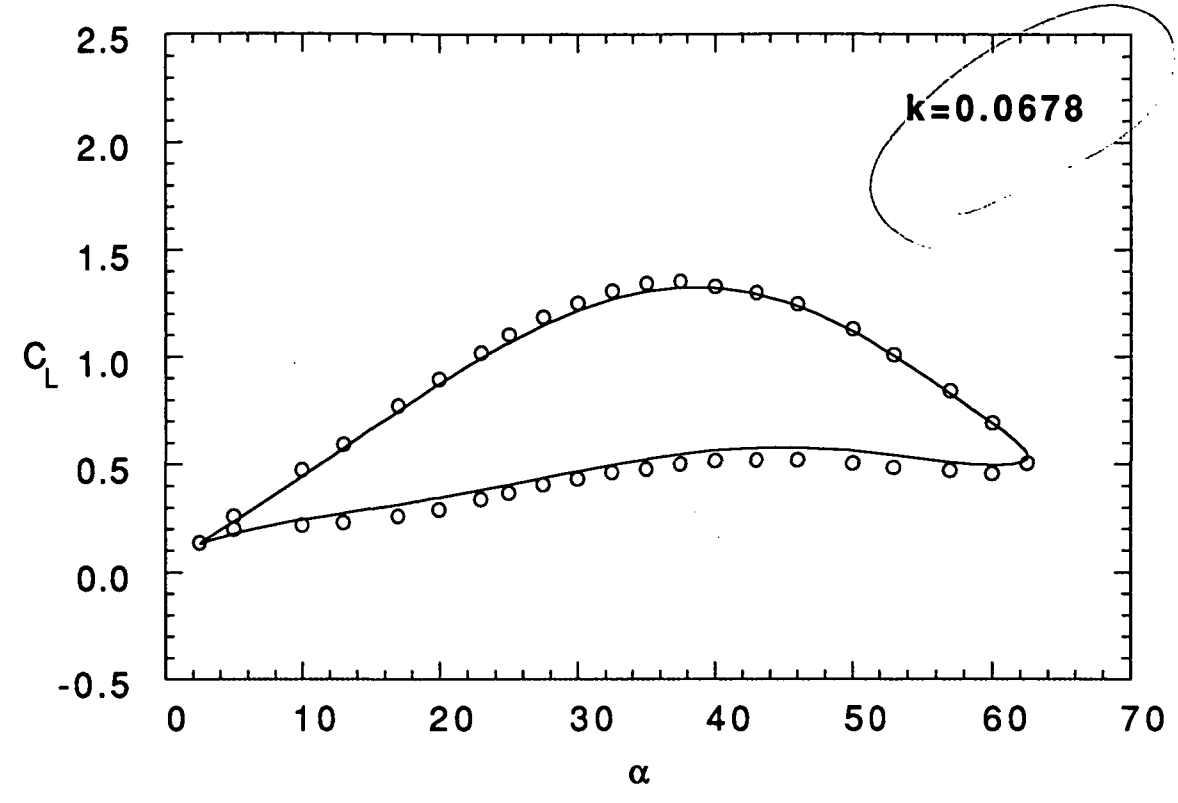

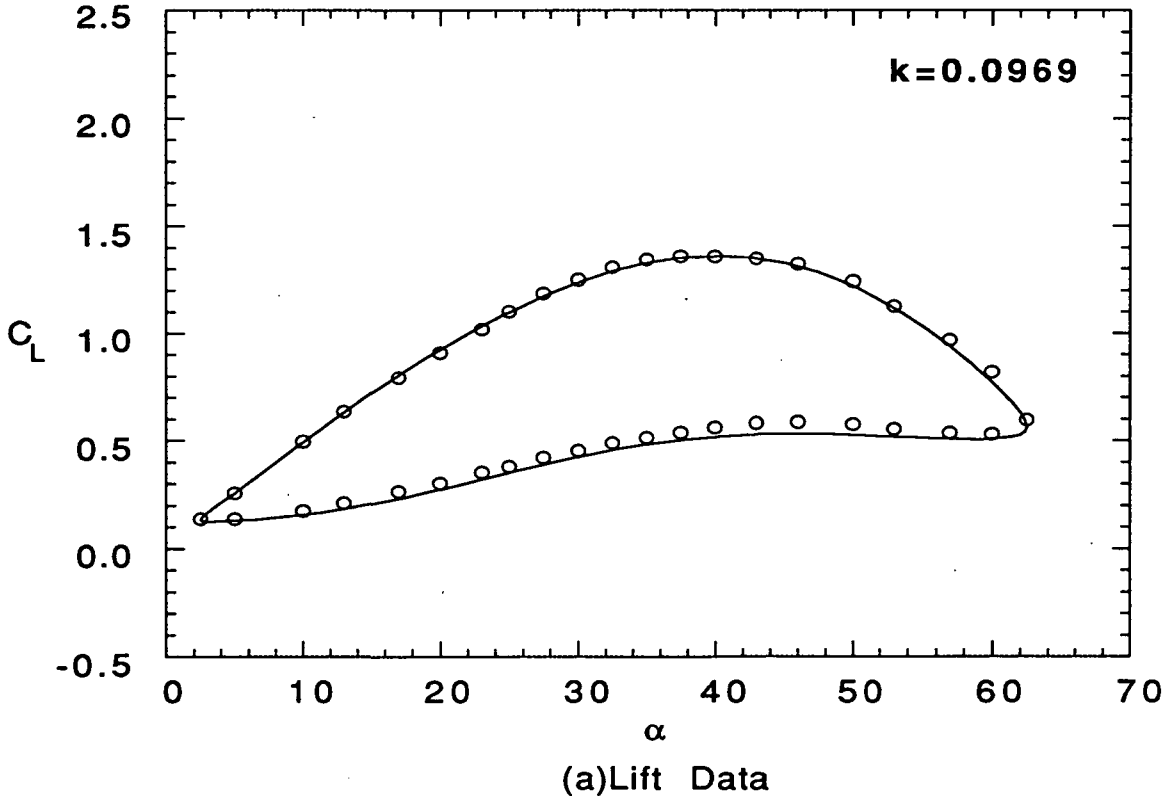

(a)Lift Data

Figure 1 Continued

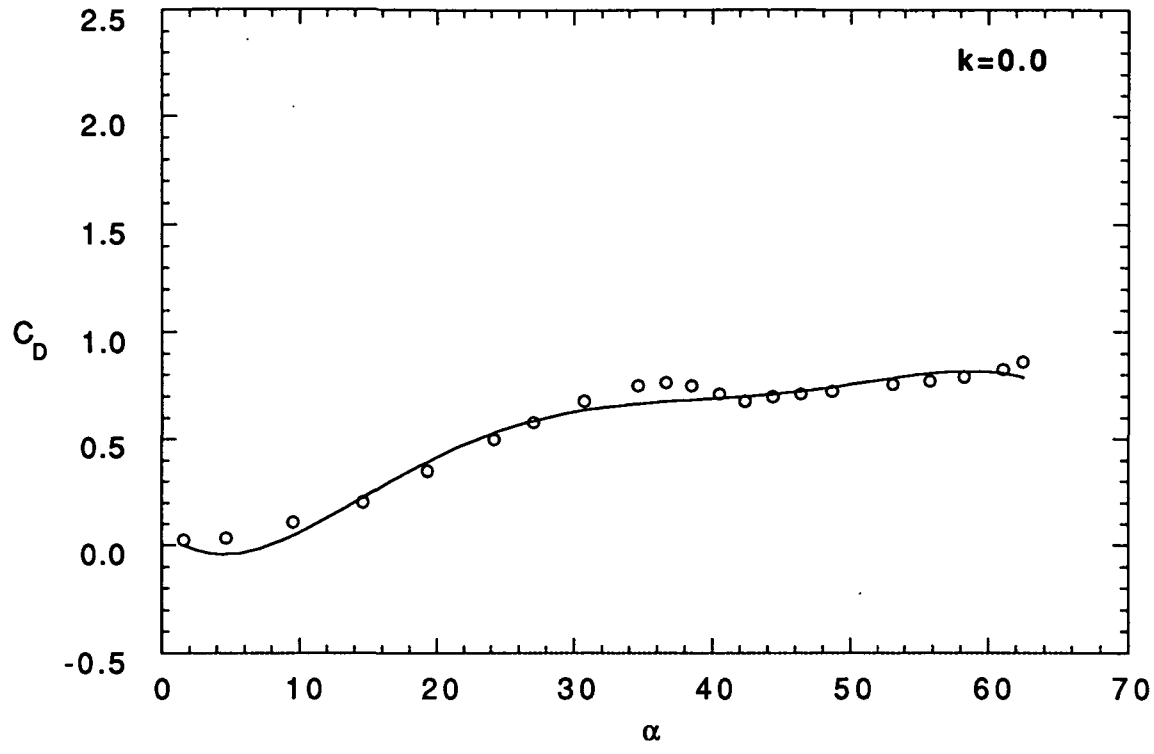

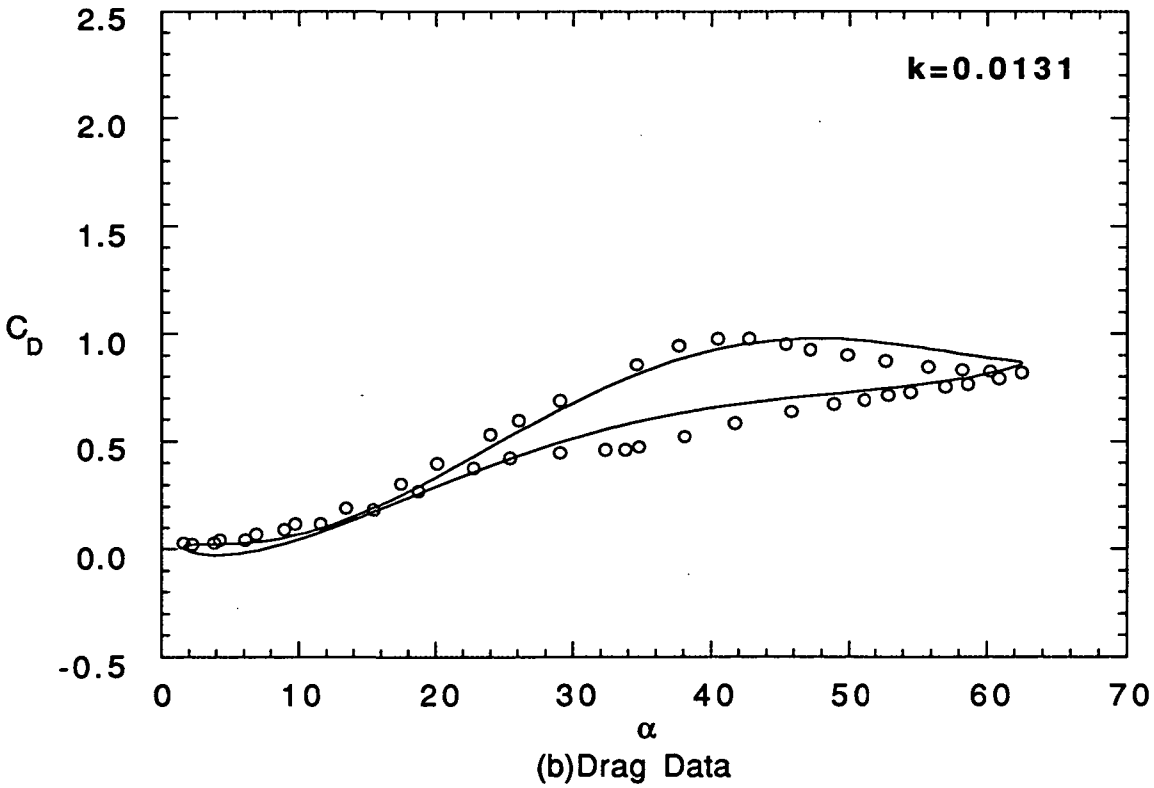

(b)Drag Data

Figure 1 Continued

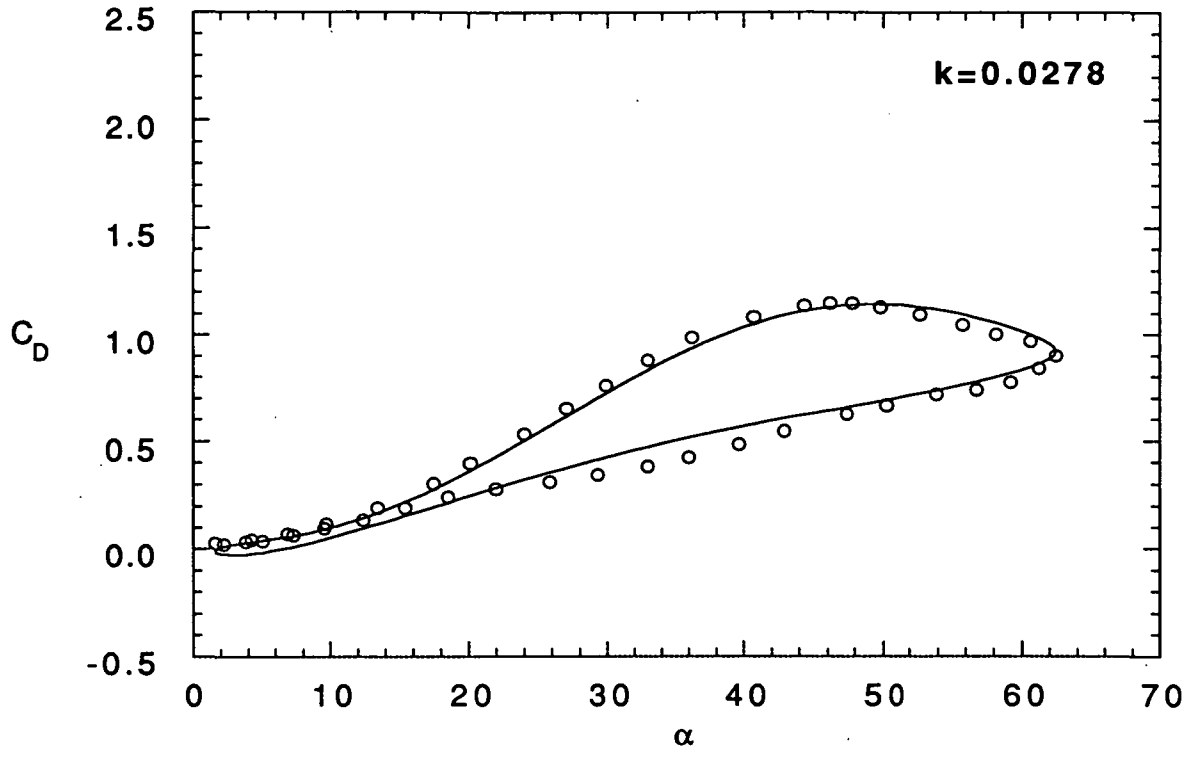

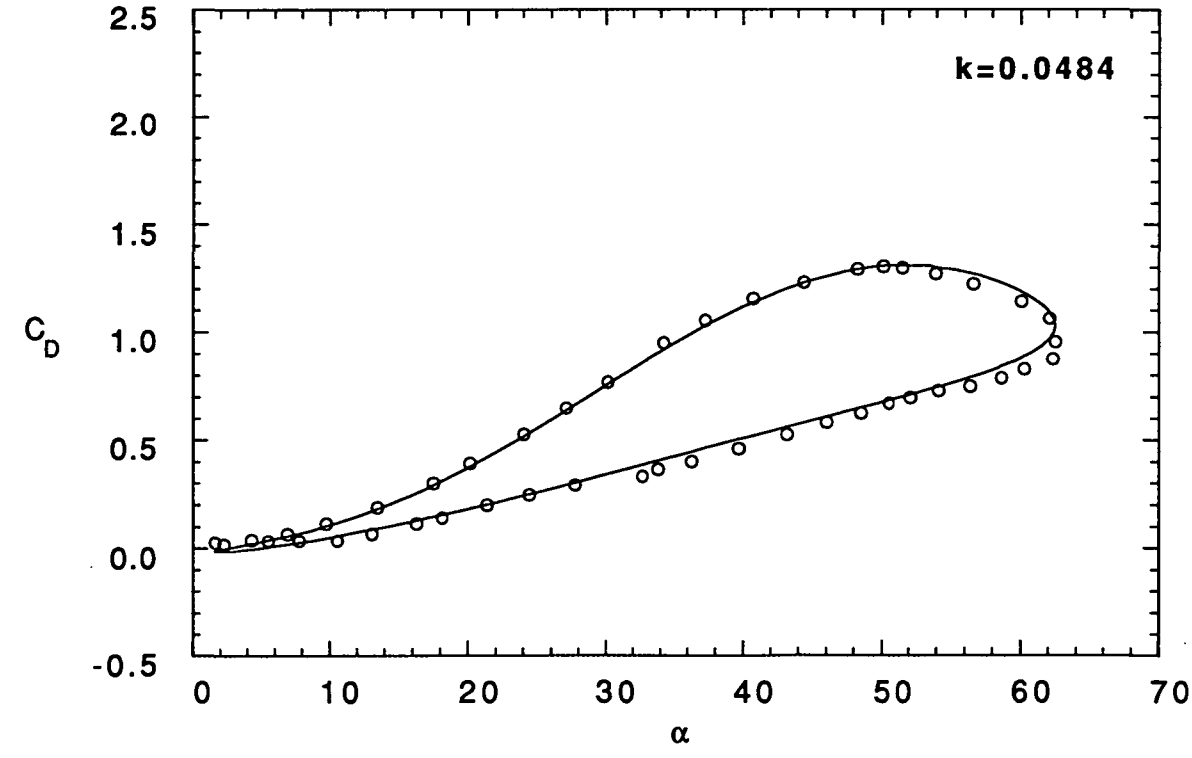

(b)Drag Data

Figure 1 Continued

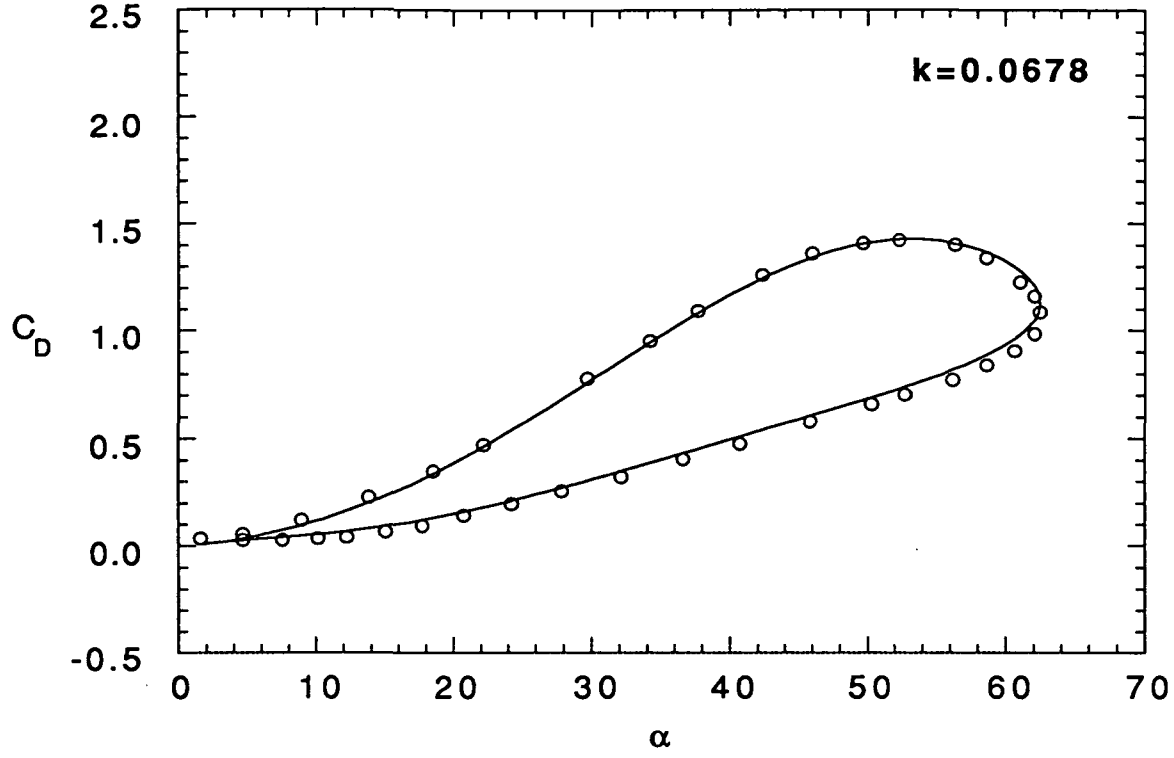

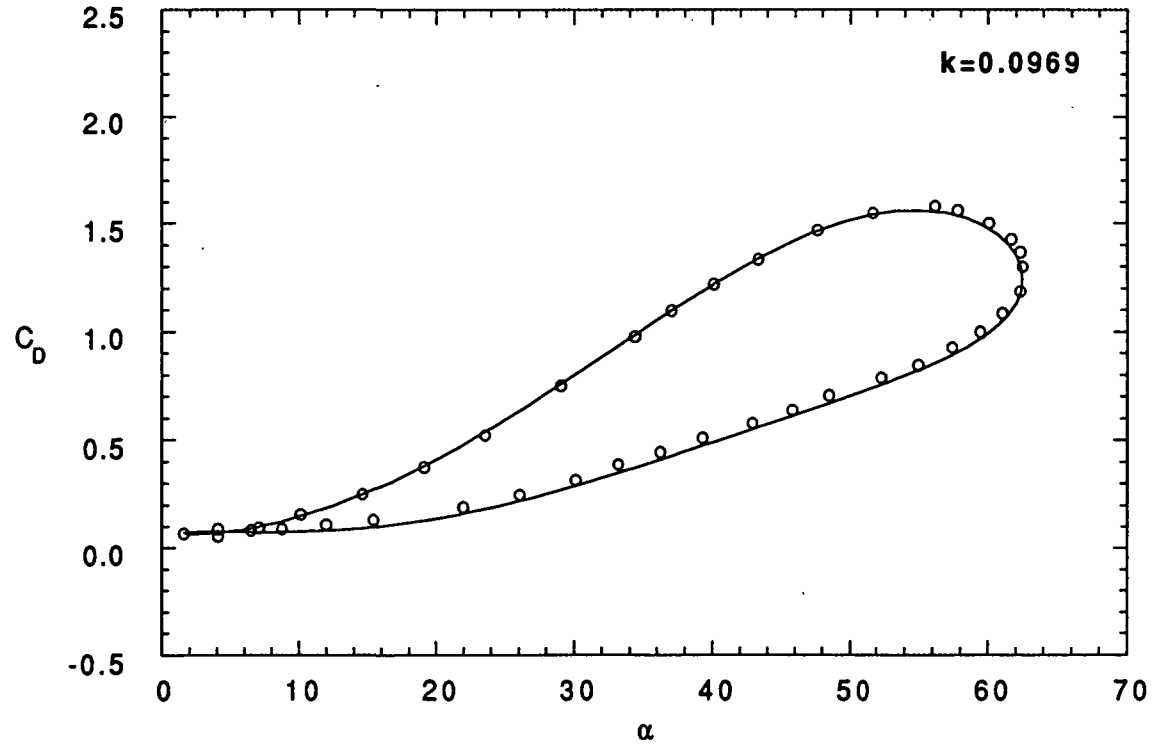

(b)Drag Data

Figure 1 Continued

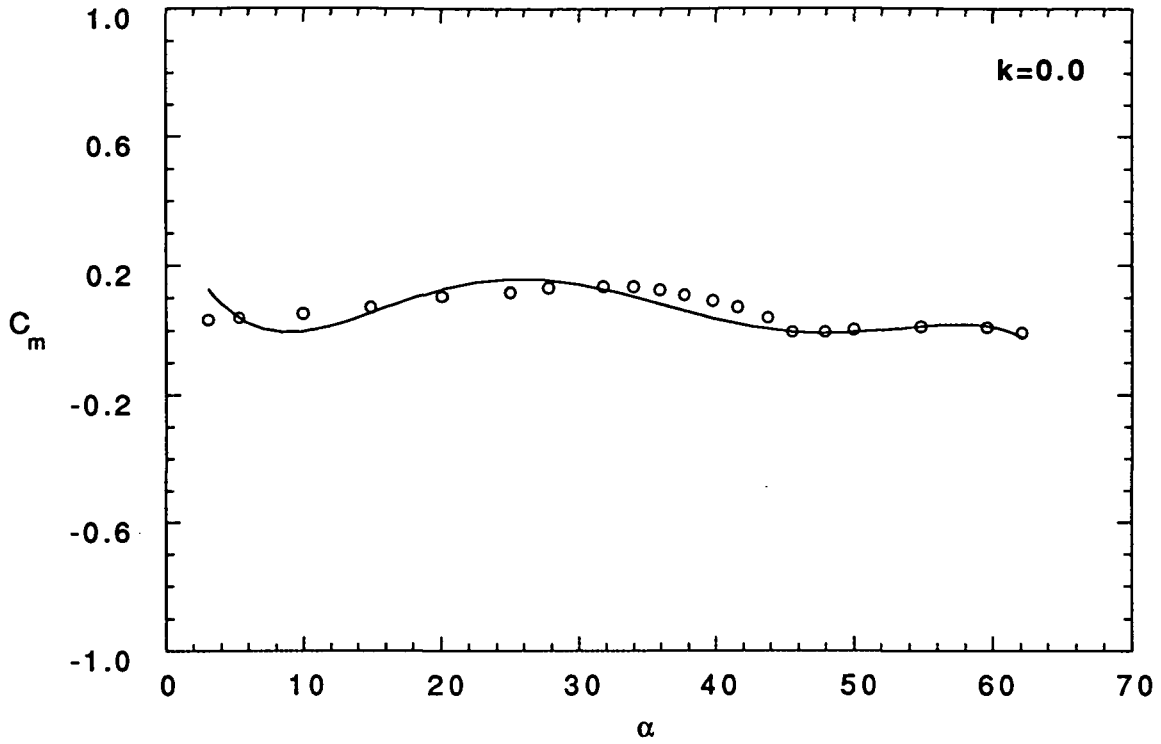

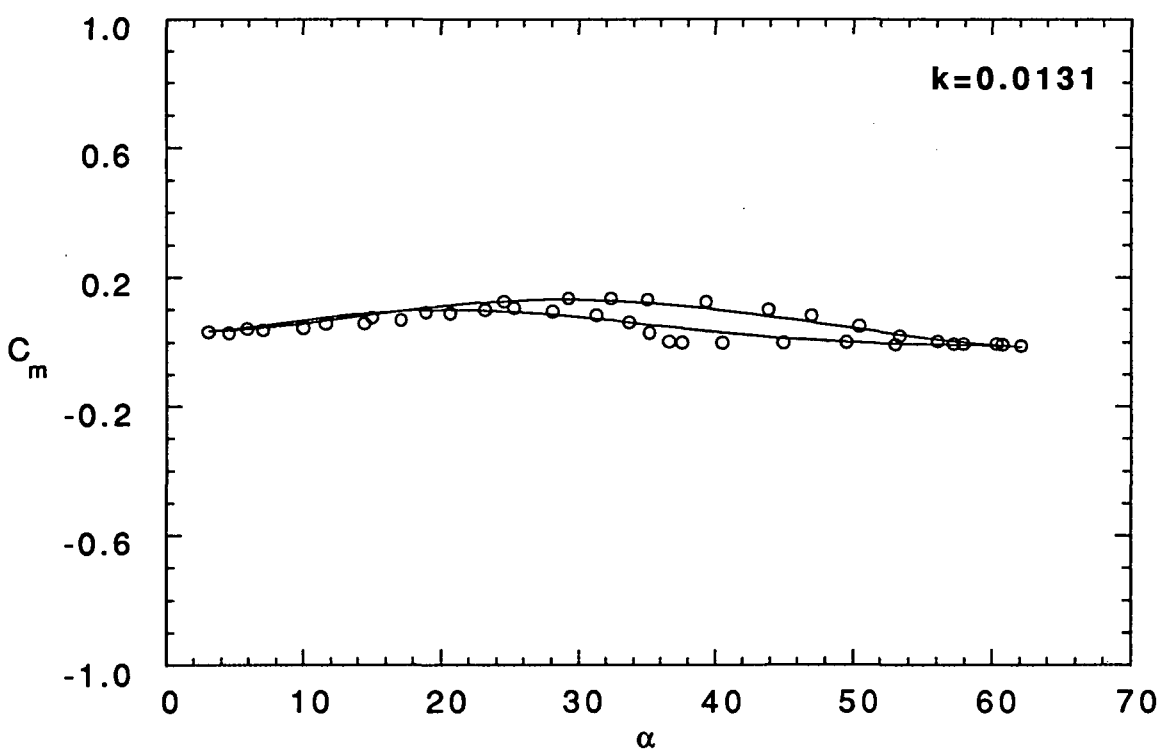

(c)Pitching Moment Data

Figure 1 Continued

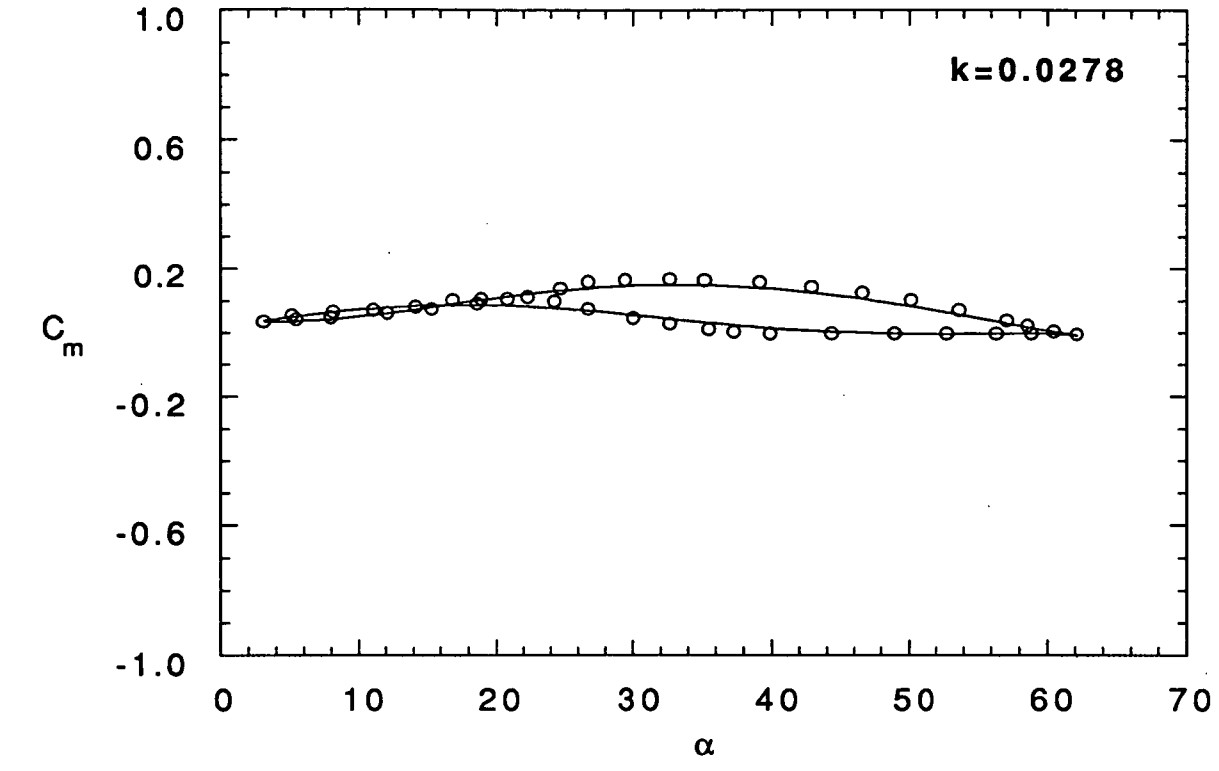

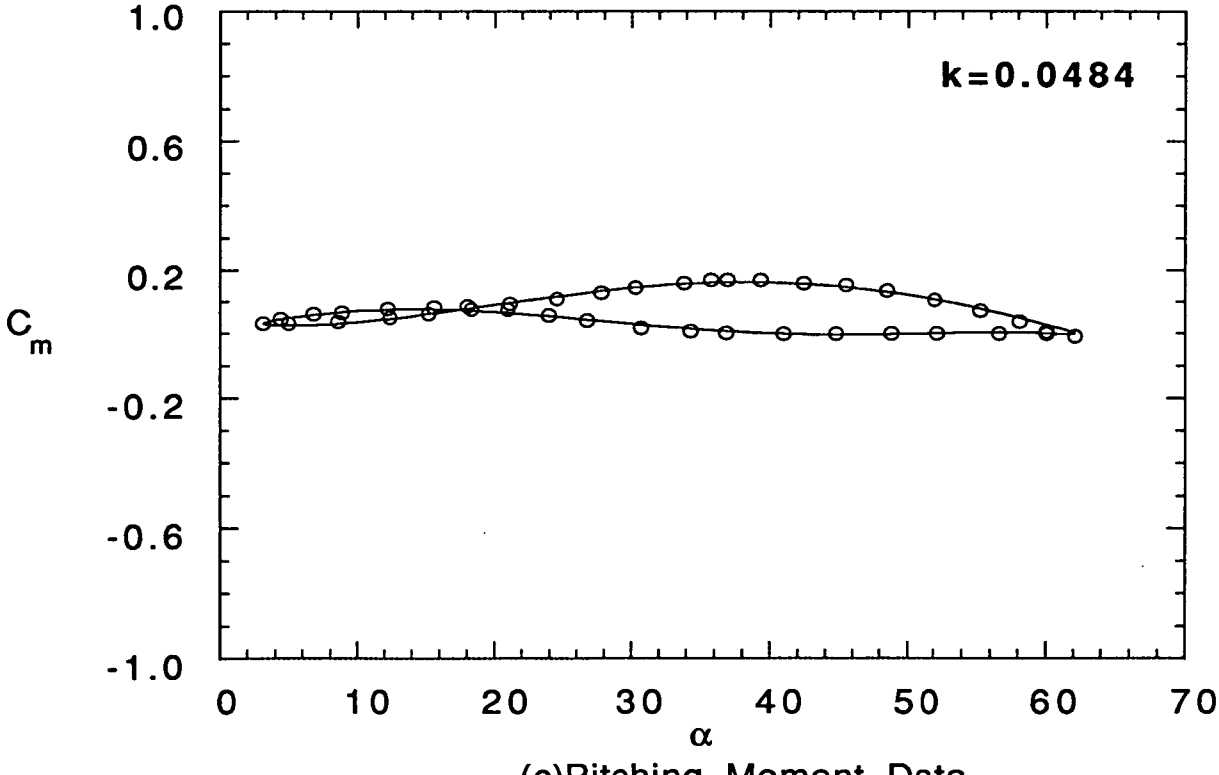

(c)Pitching Moment Data

Figure 1 Continued

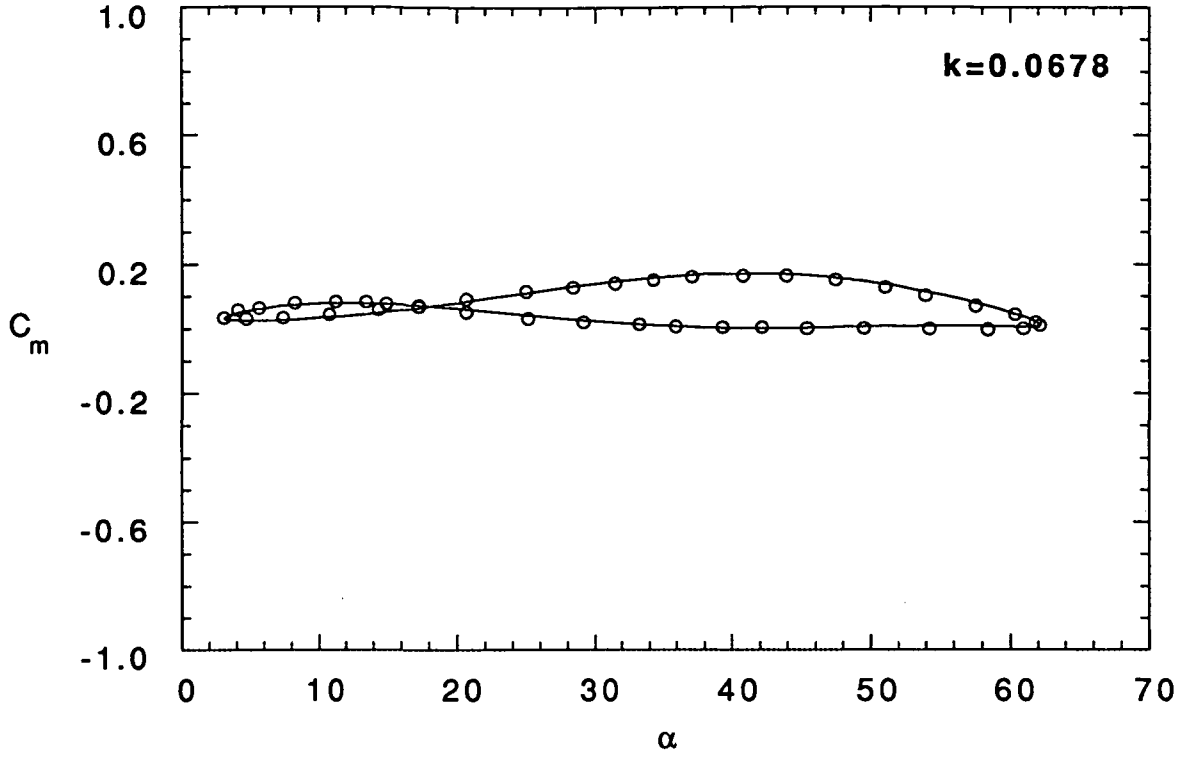

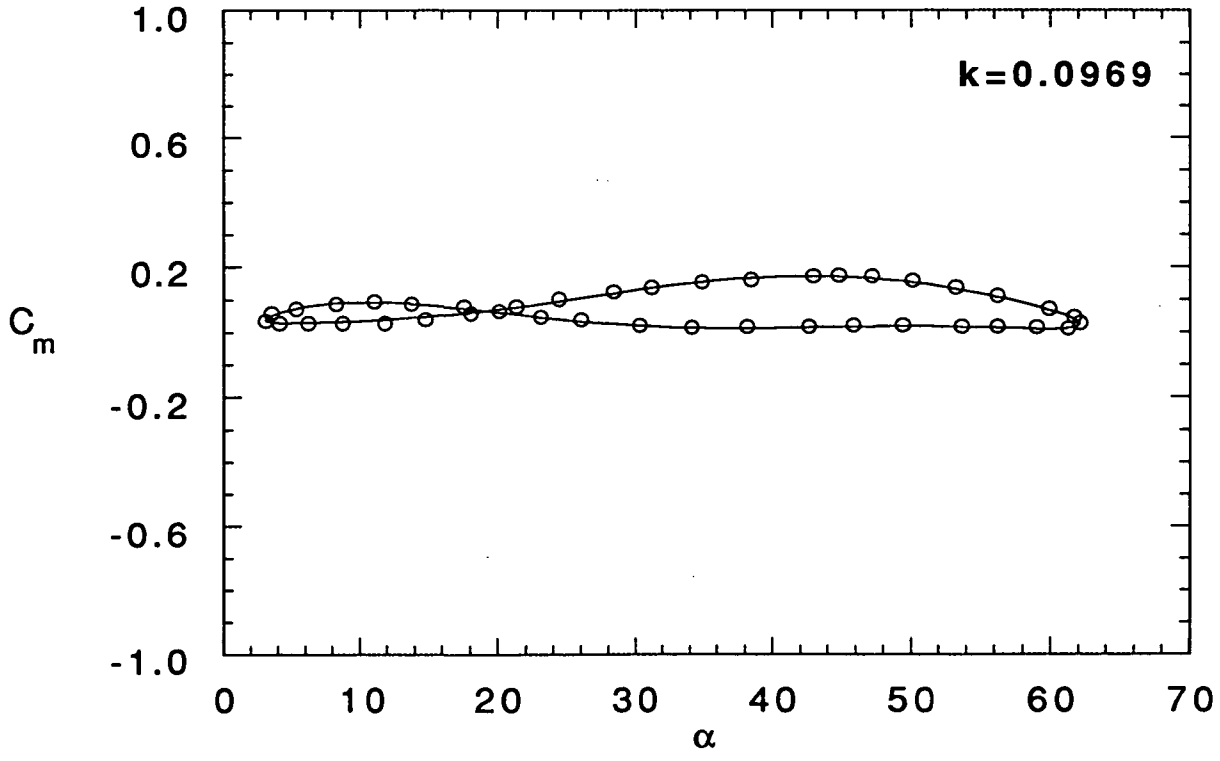

(c)Pitching Moment Data

Figure 1 Concluded

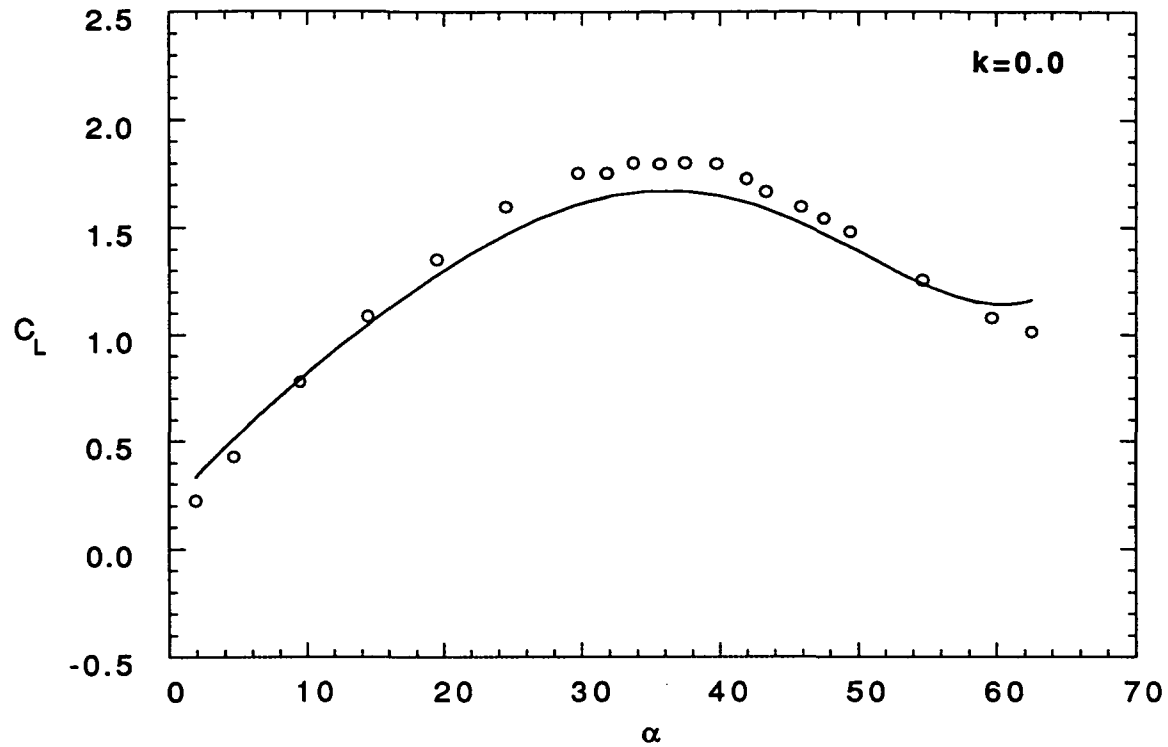

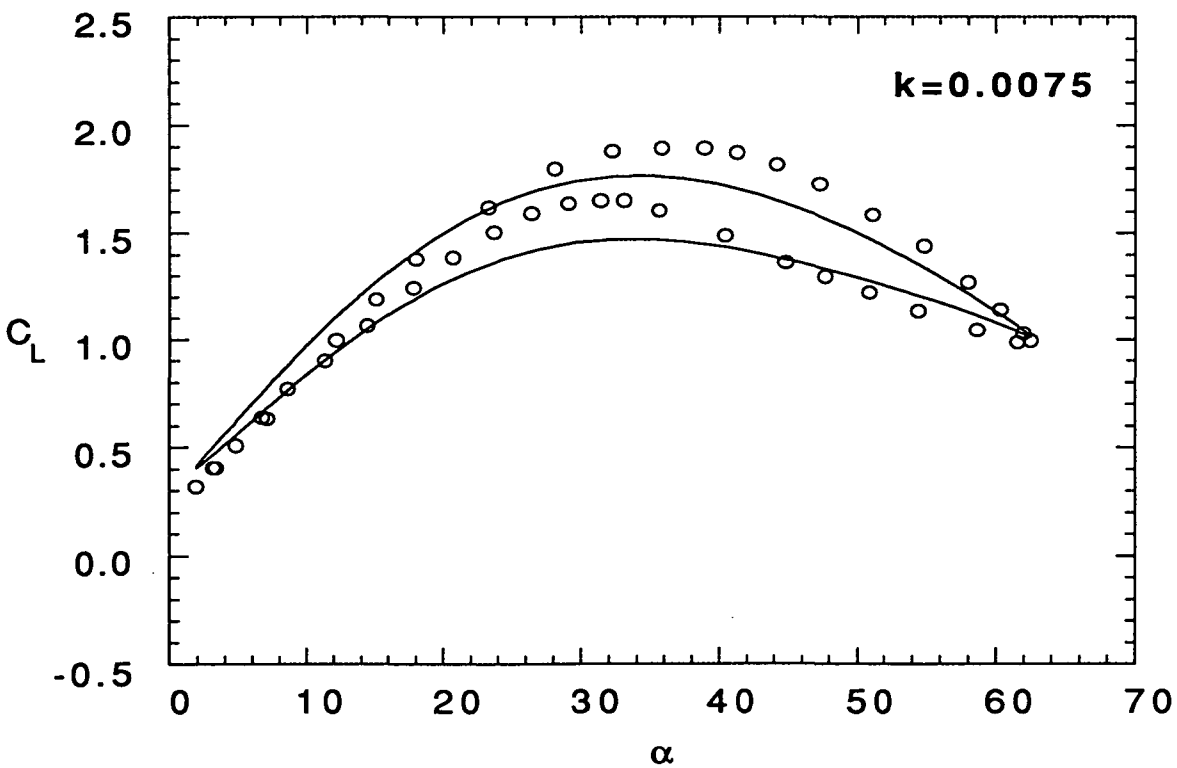

(a)Lift Data

Figure 2 Analysis of F-18 Dynamic Stall Data

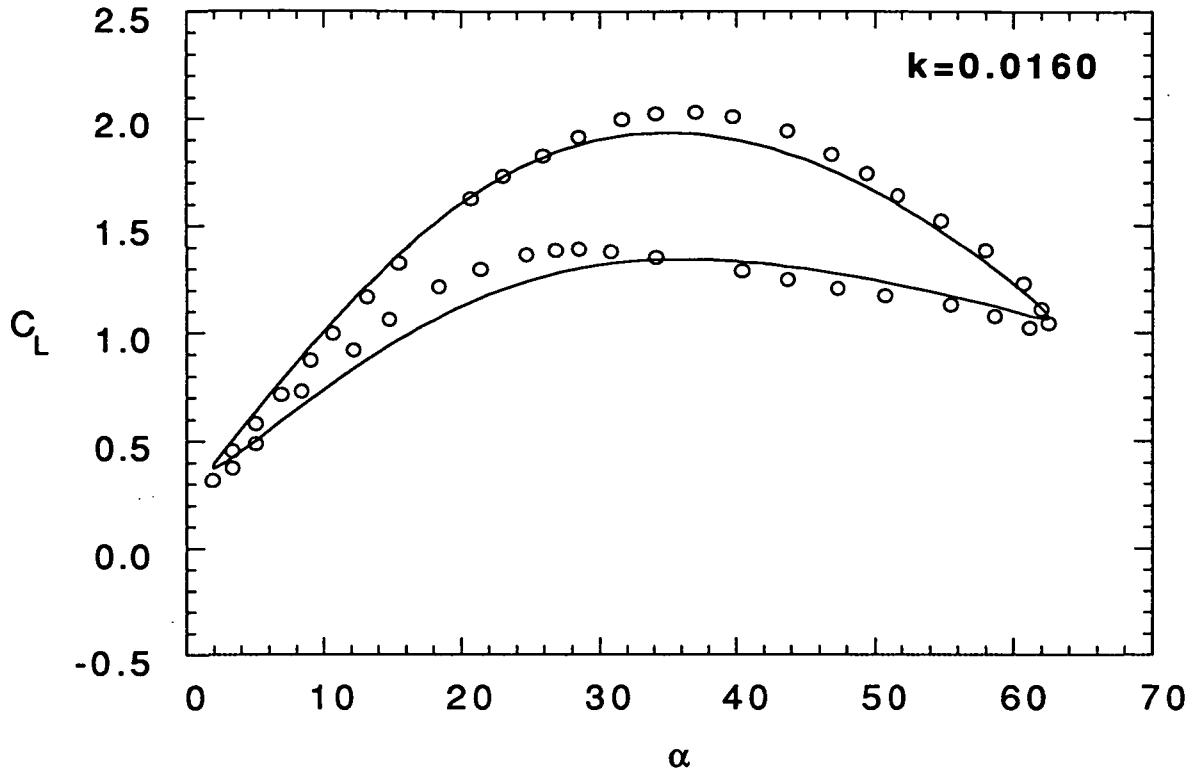

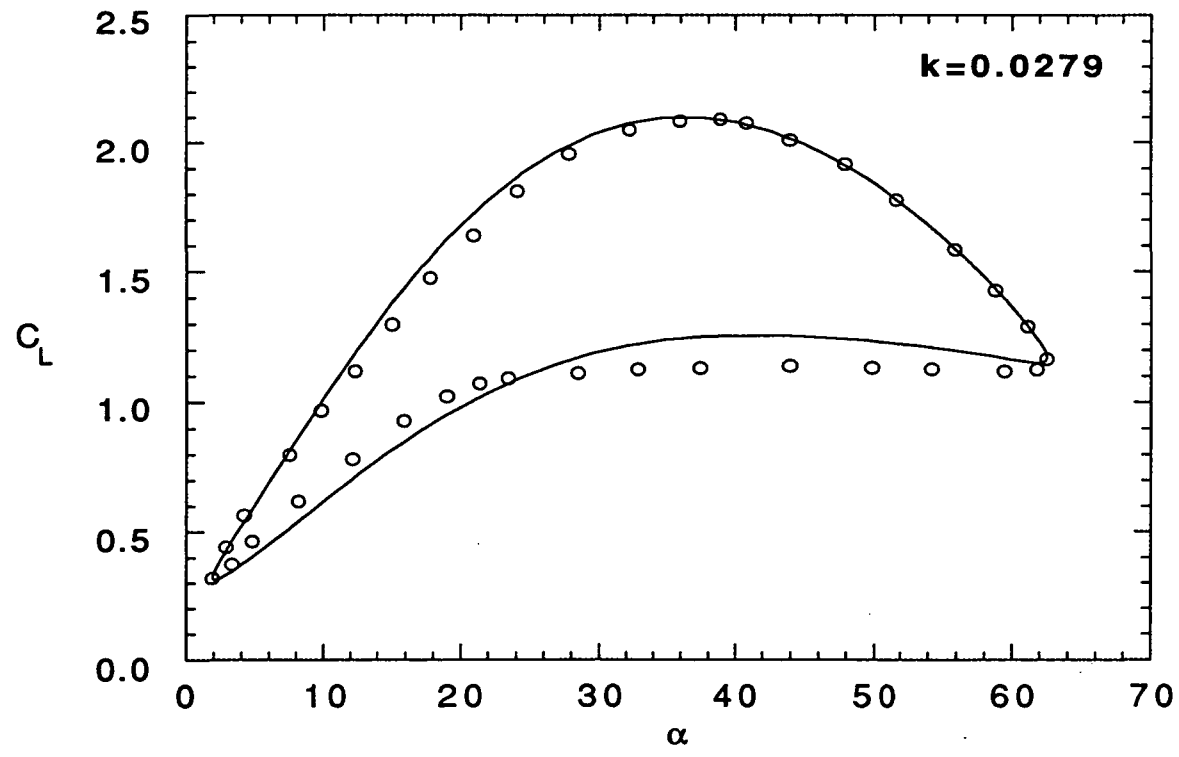

(a)Lift Data

Figure 2 Continued

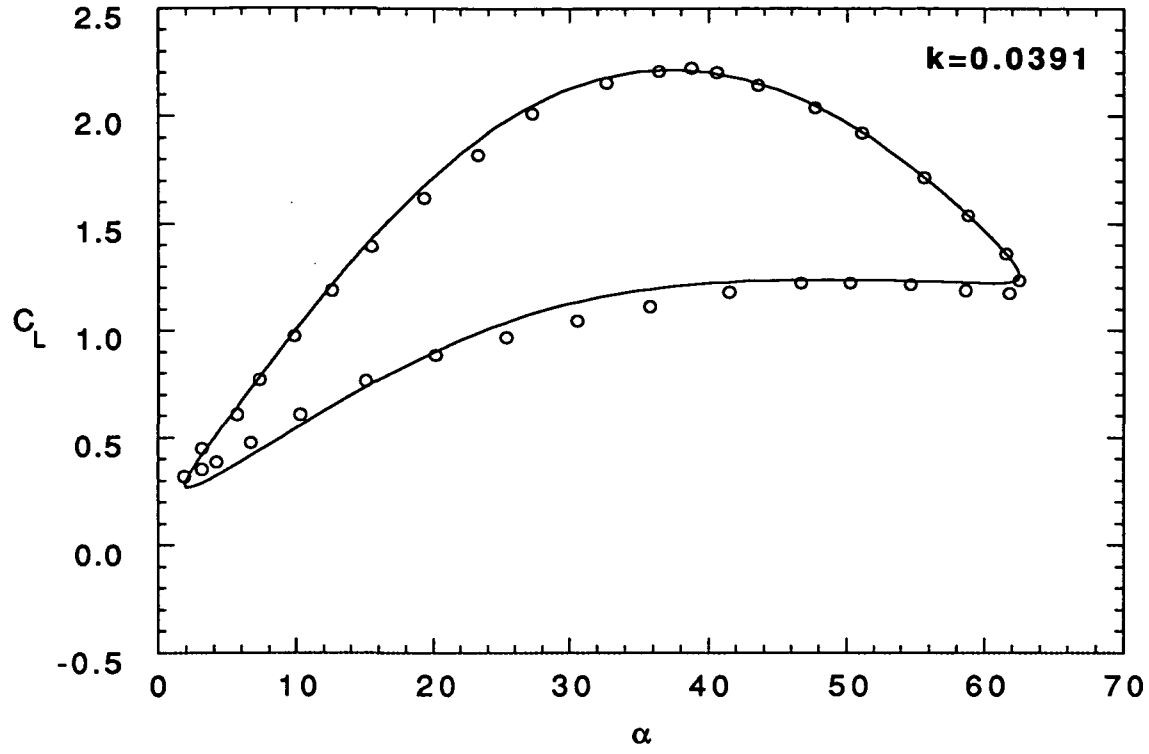

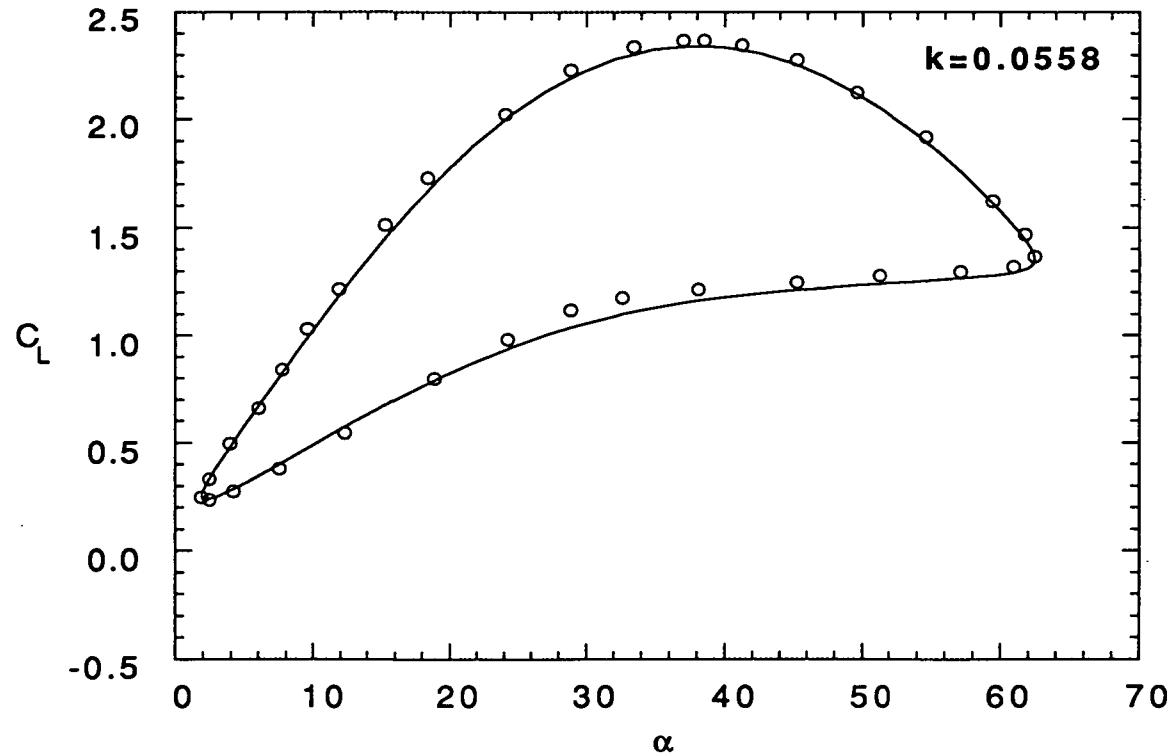

(a)Lift Data

Figure 2 Continued

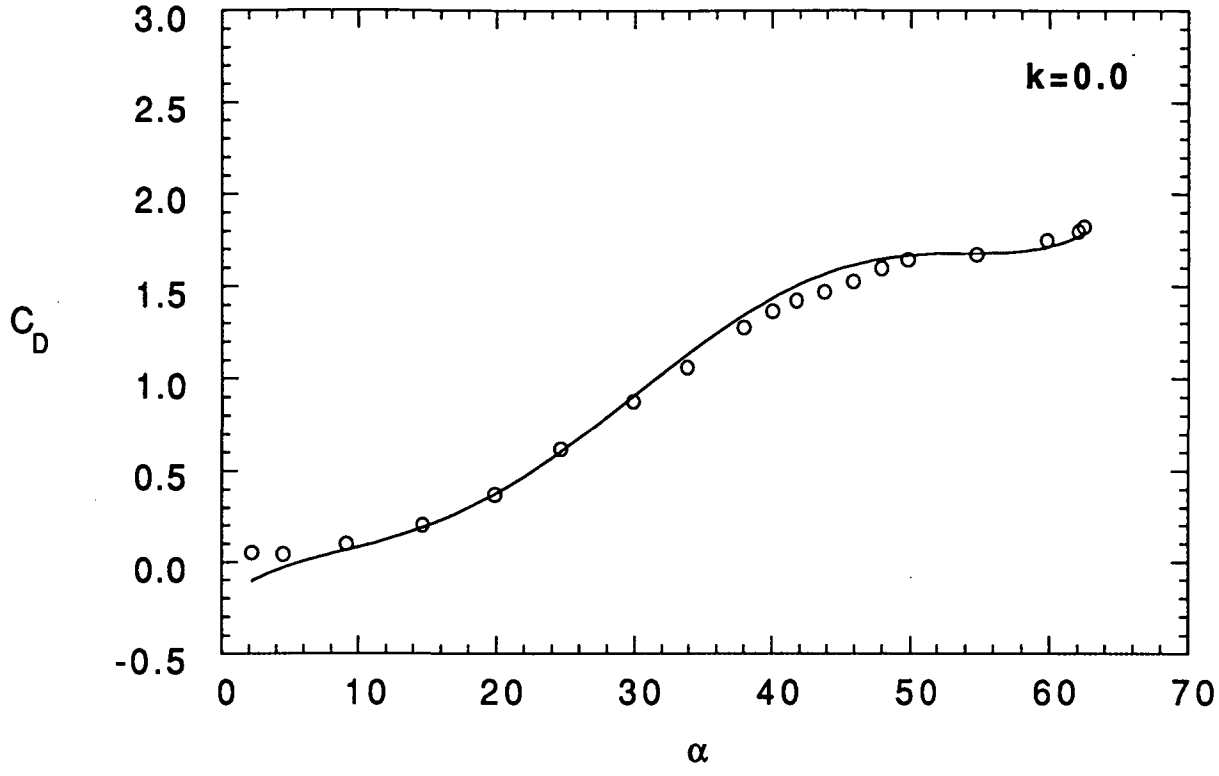

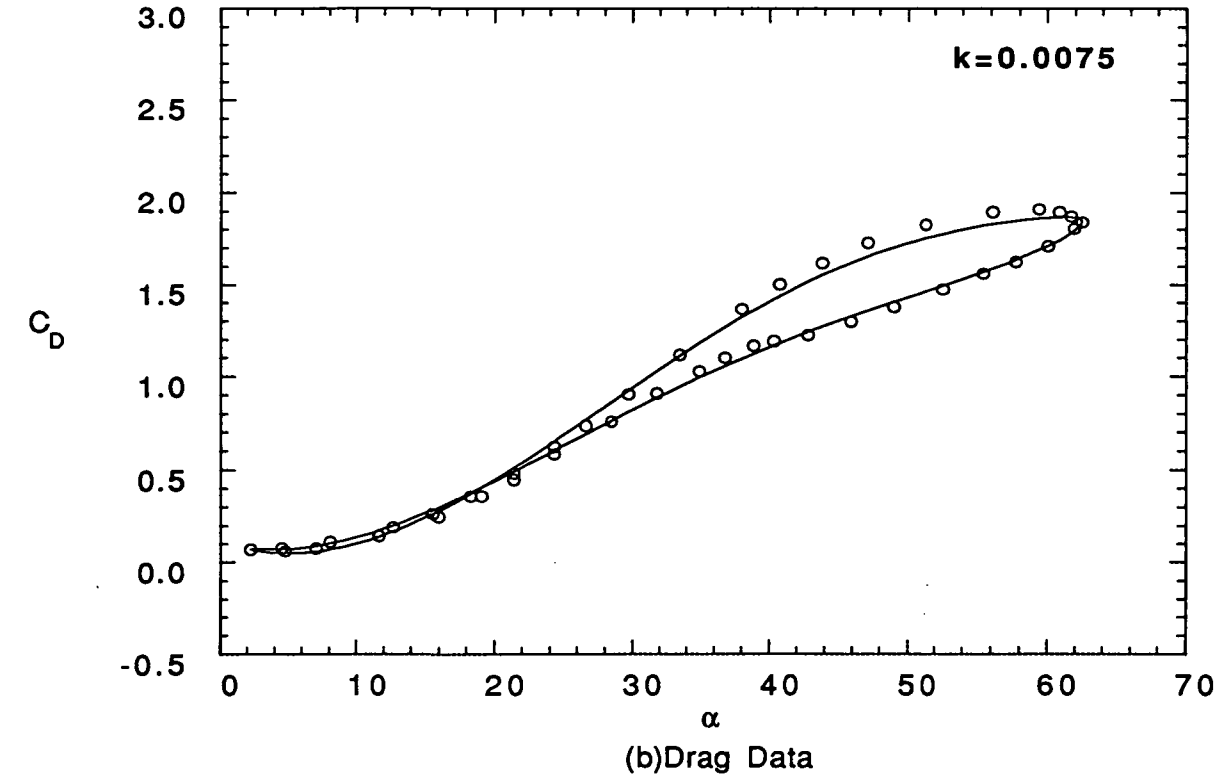

(b)Drag Data

Figure 2 Continued

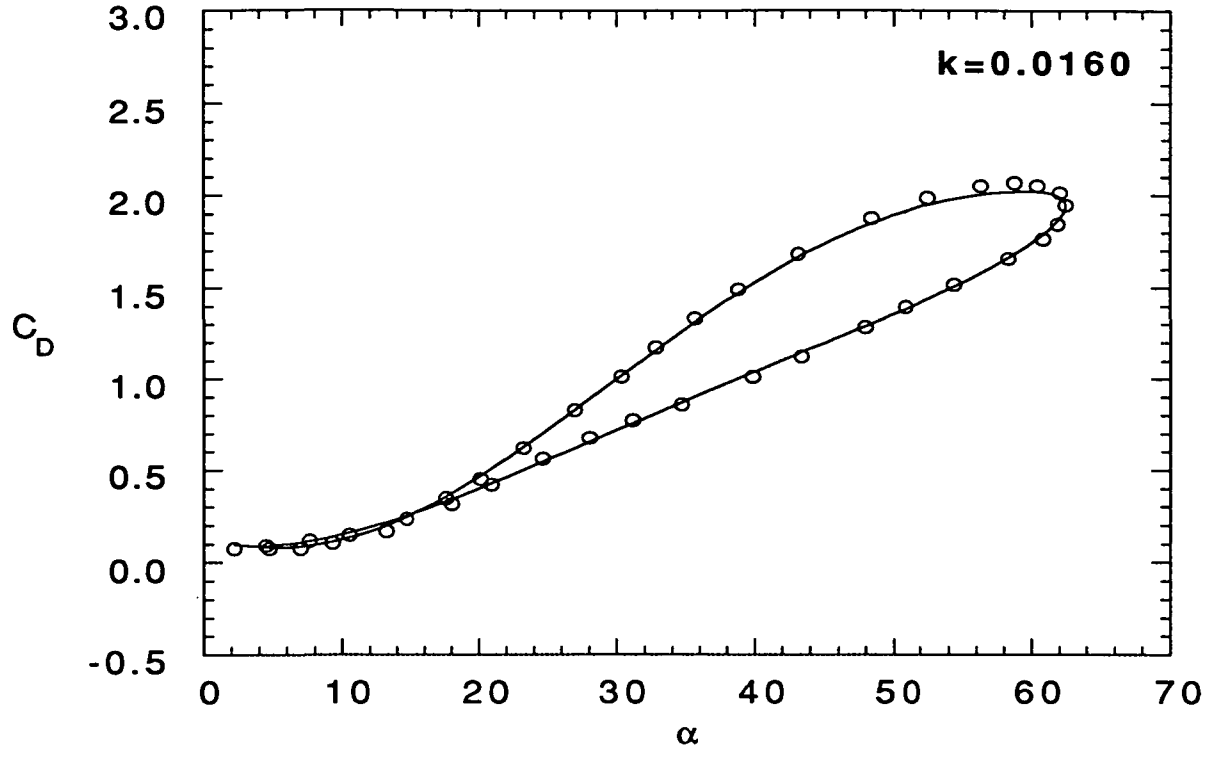

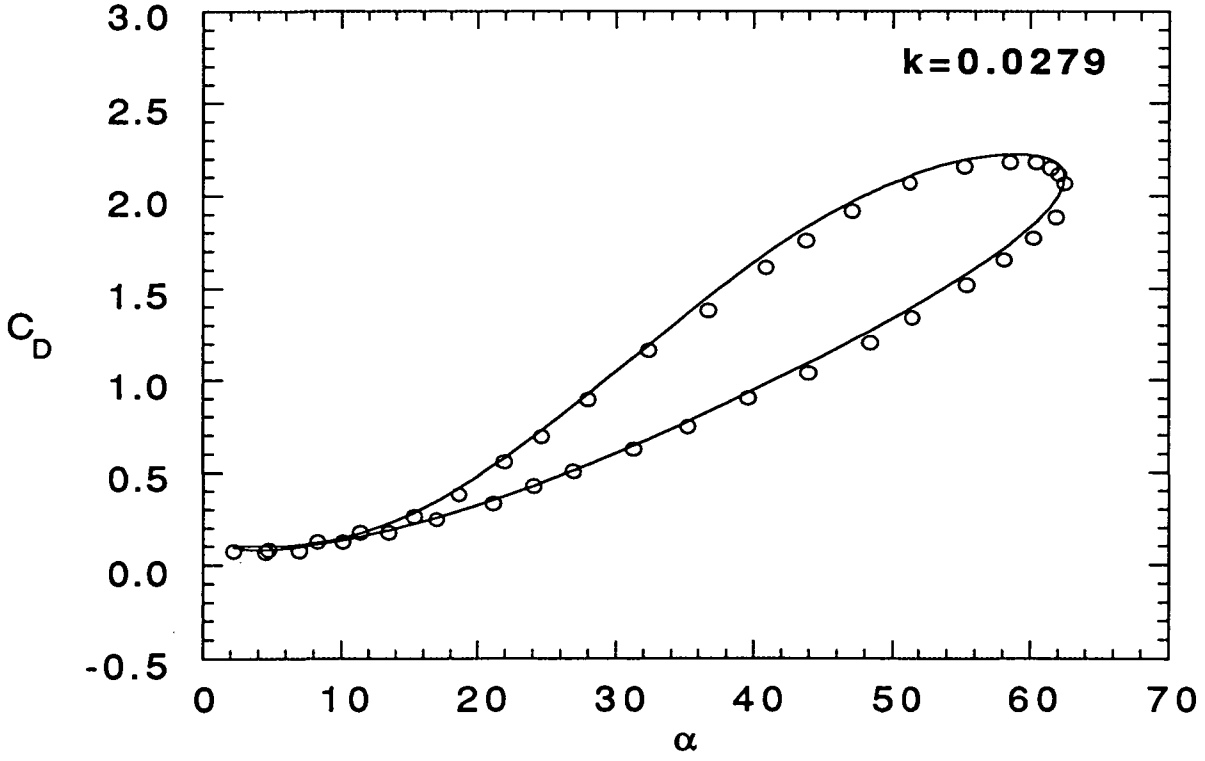

(b)Drag Data

Figure 2 Continued

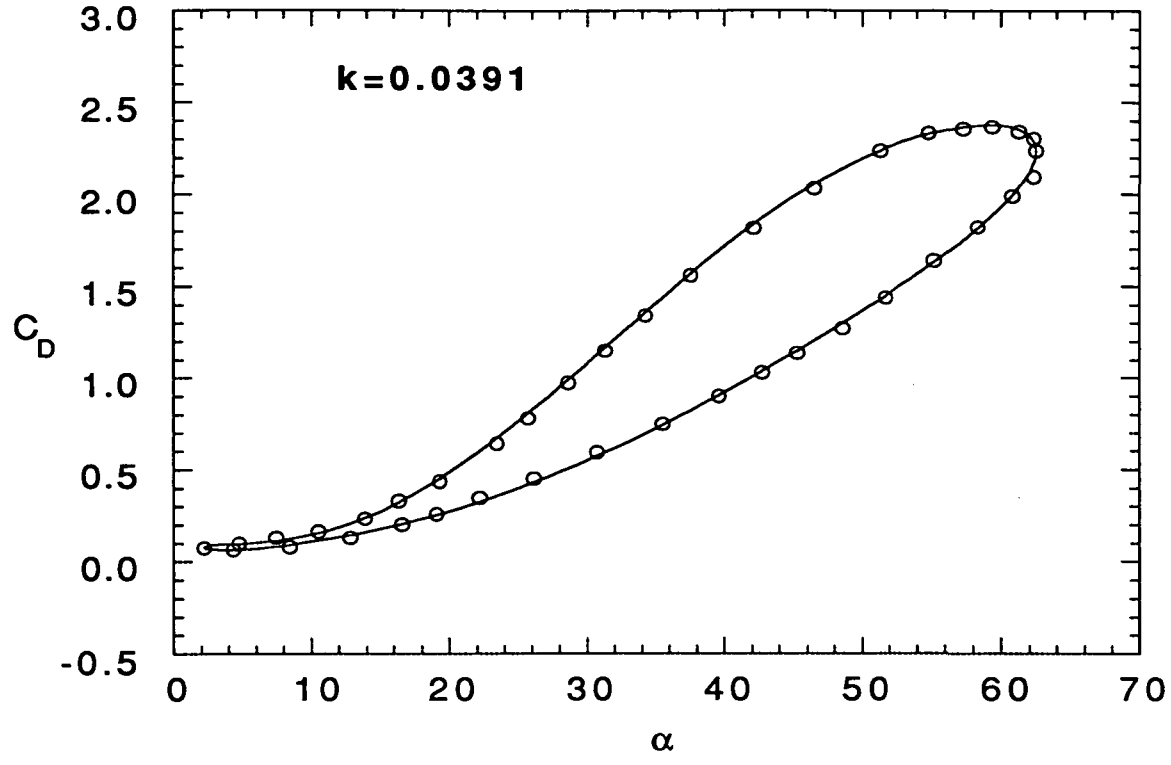

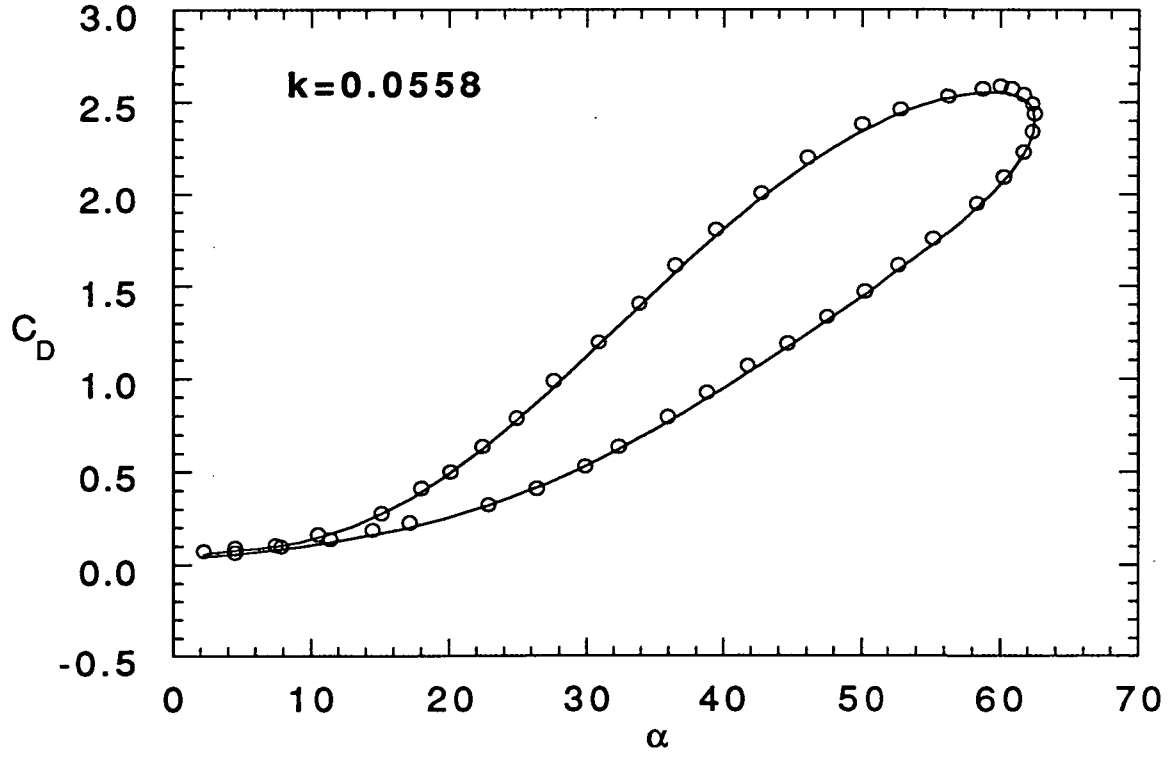

(b)Drag Data

Figure 2 Continued

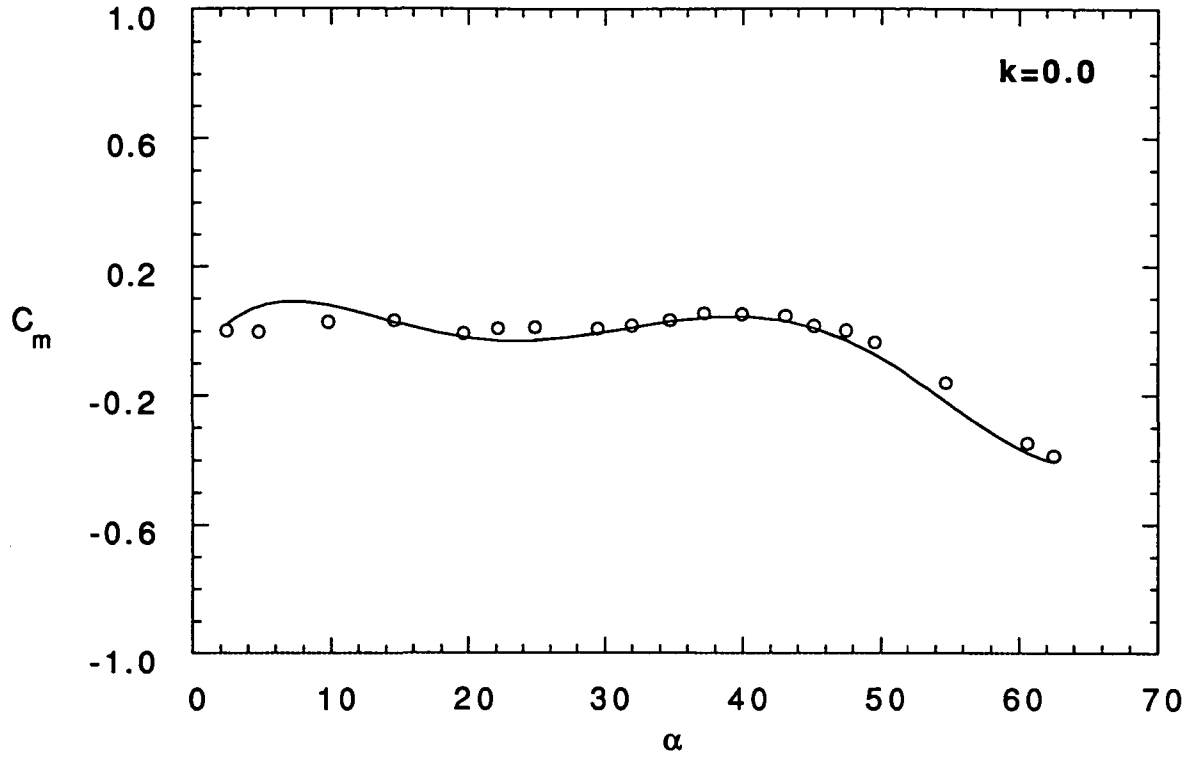

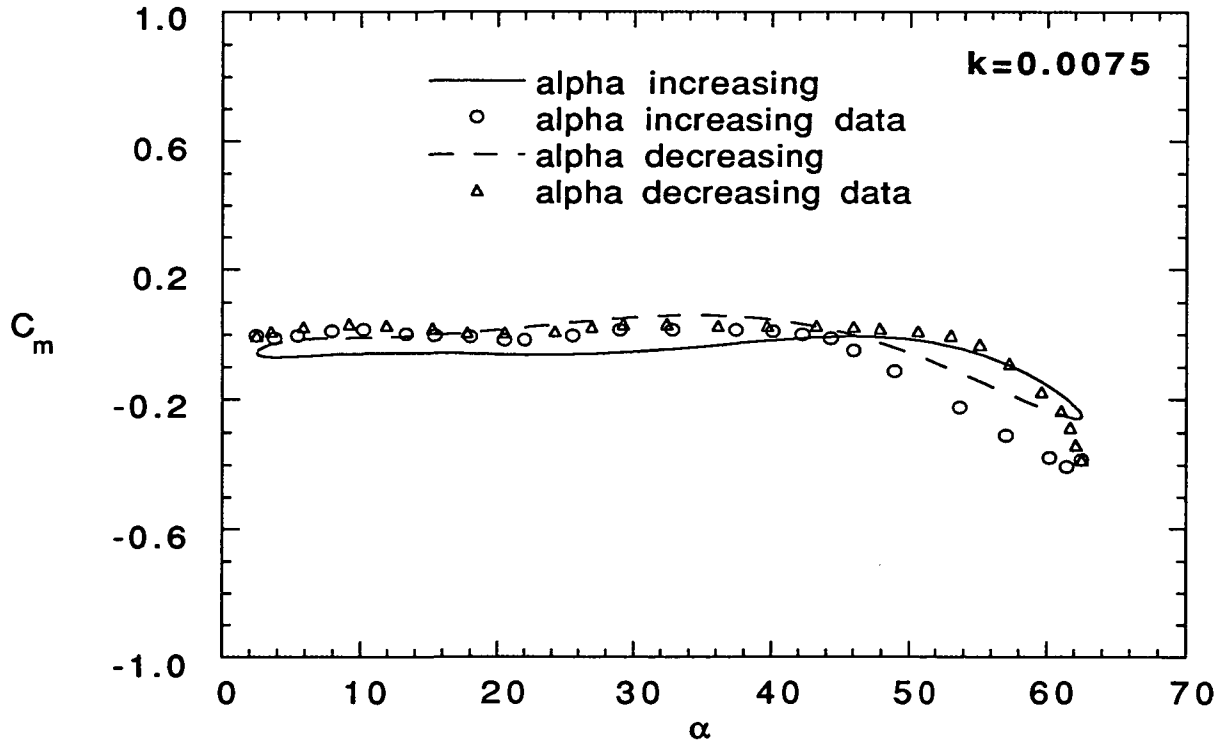

(c)Pitching Moment Data

Figure 2 Continued

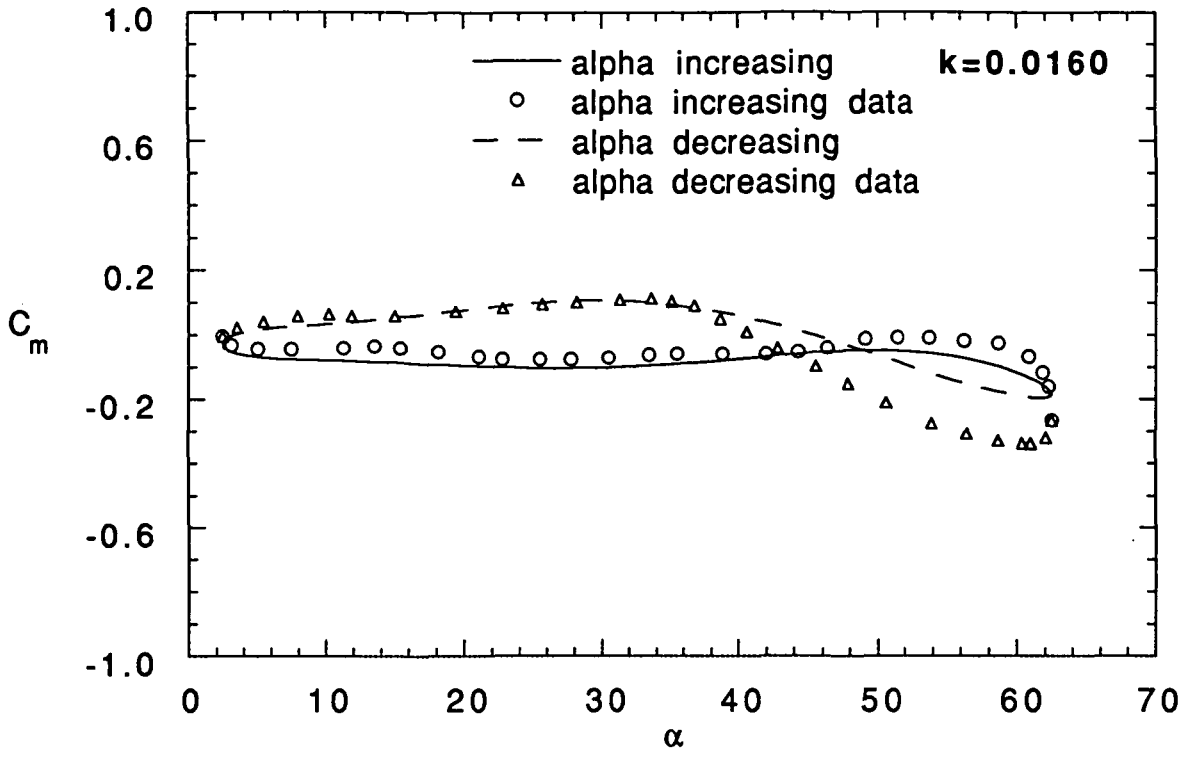

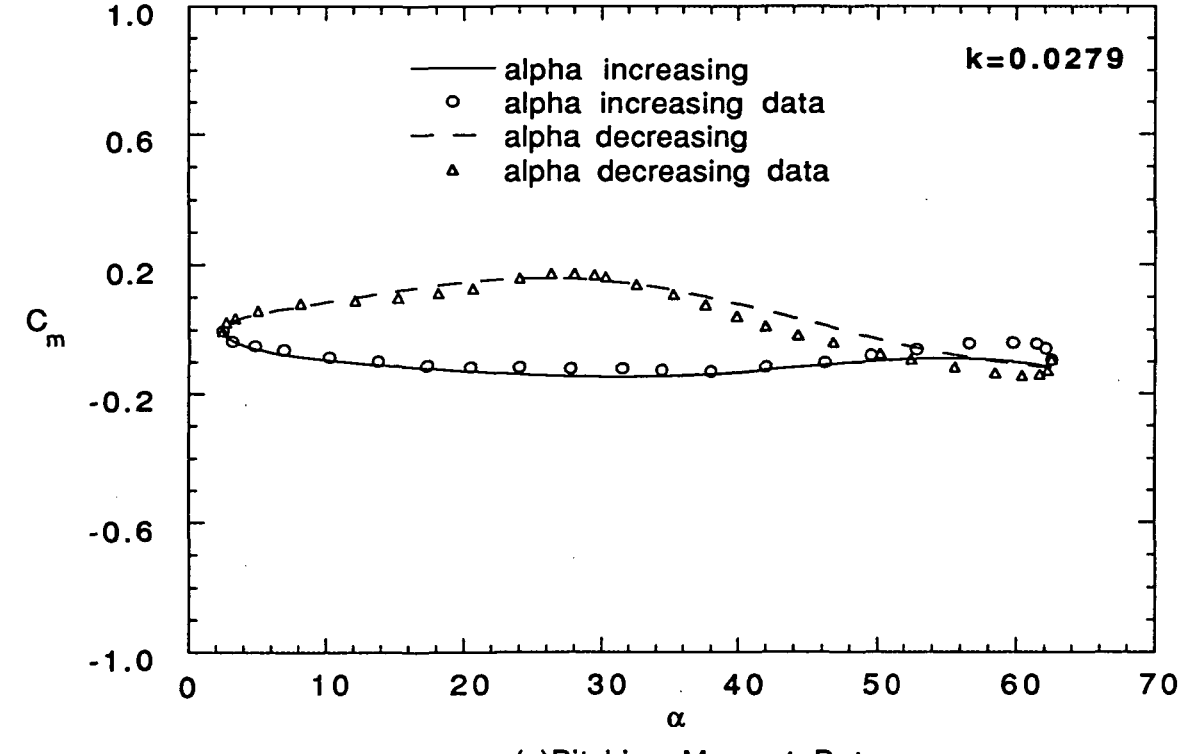

(c)Pitching Moment Data

Figure 2 Continued

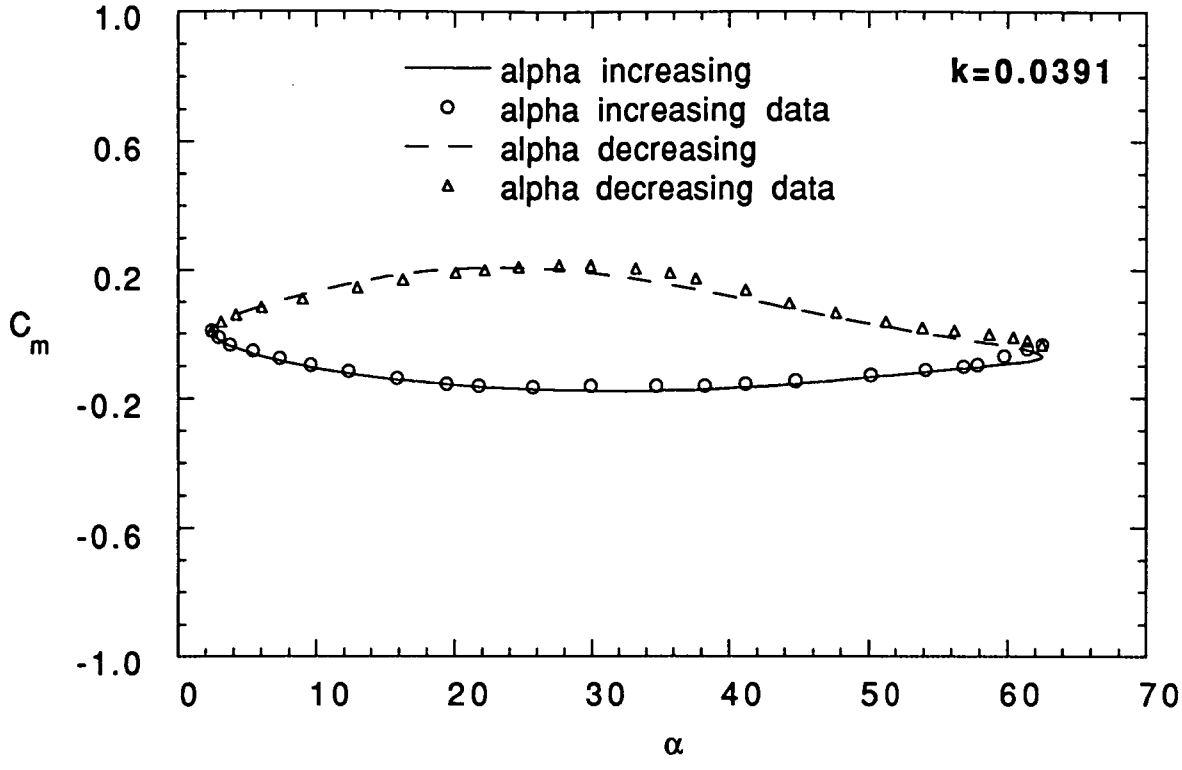

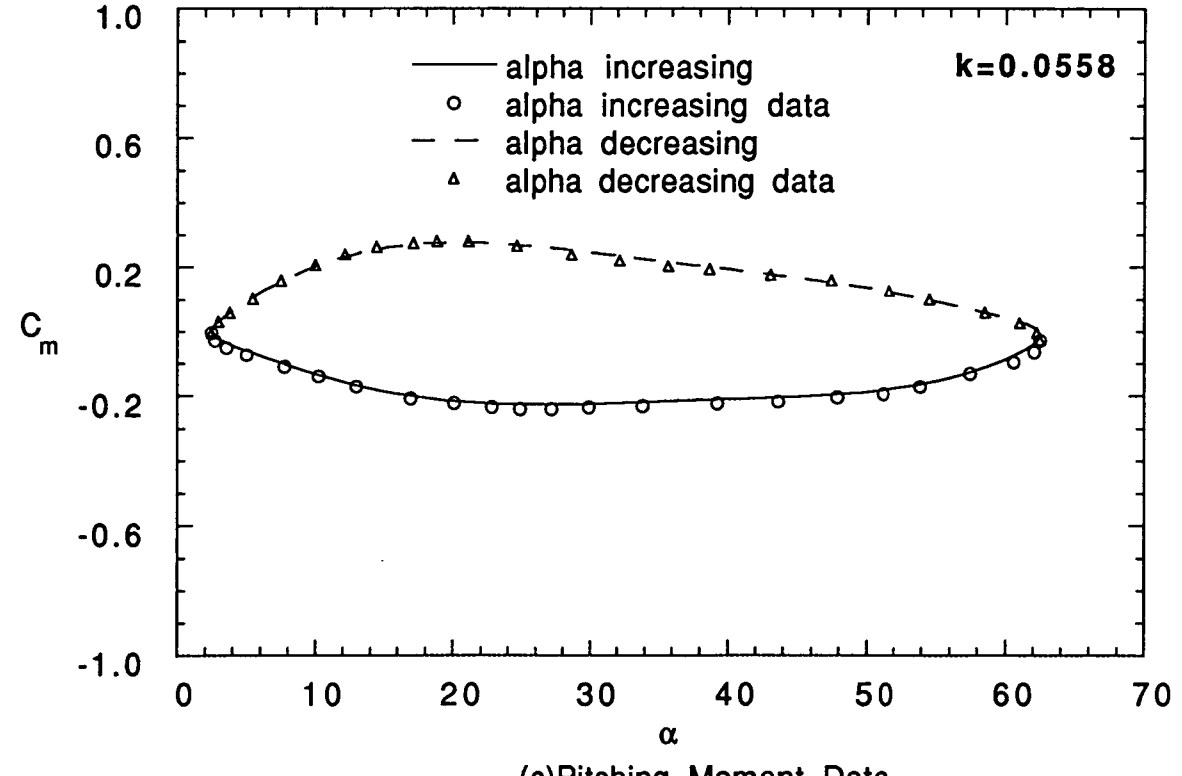

(c)Pitching Moment Data

Figure 2 Concluded

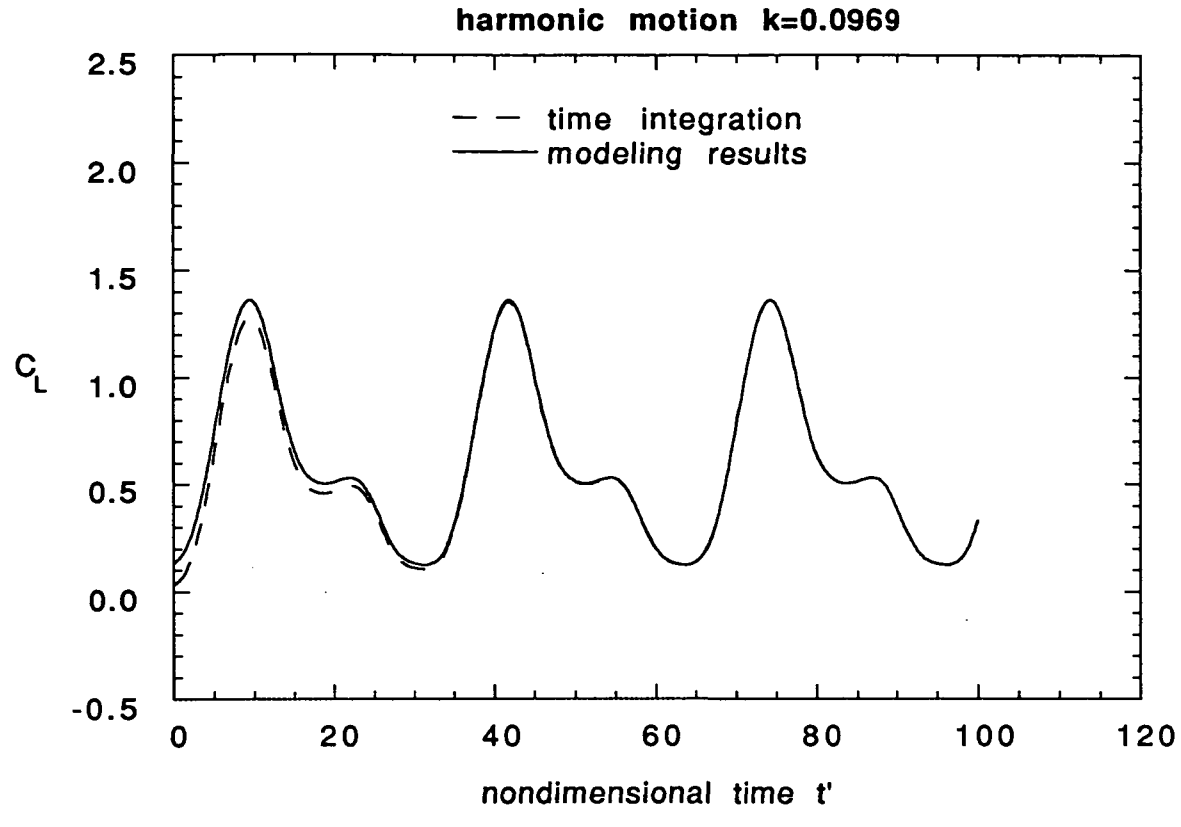

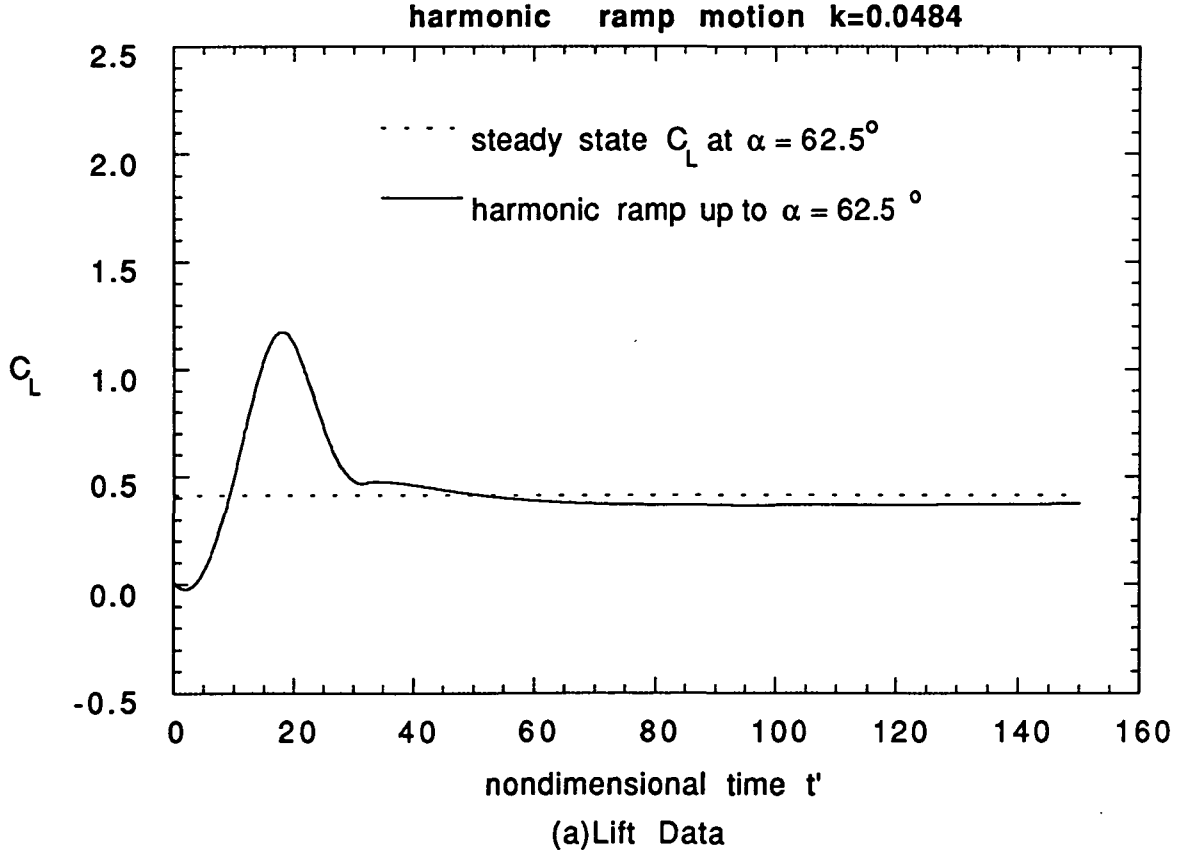

(a)Lift Data

Figure 3 Delta Wing Responses by Time Integration for Harmonic Motion and Harmonic Ramp Motion

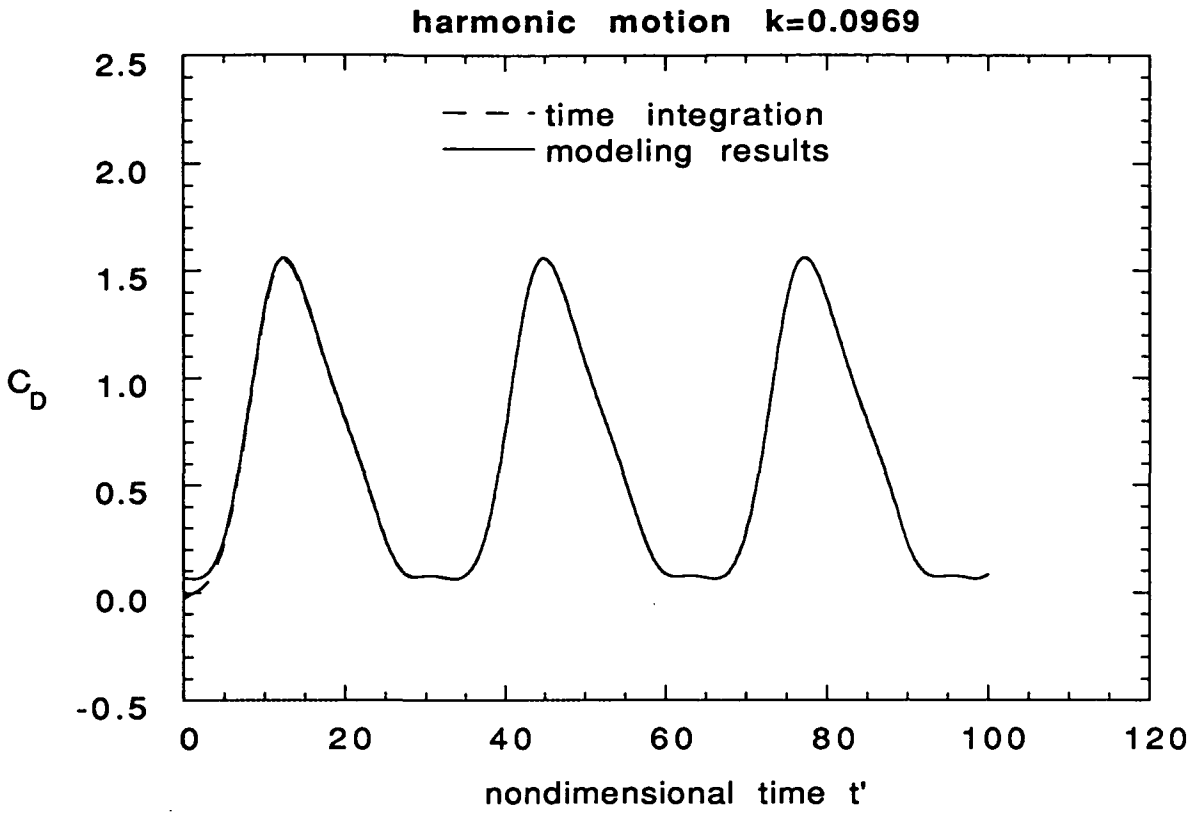

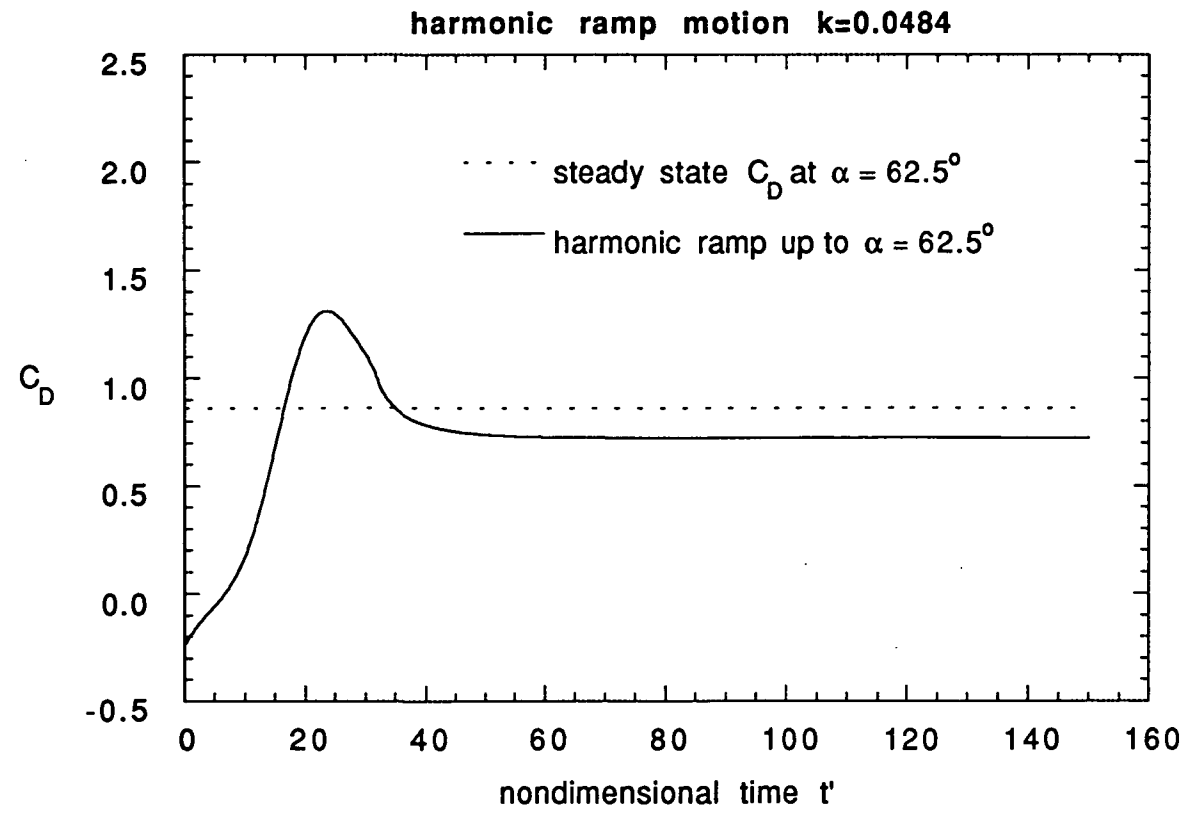

(b)Drag Data

Figure 3 Continued

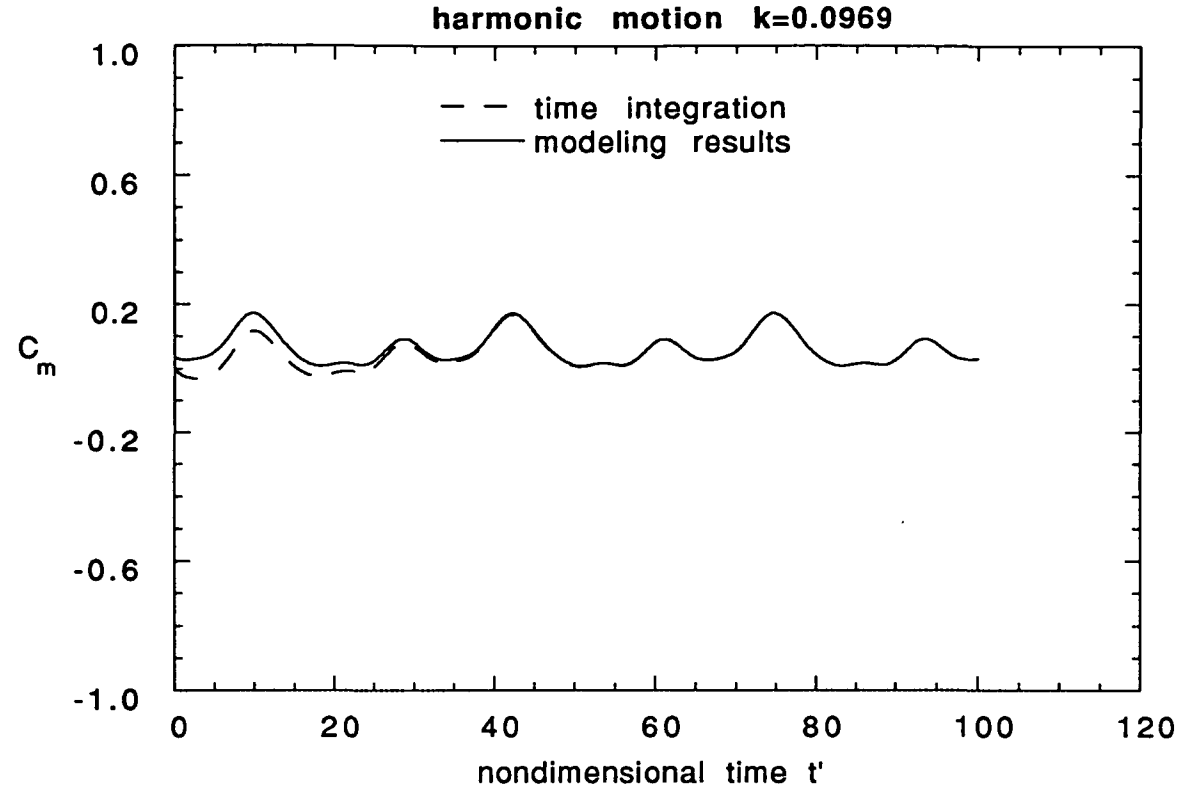

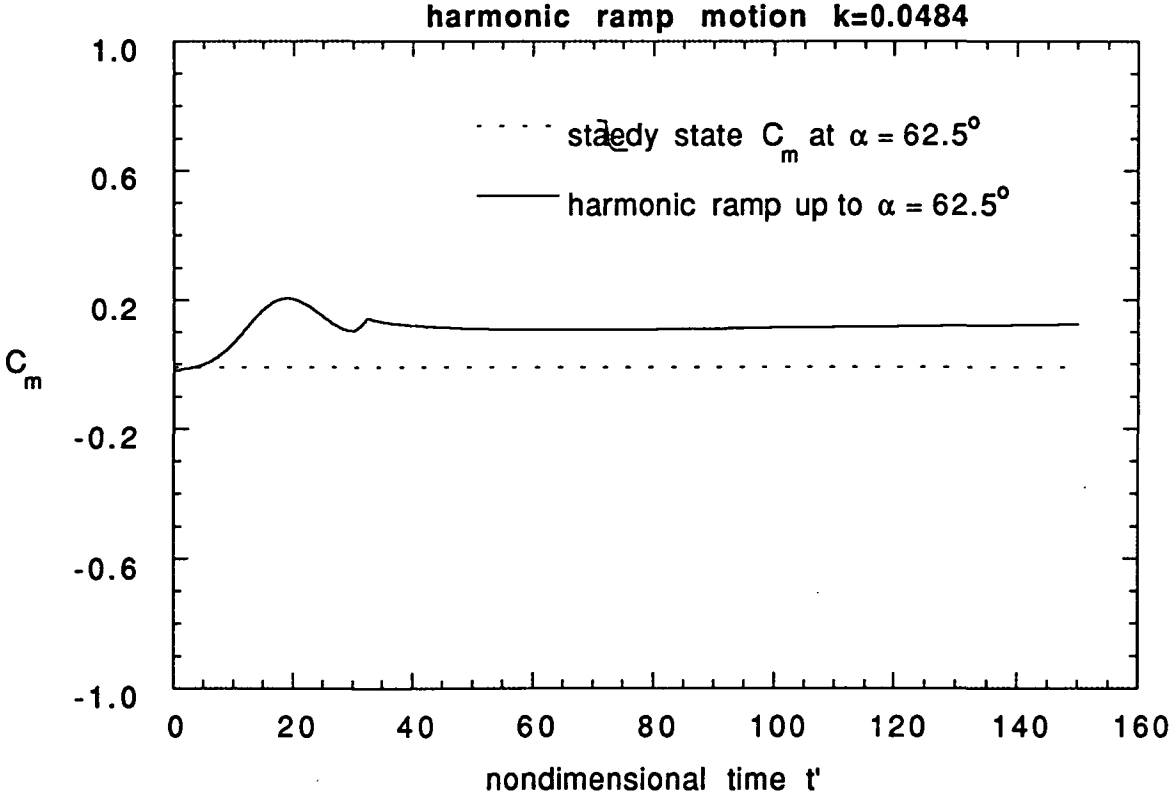

(c)Pitching Moment Data

Figure 3 Concluded

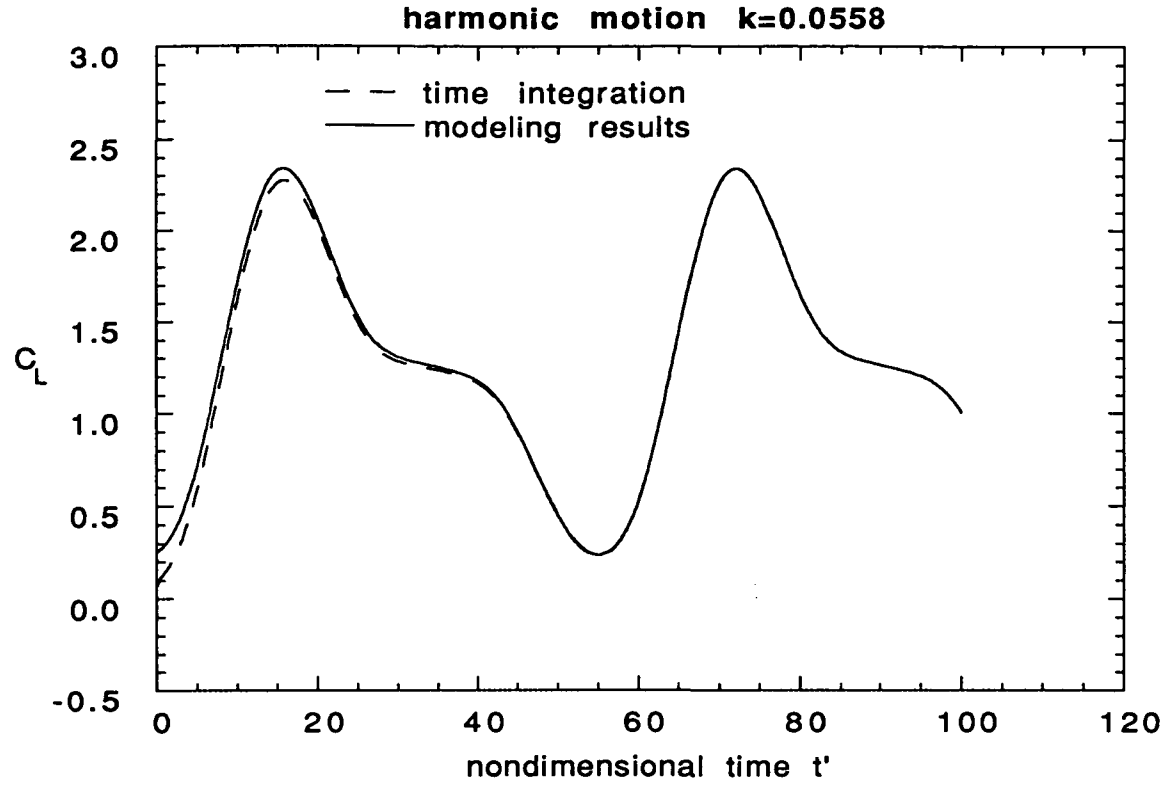

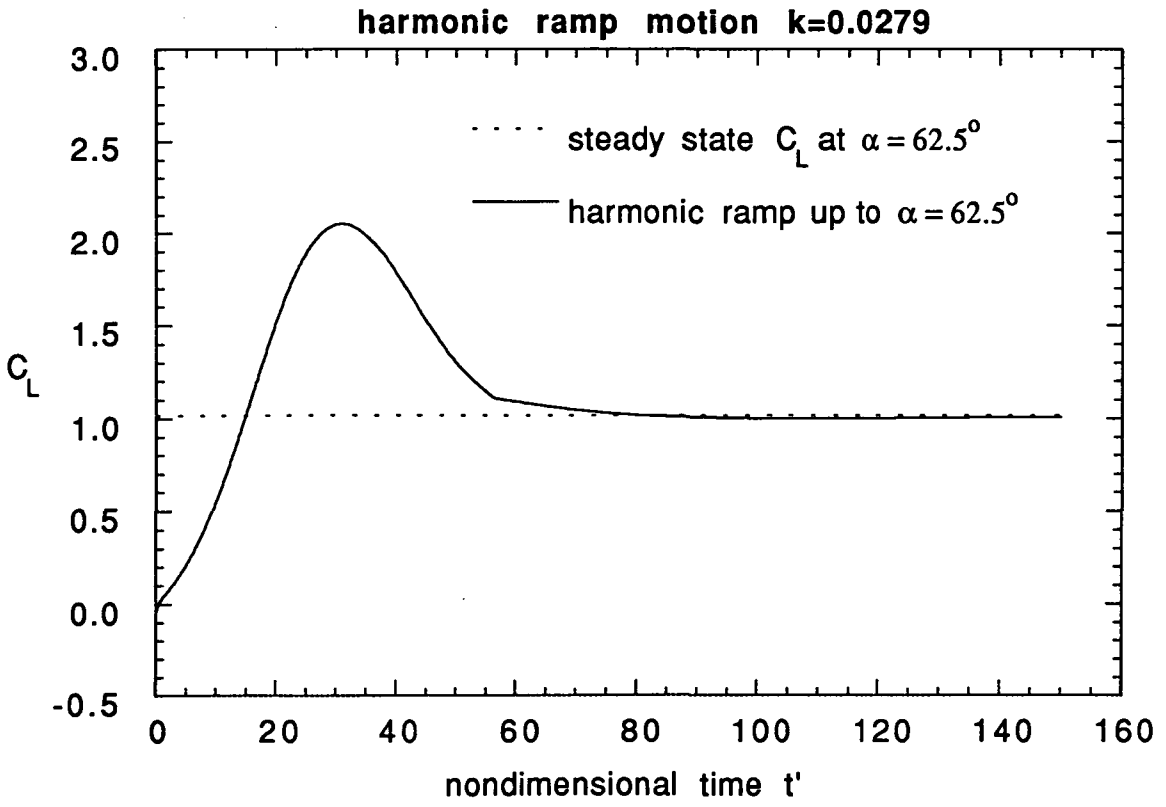

(a)Lift Data

Figure 4 F-18 Responses by Time Integration for Harmonic Motion and Harmonic Ramp Motion

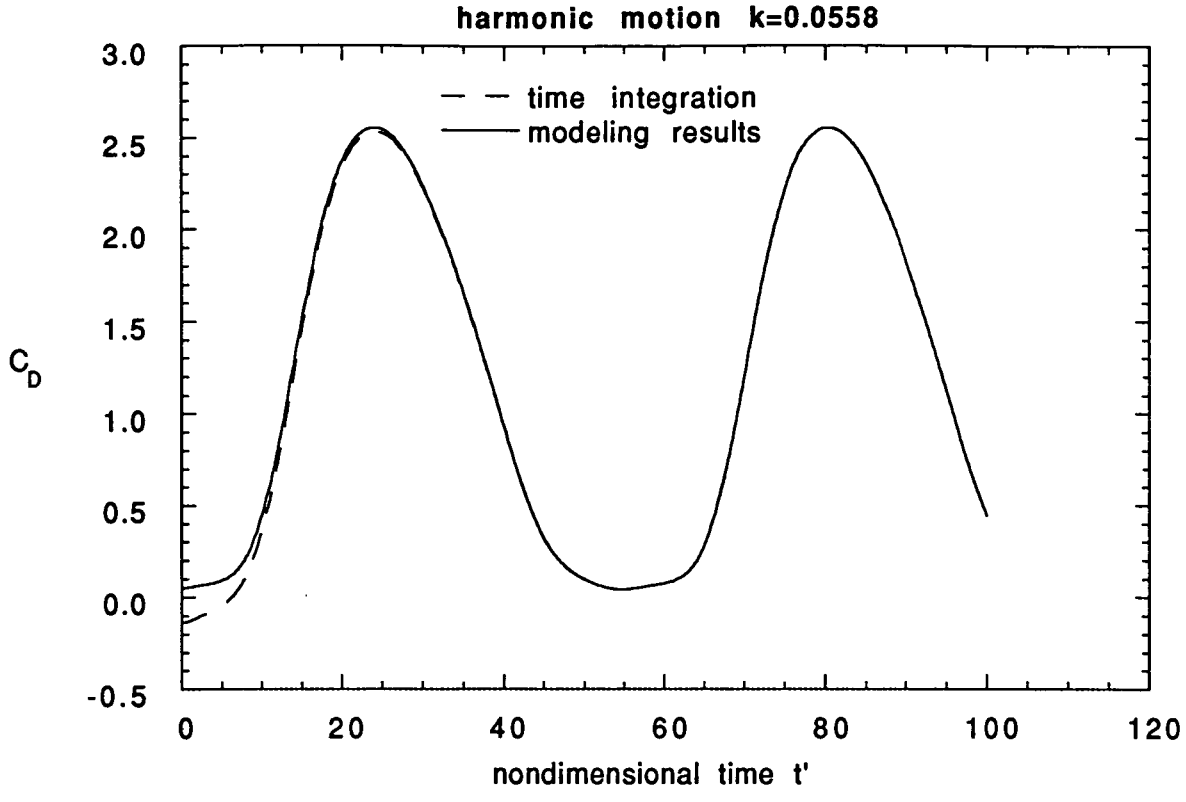

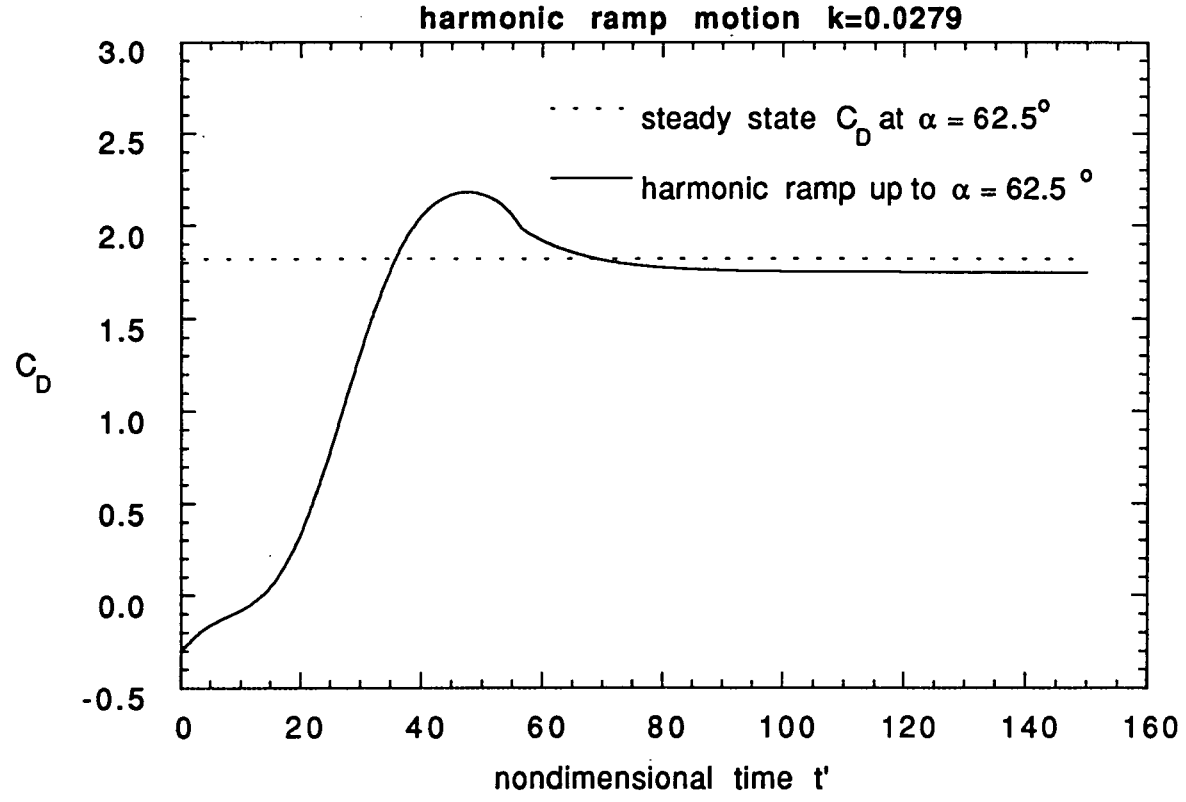

(b)Drag Data

Figure 4 Continued

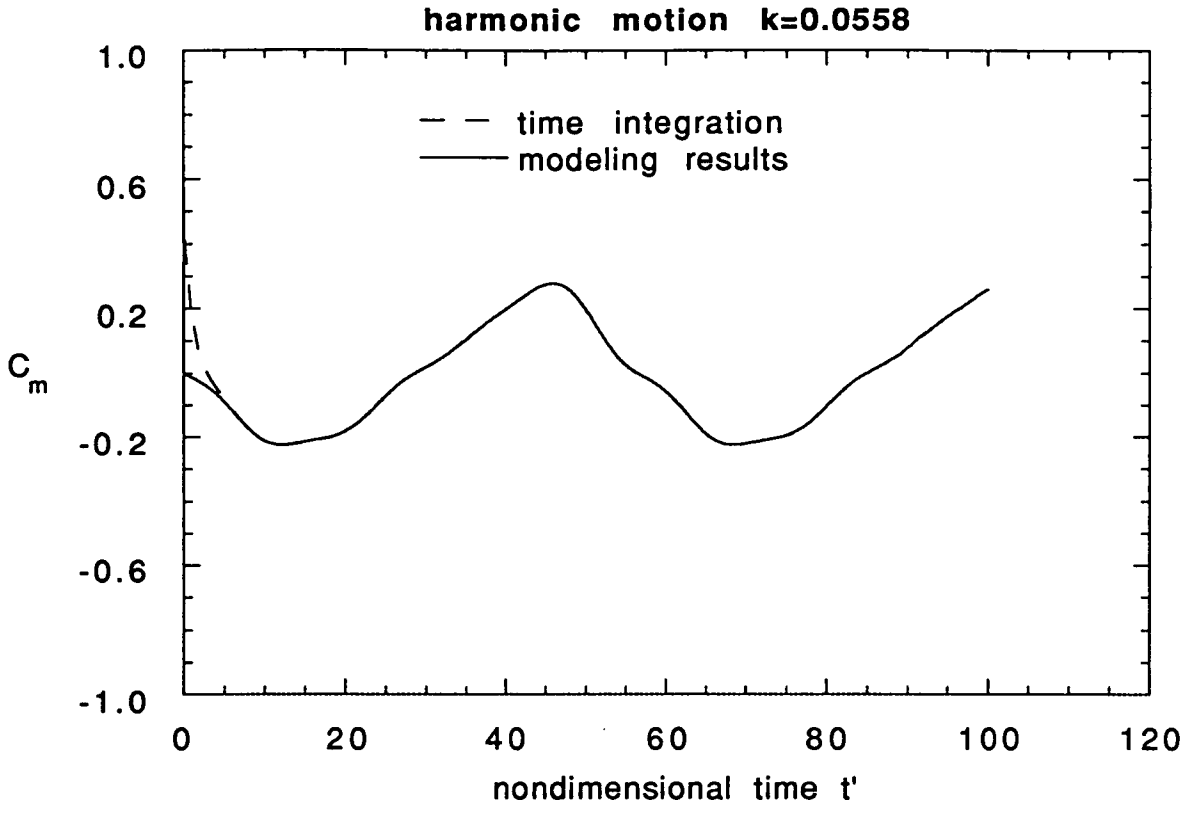

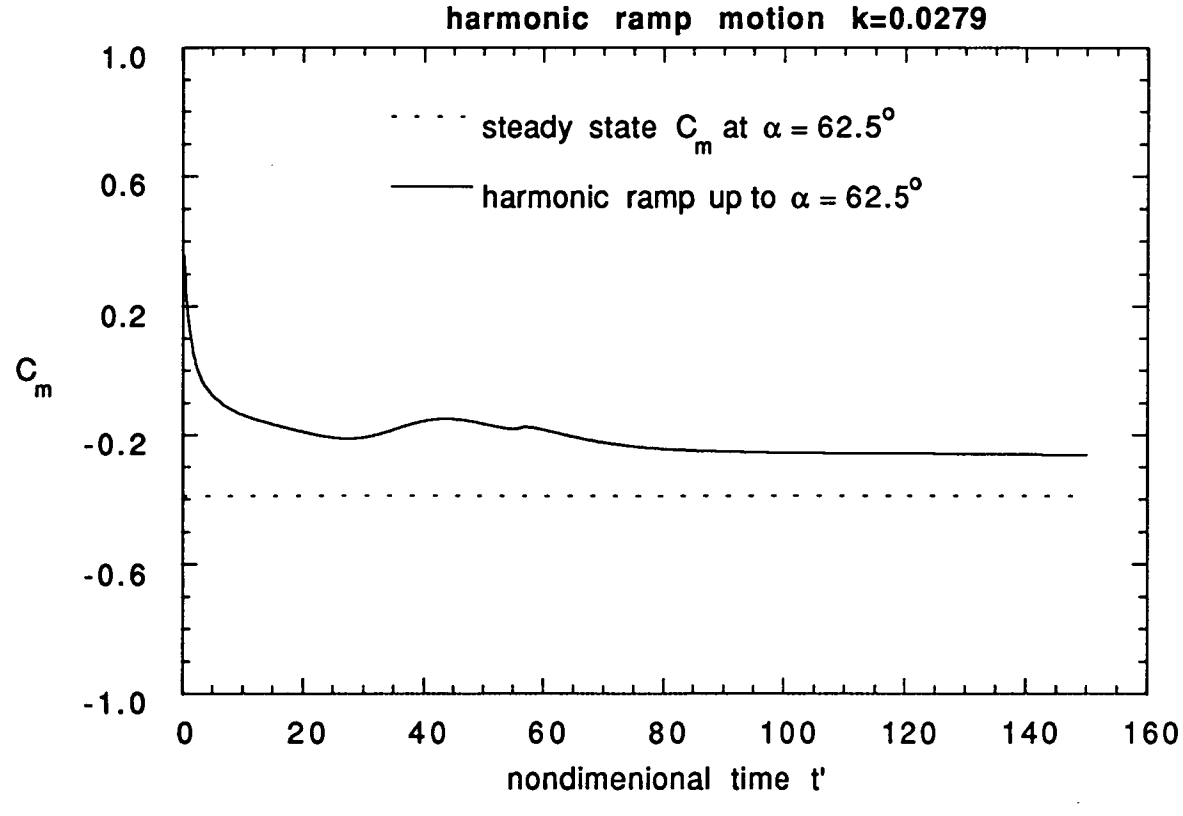

(c)Pitching Moment Data

Figure 4 Concluded

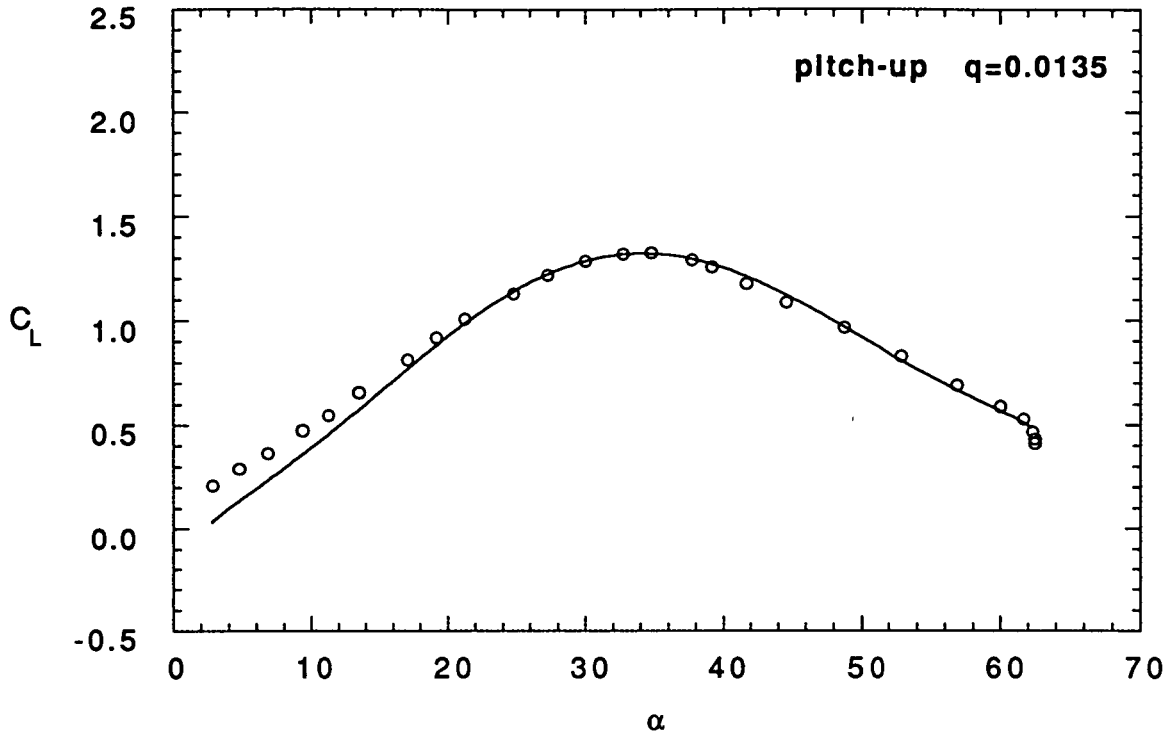

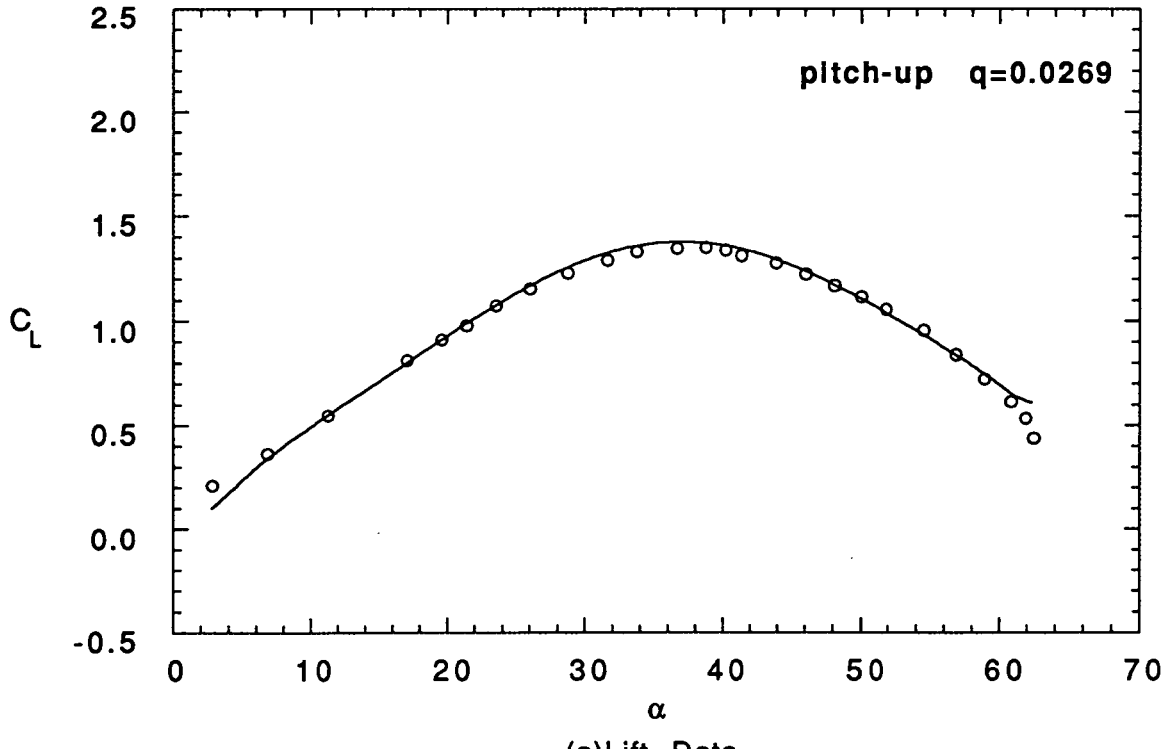

(a)Lift Data

Figure 5 Delta Wing Responses by Time Integration
for Constant Rate Pitching Motion

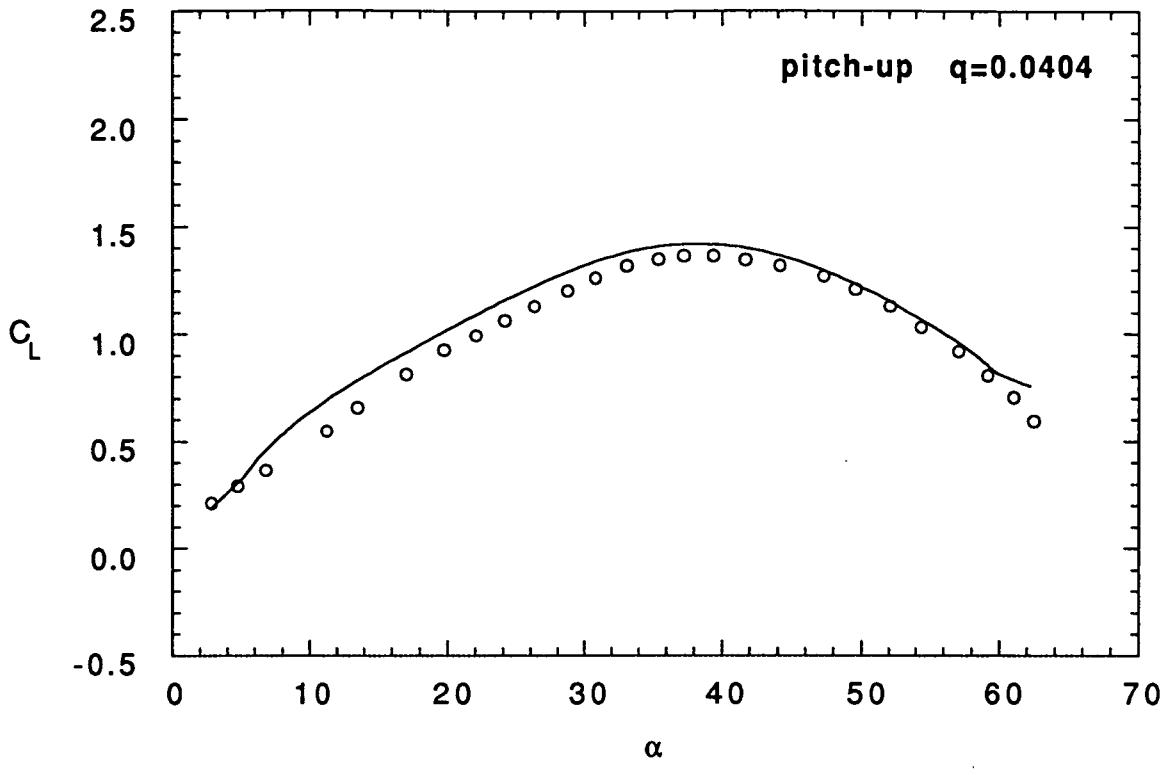

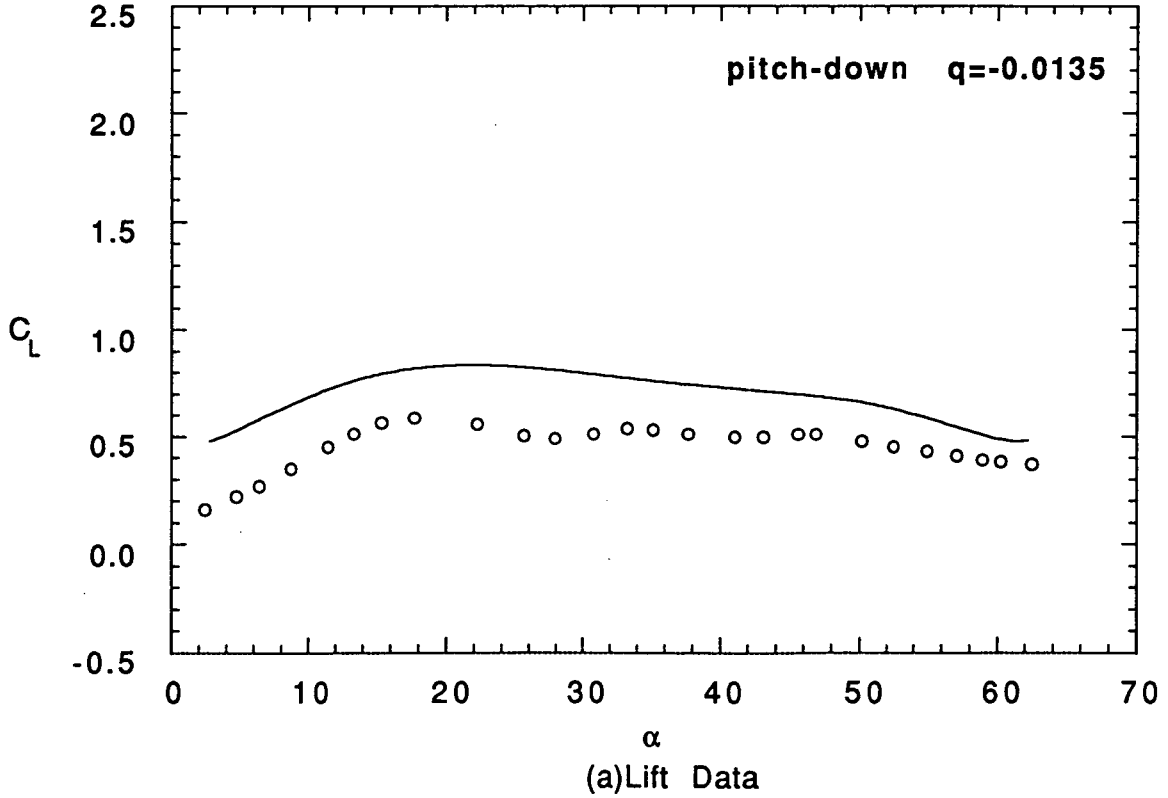

(a)Lift Data

Figure 5 Continued

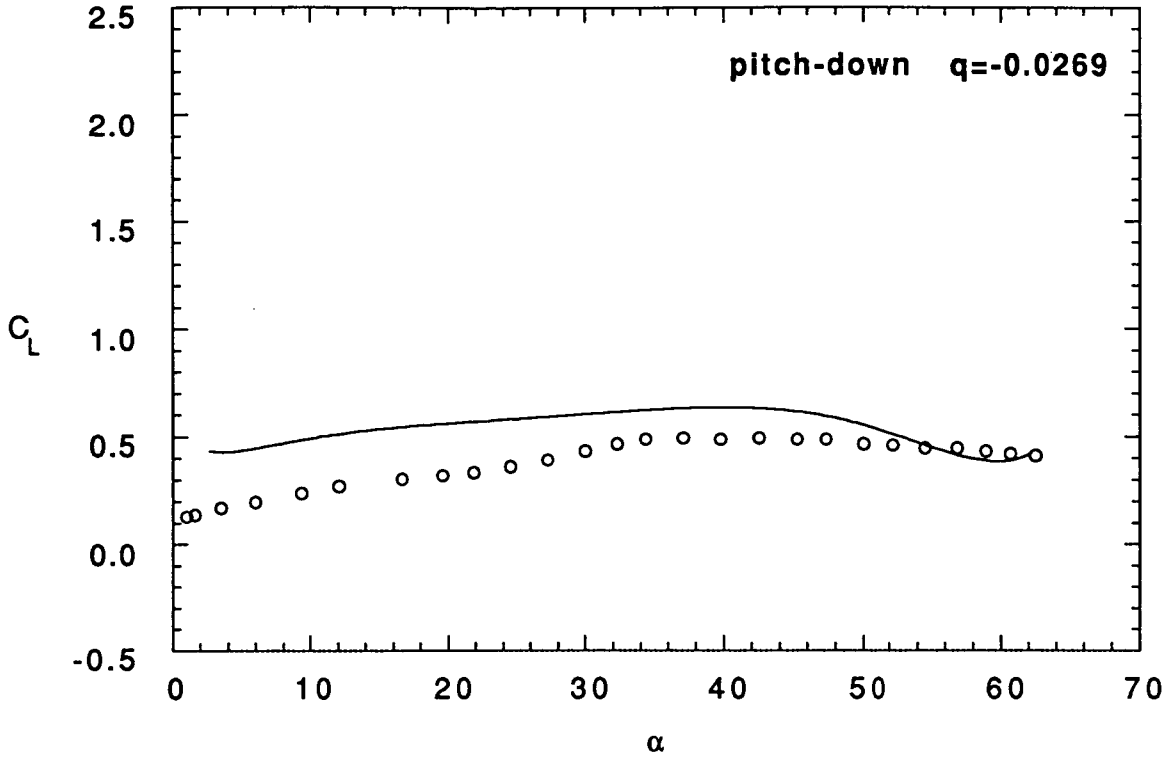

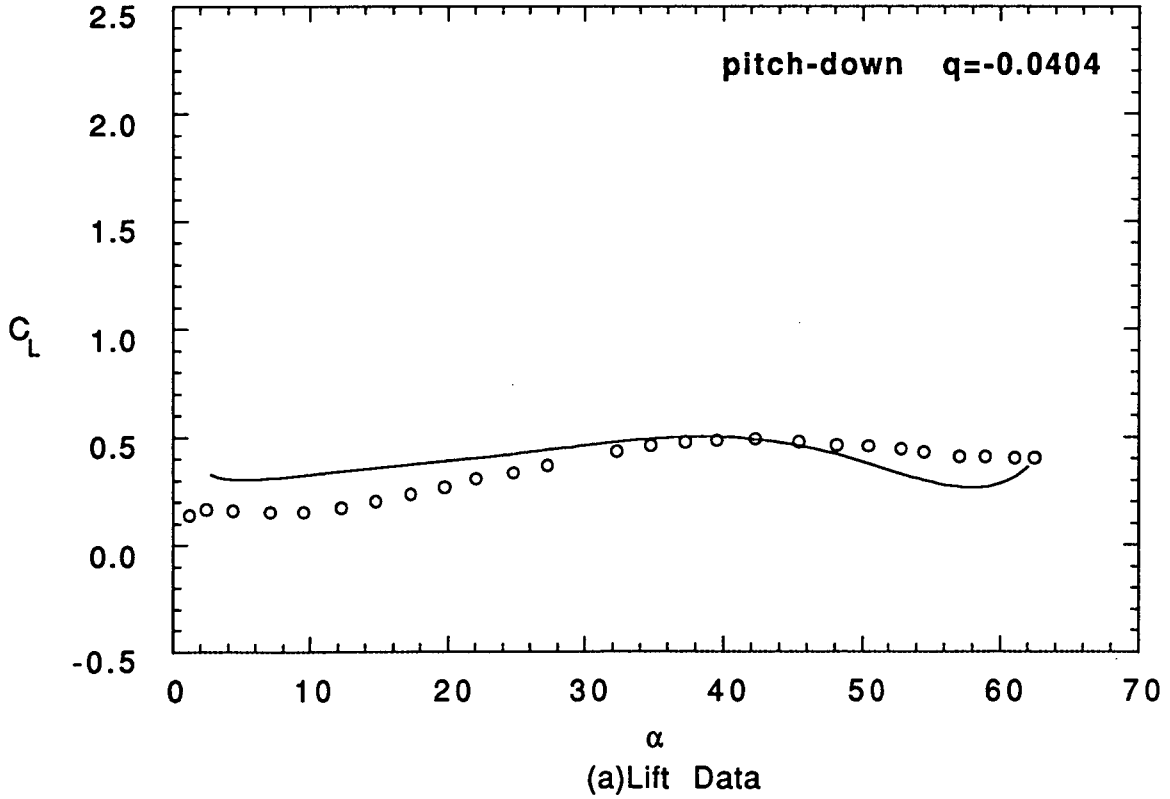

(a)Lift Data

Figure 5 Continued

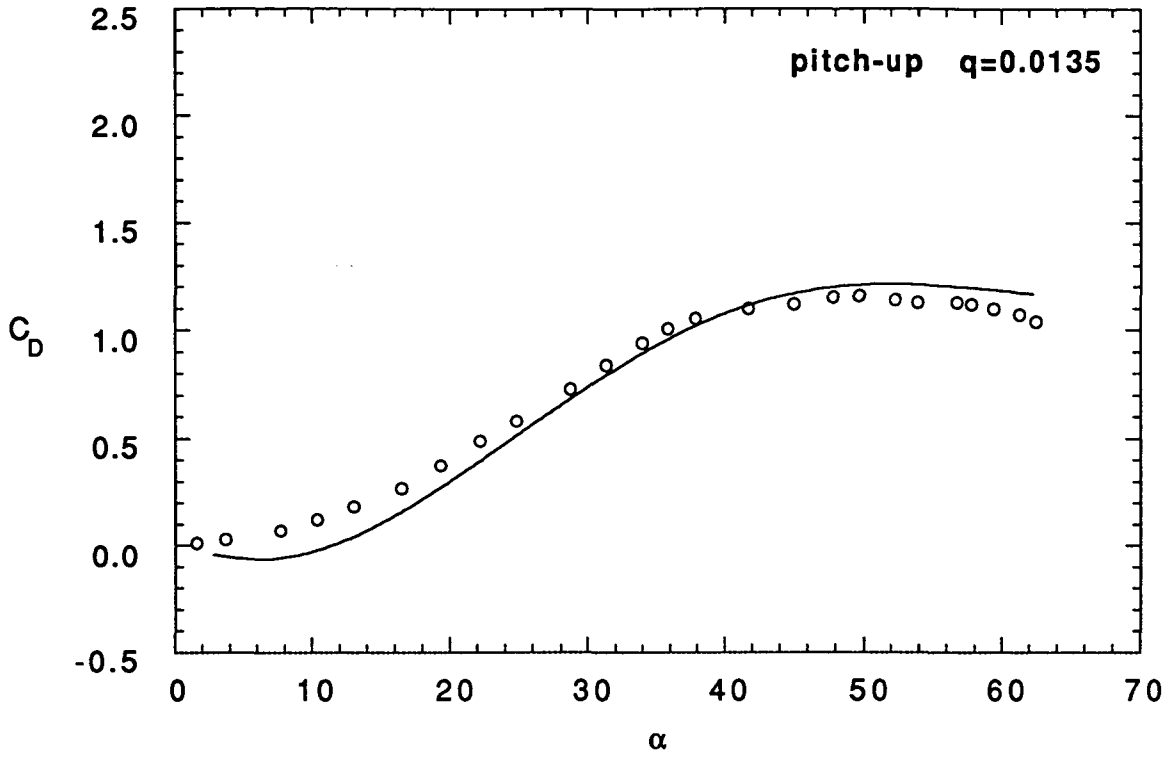

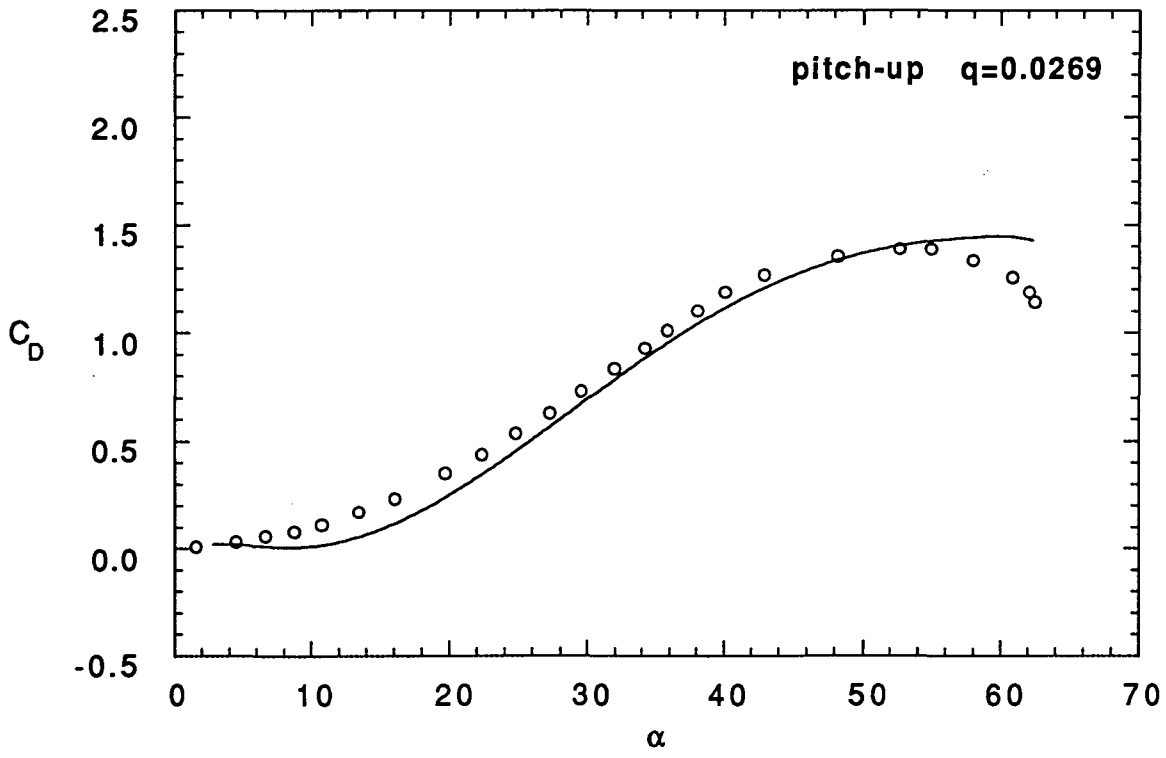

(b)Drag Data

Figure 5 Continued

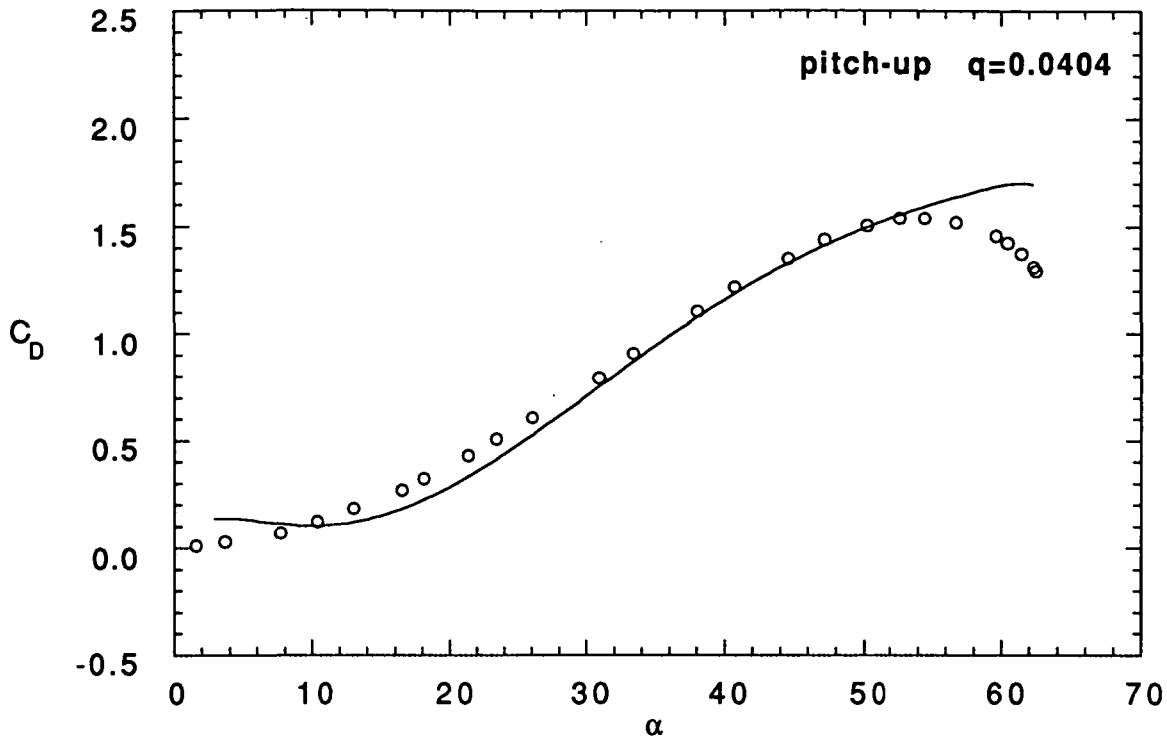

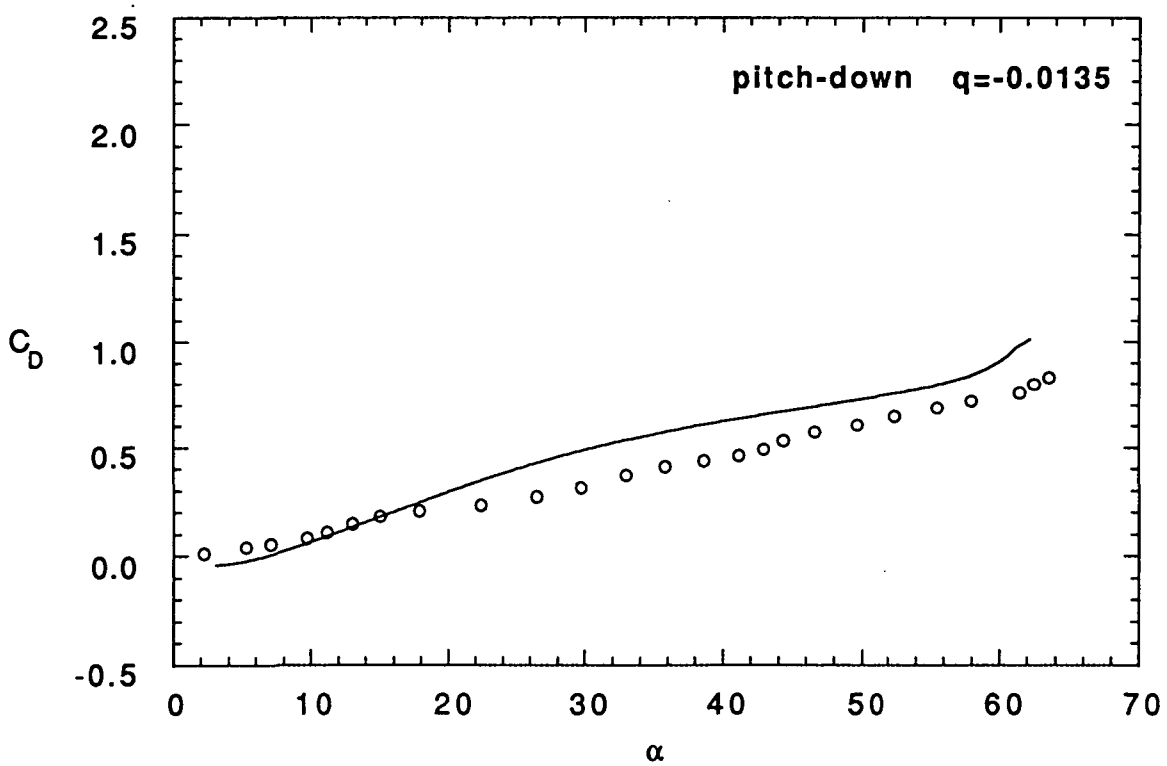

(b)Drag Data

Figure 5 Continued

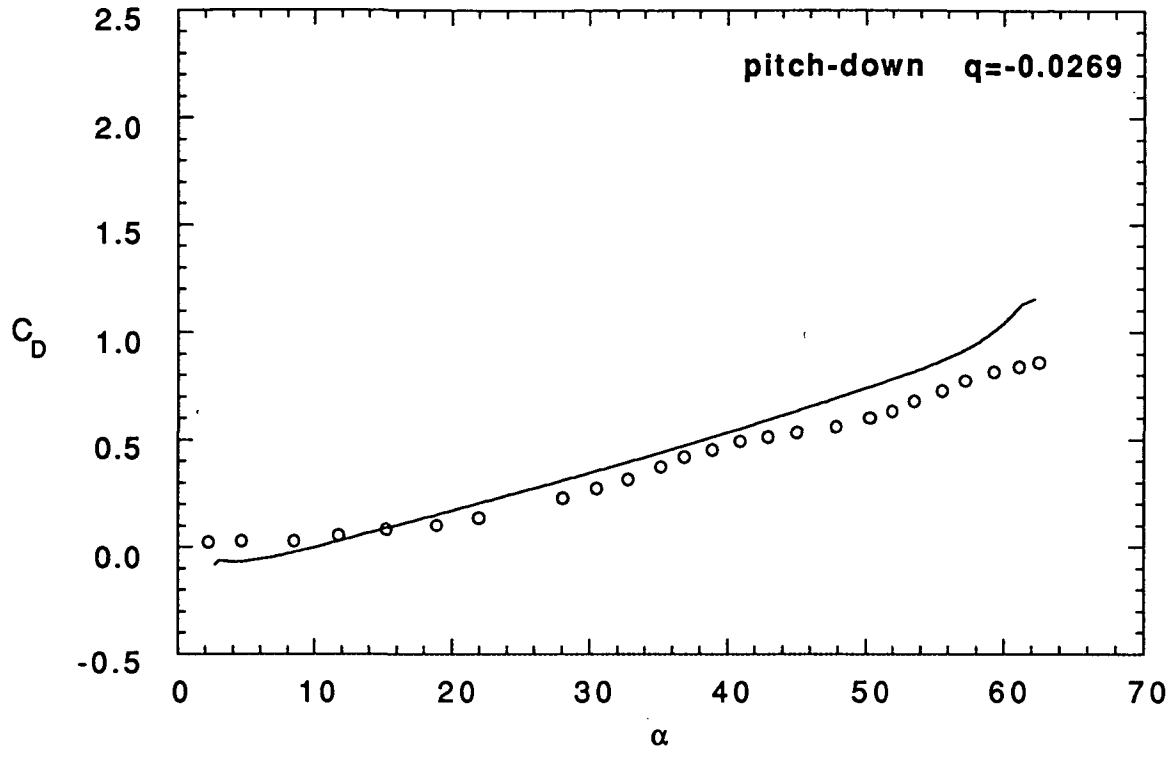

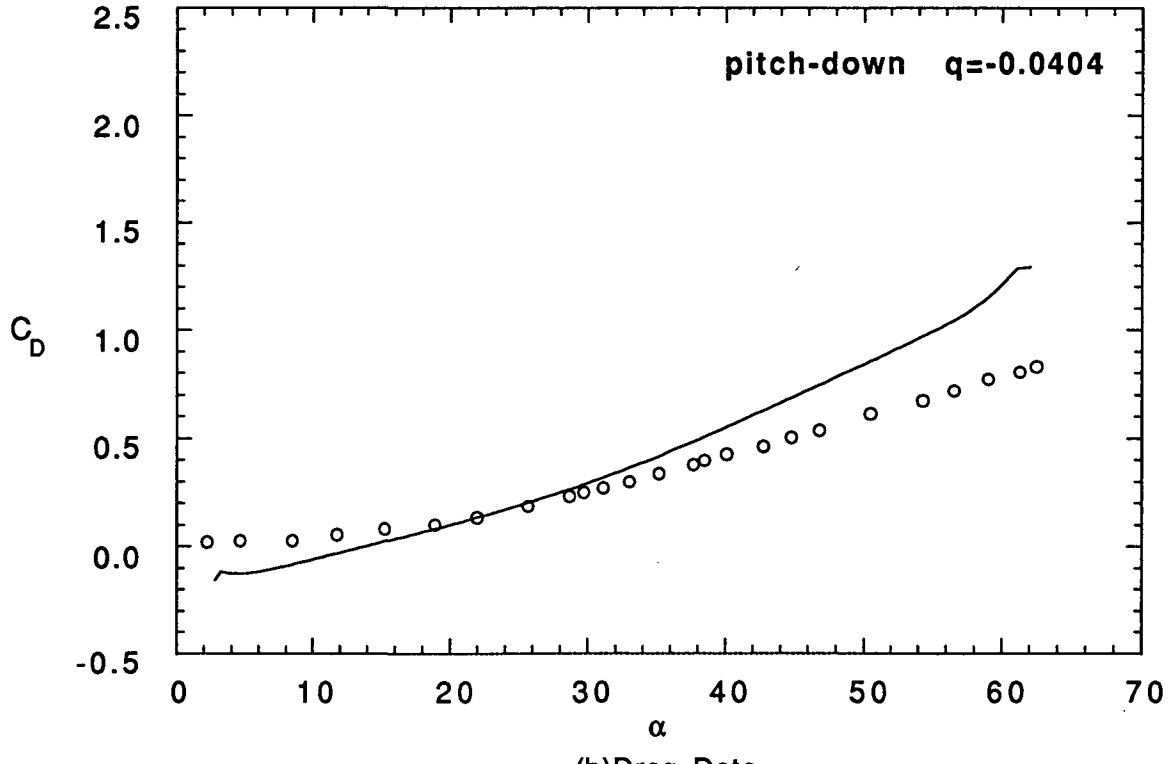

(b)Drag Data

Figure 5 Continued

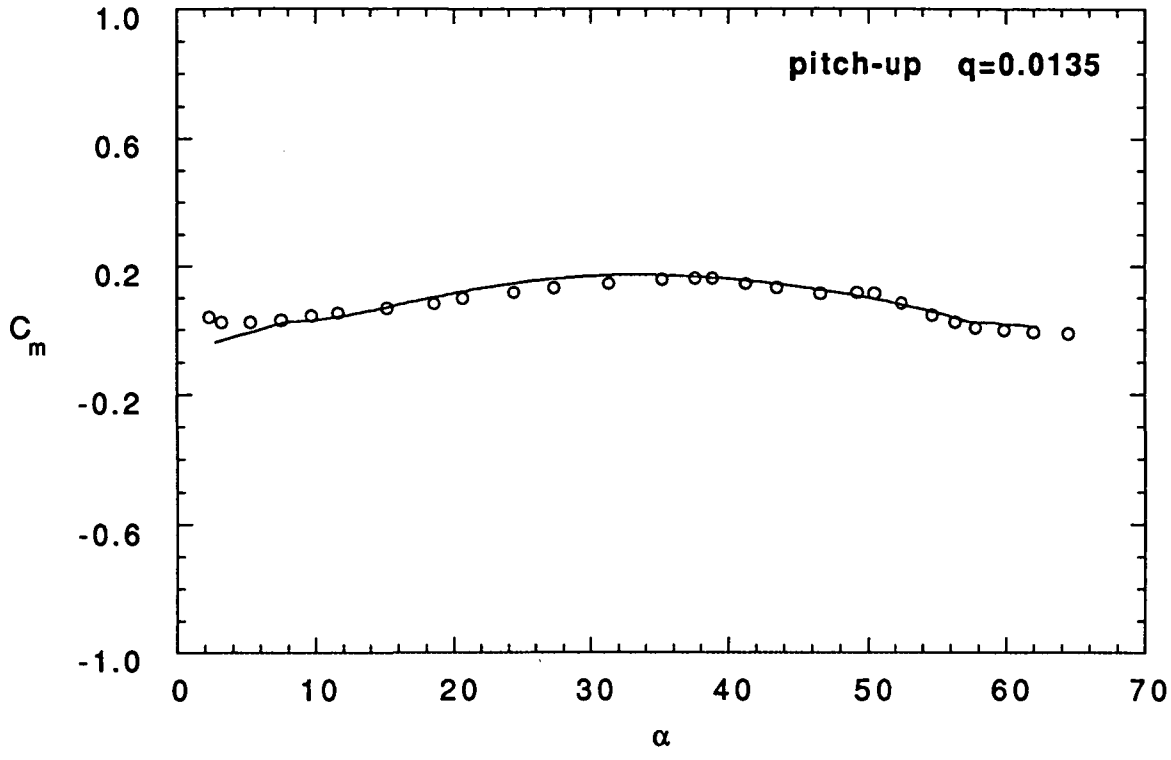

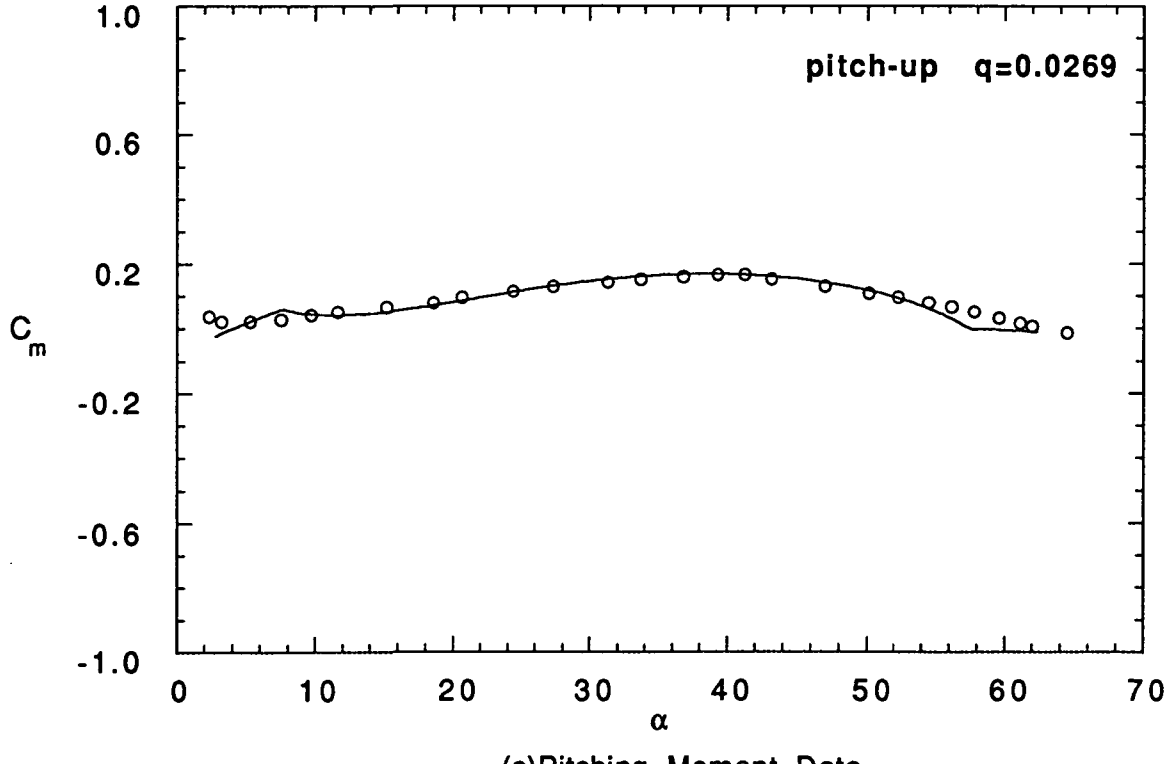

(c)Pitching Moment Data

Figure 5 Continued

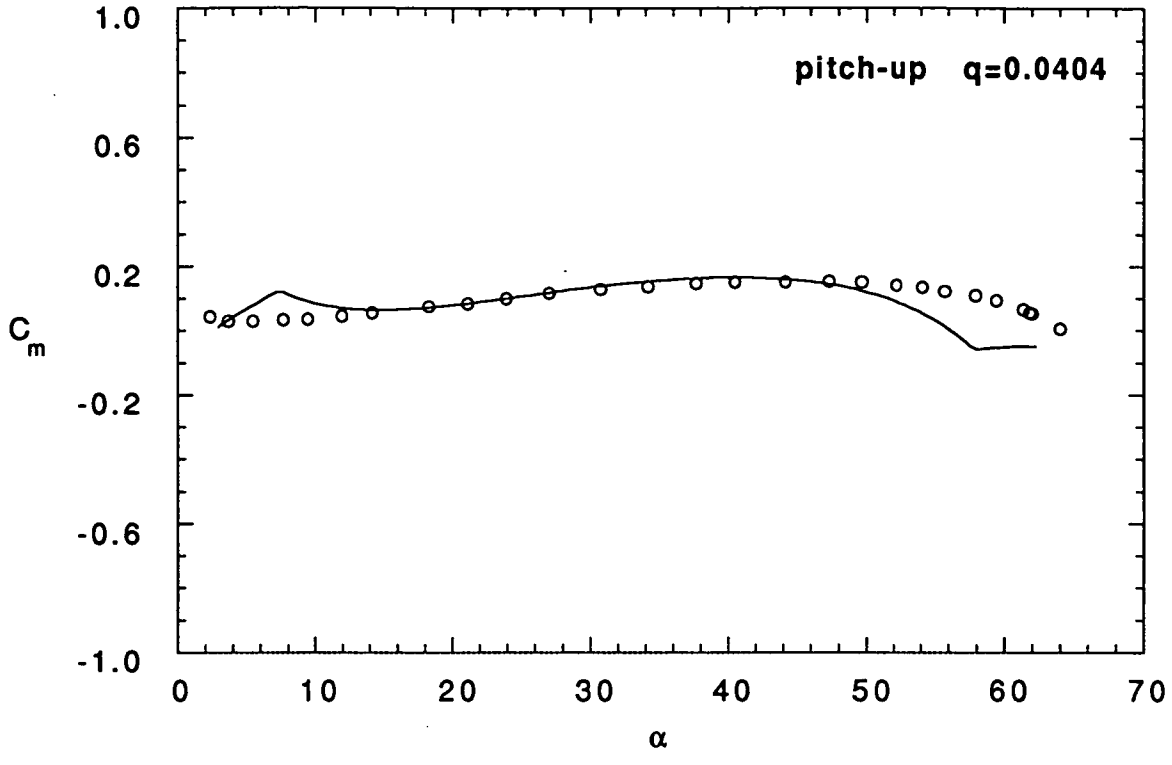

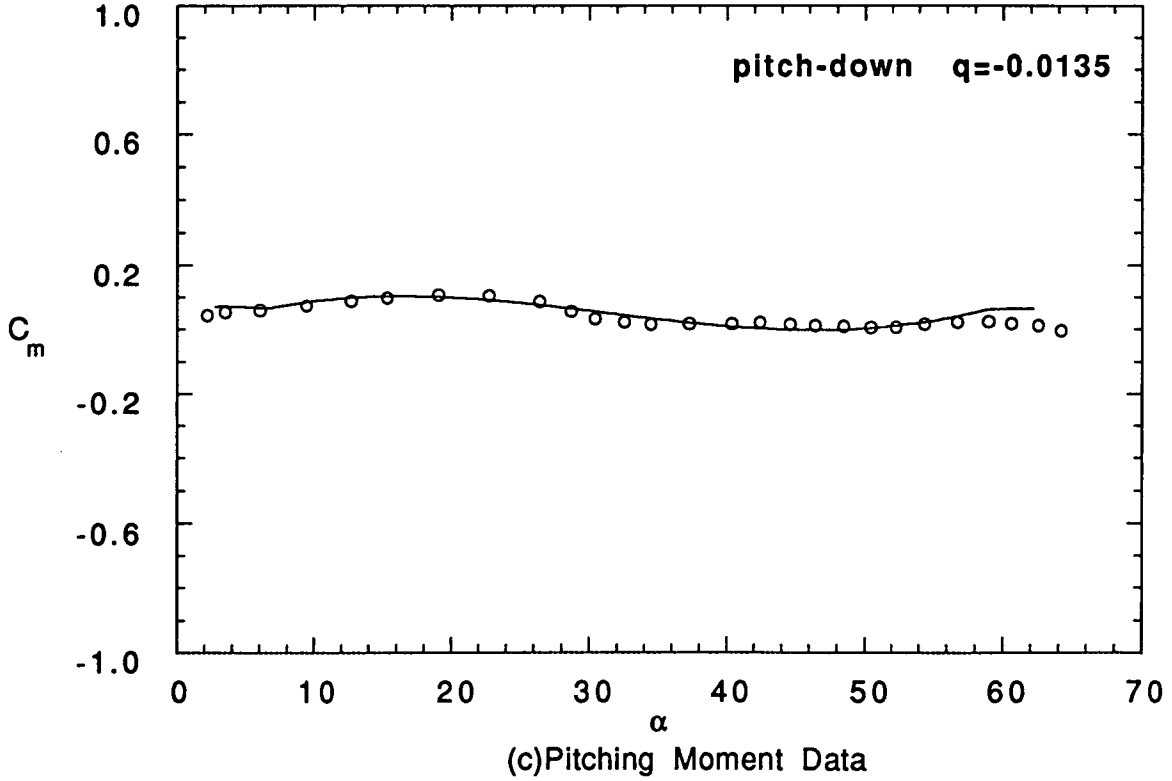

(c)Pitching Moment Data

Figure 5 Continued

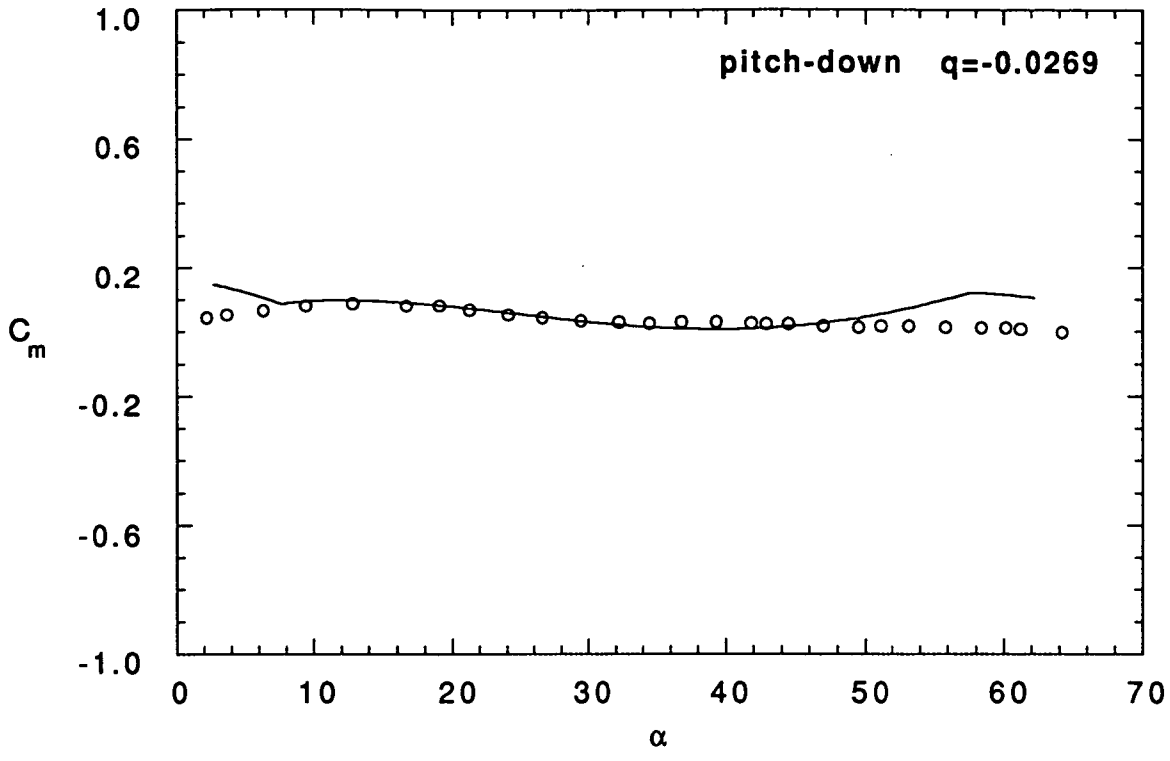

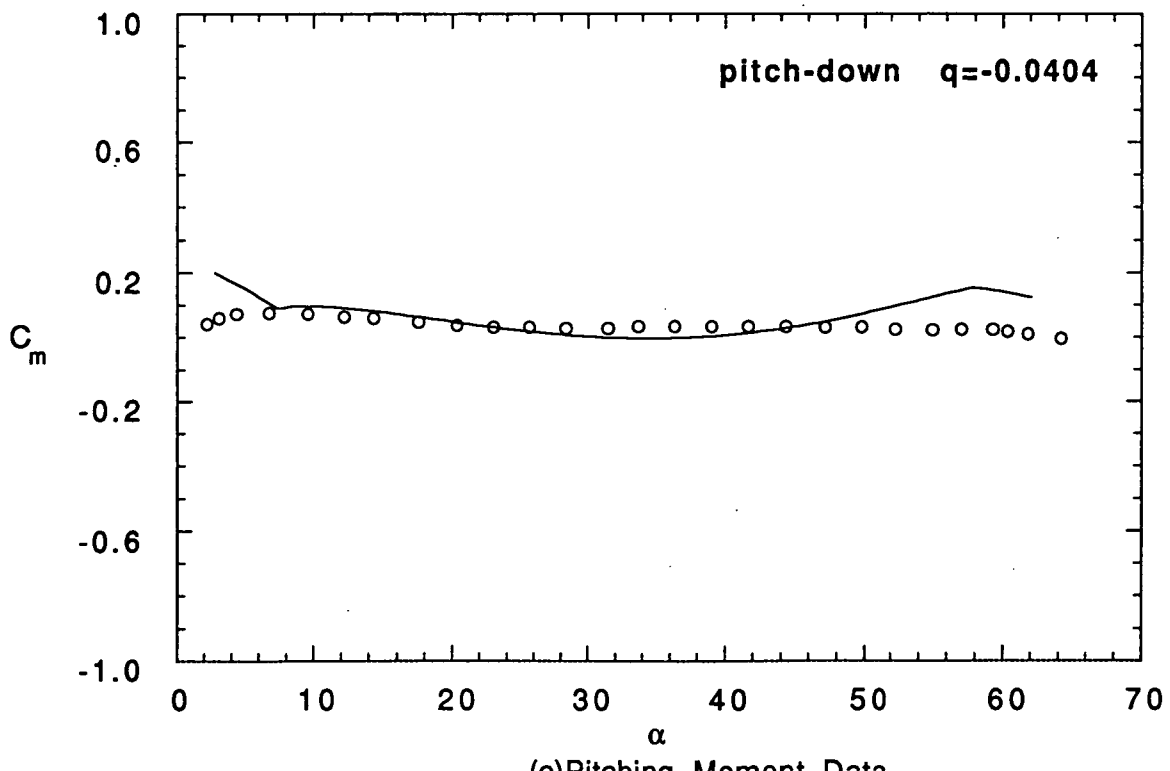

(c)Pitching Moment Data

Figure 5 Concluded

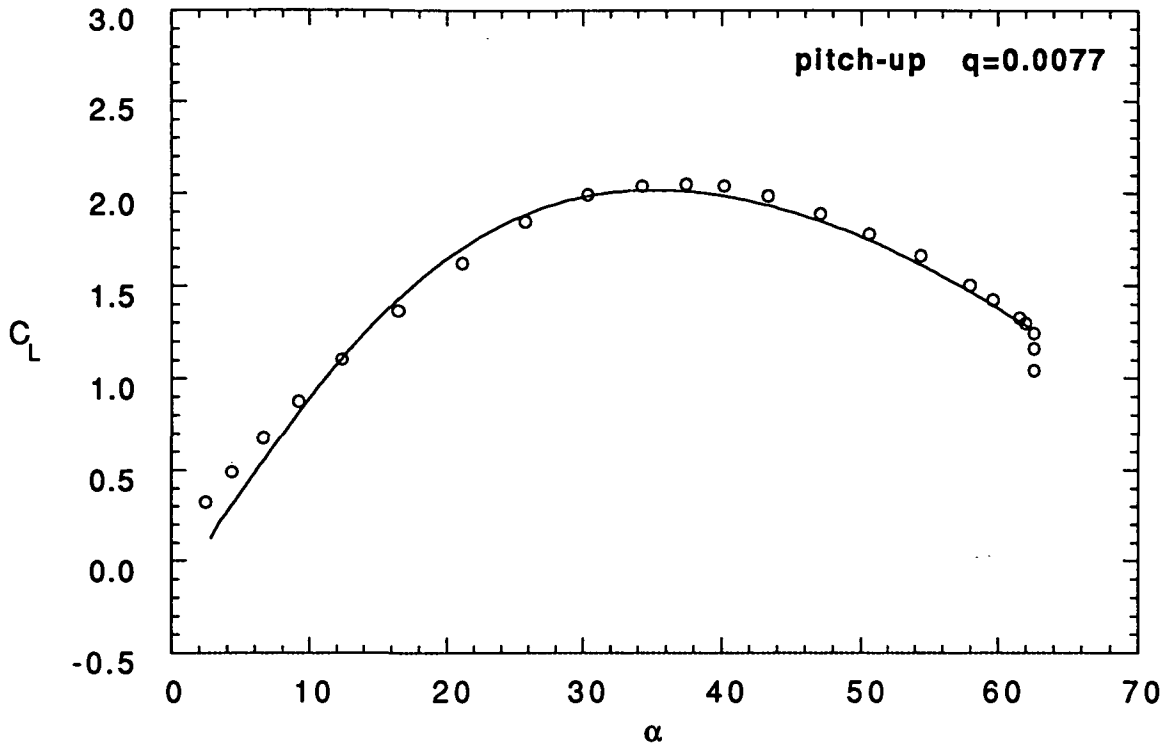

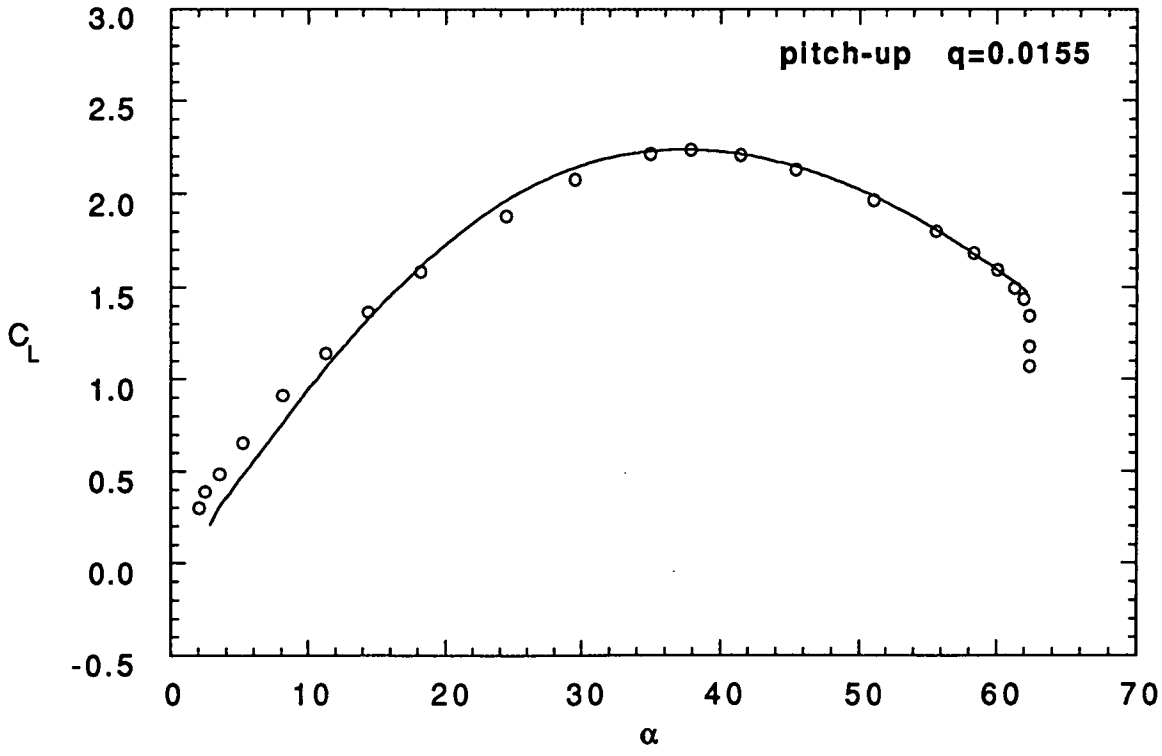

(a)Lift Data

Figure 6 F-18 Responses by Time Integration for Constant Rate Pitching Motion

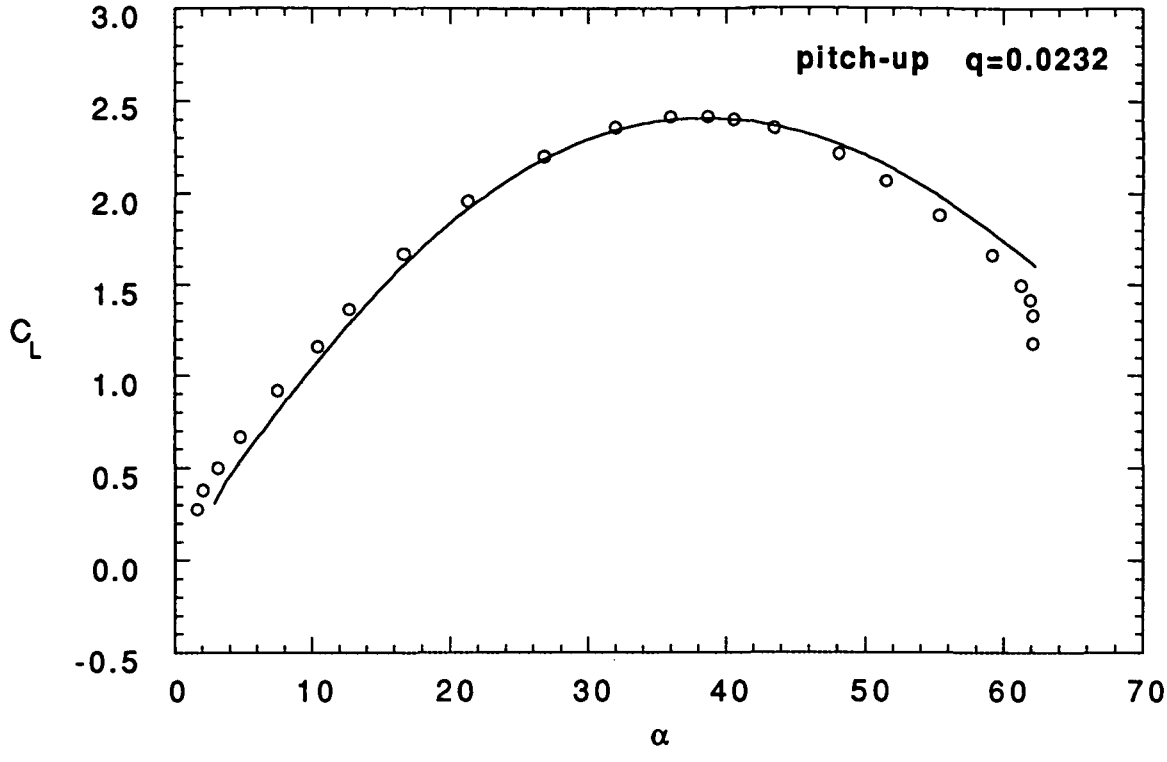

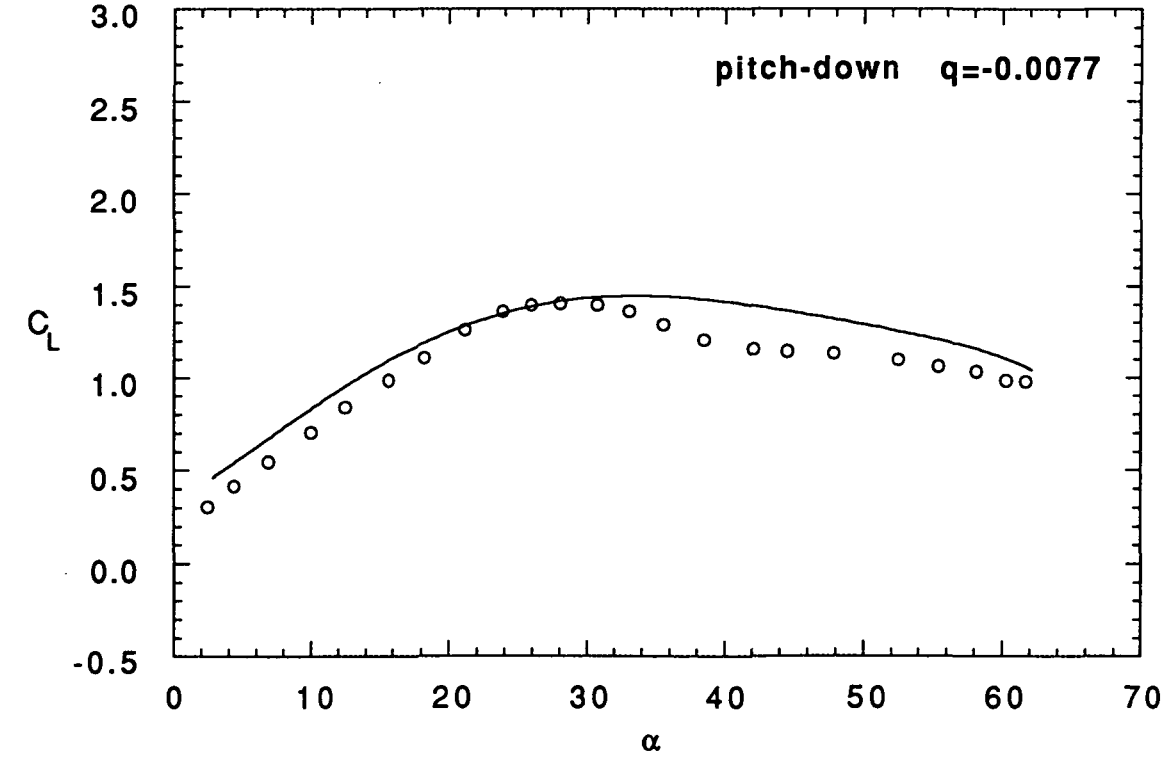

(a)Lift Data

Figure 6 Continued

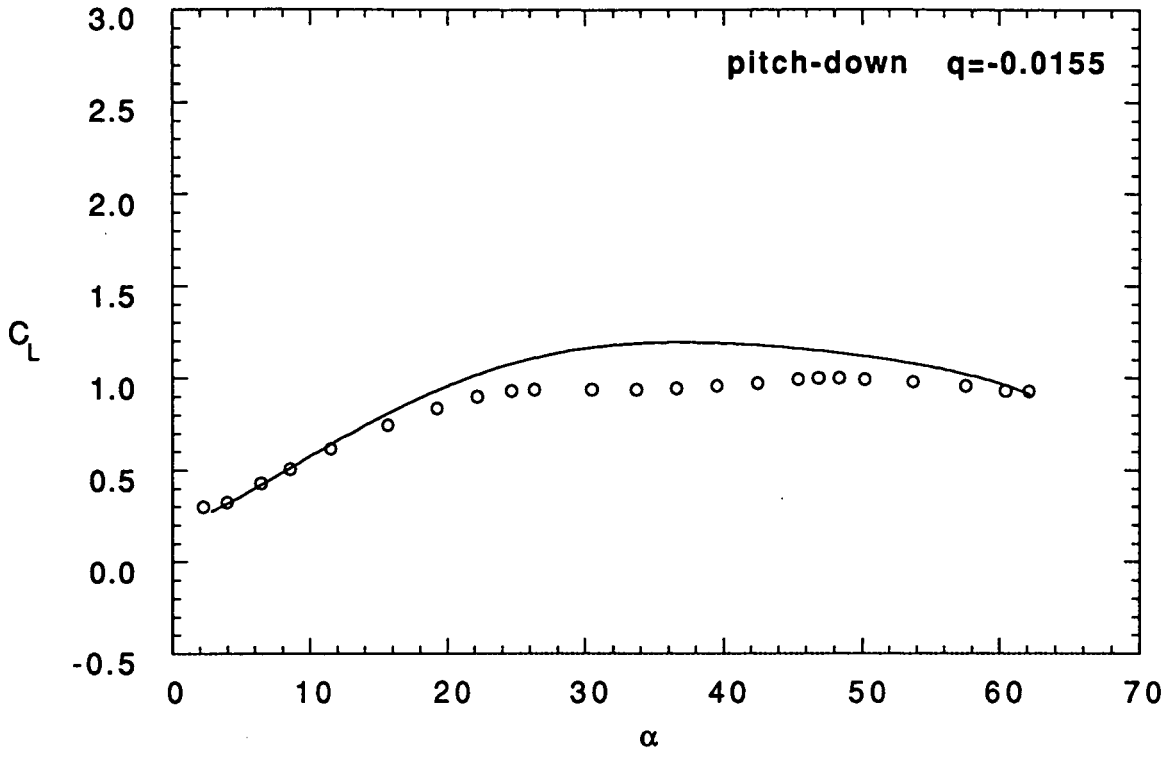

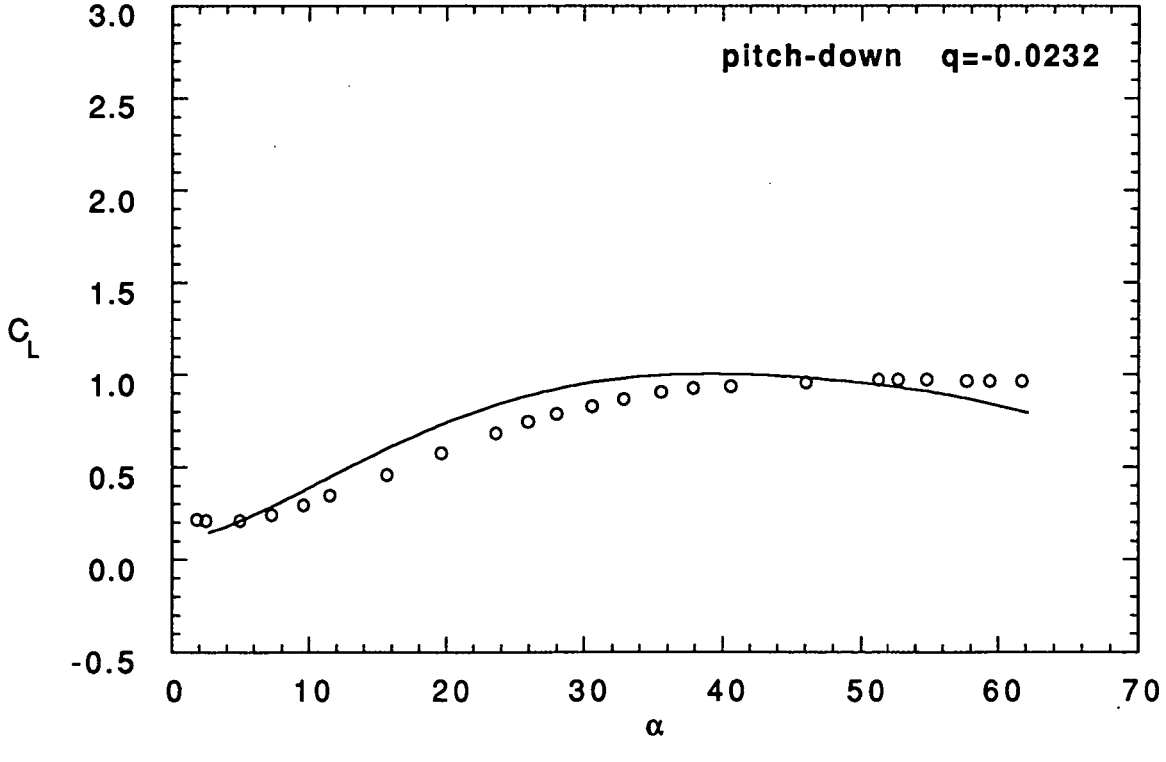

(a)Lift Data

Figure 6 Continued

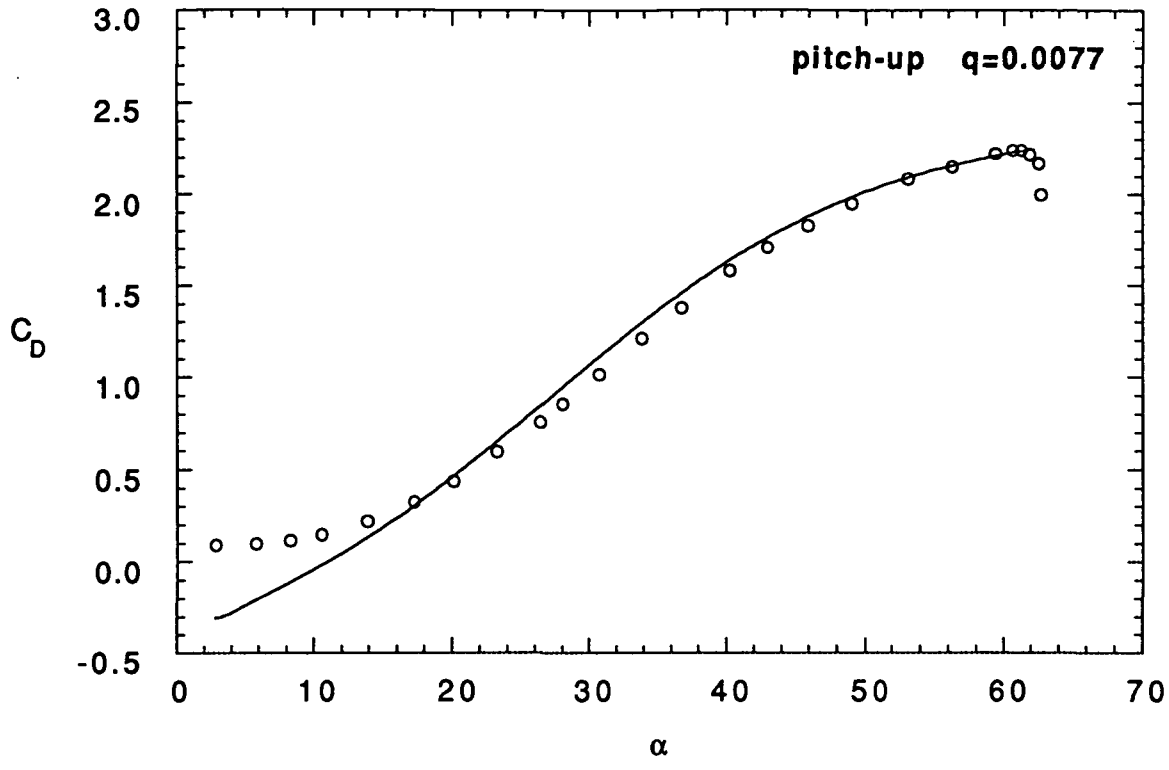

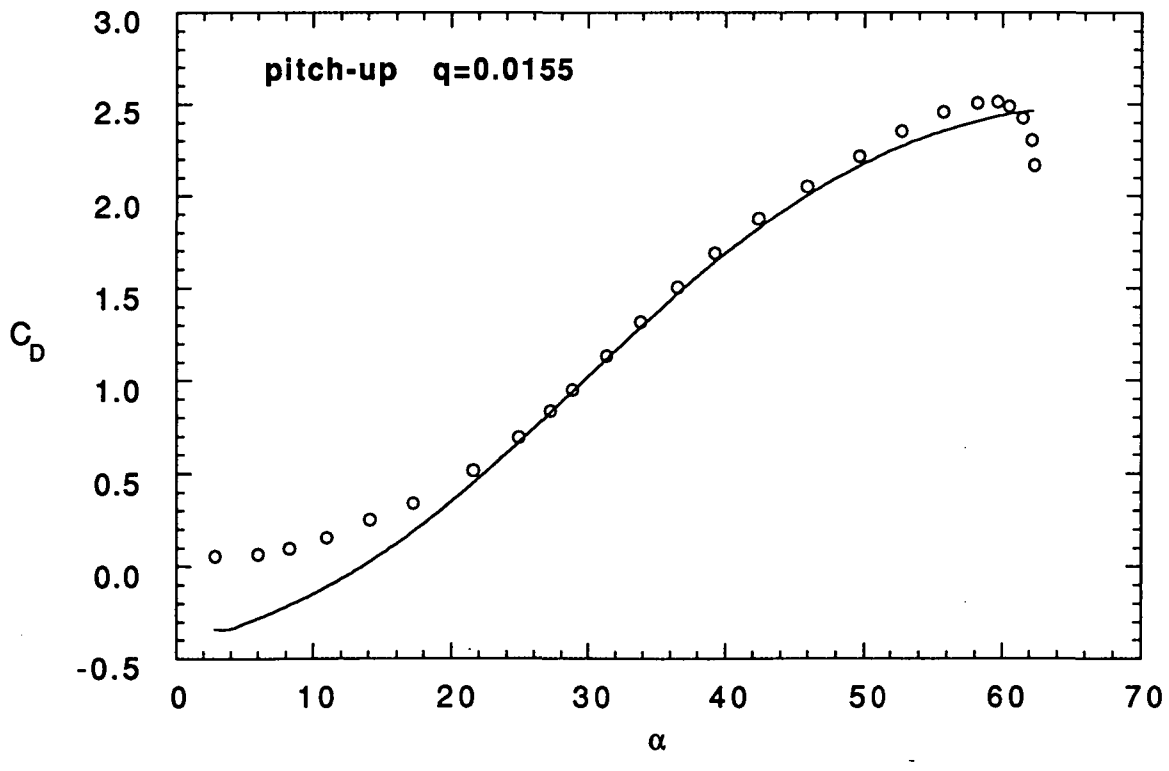

(b)Drag Data

Figure 6 Continued

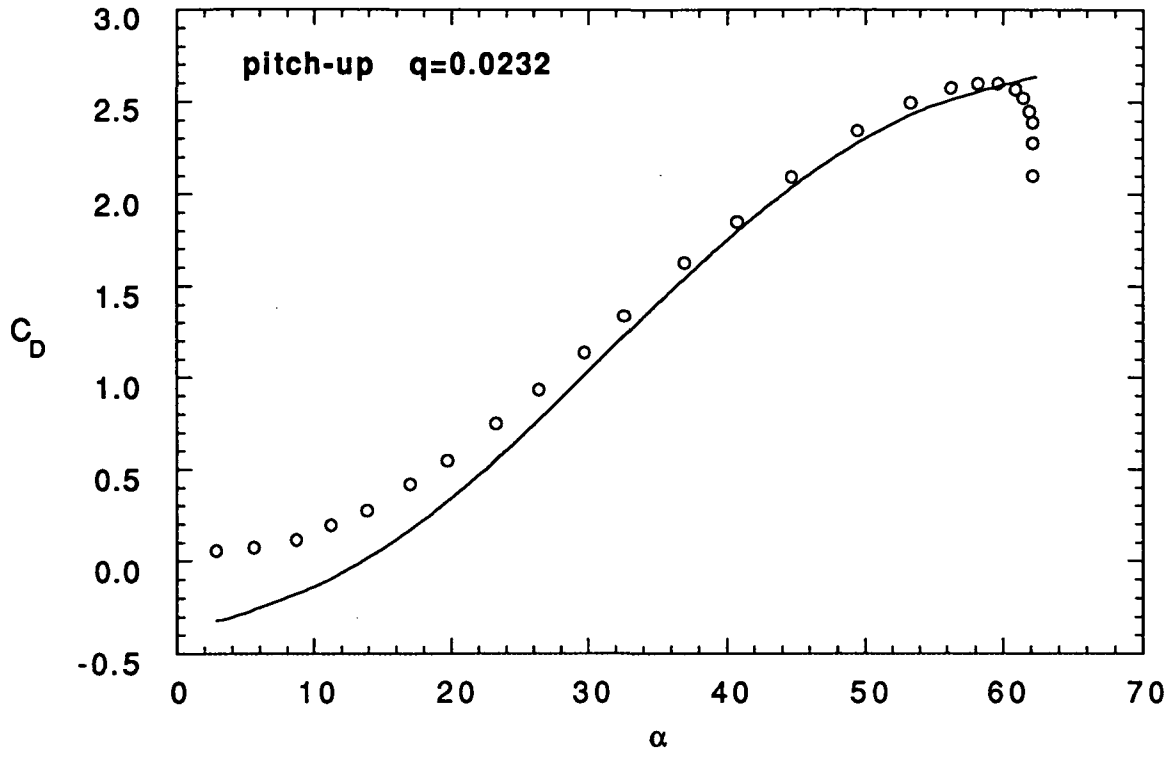

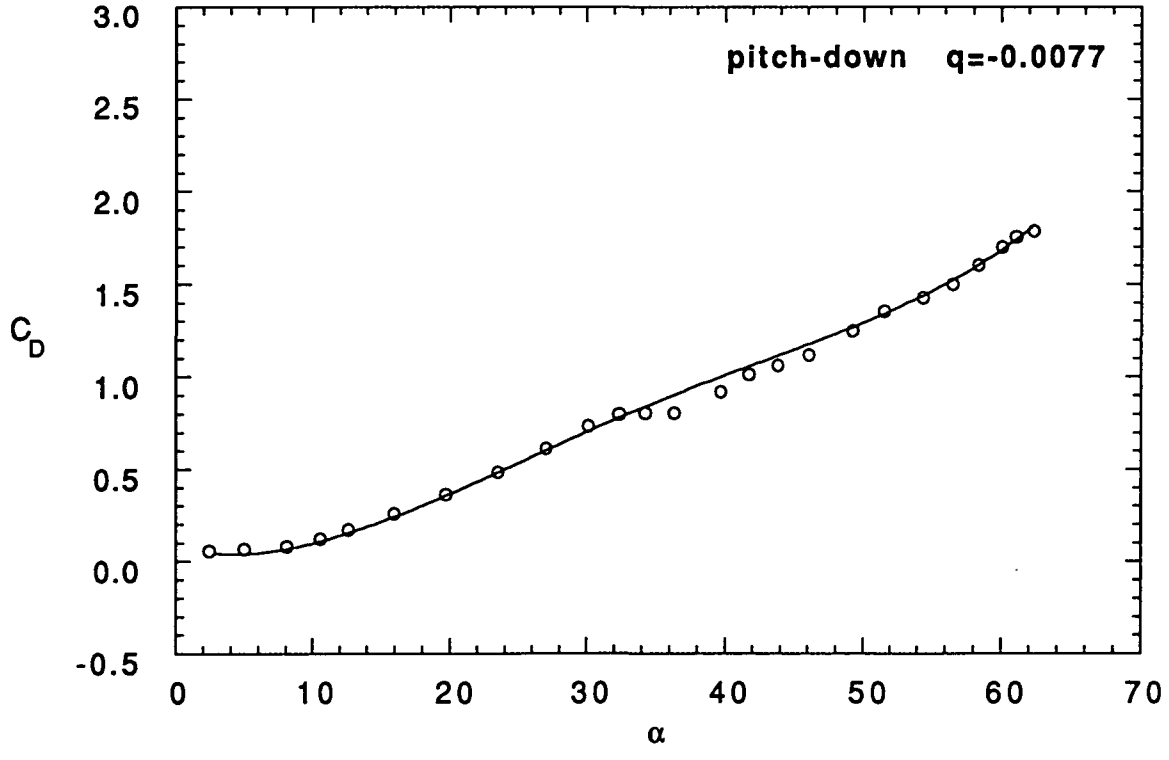

(b)Drag Data

Figure 6 Continued

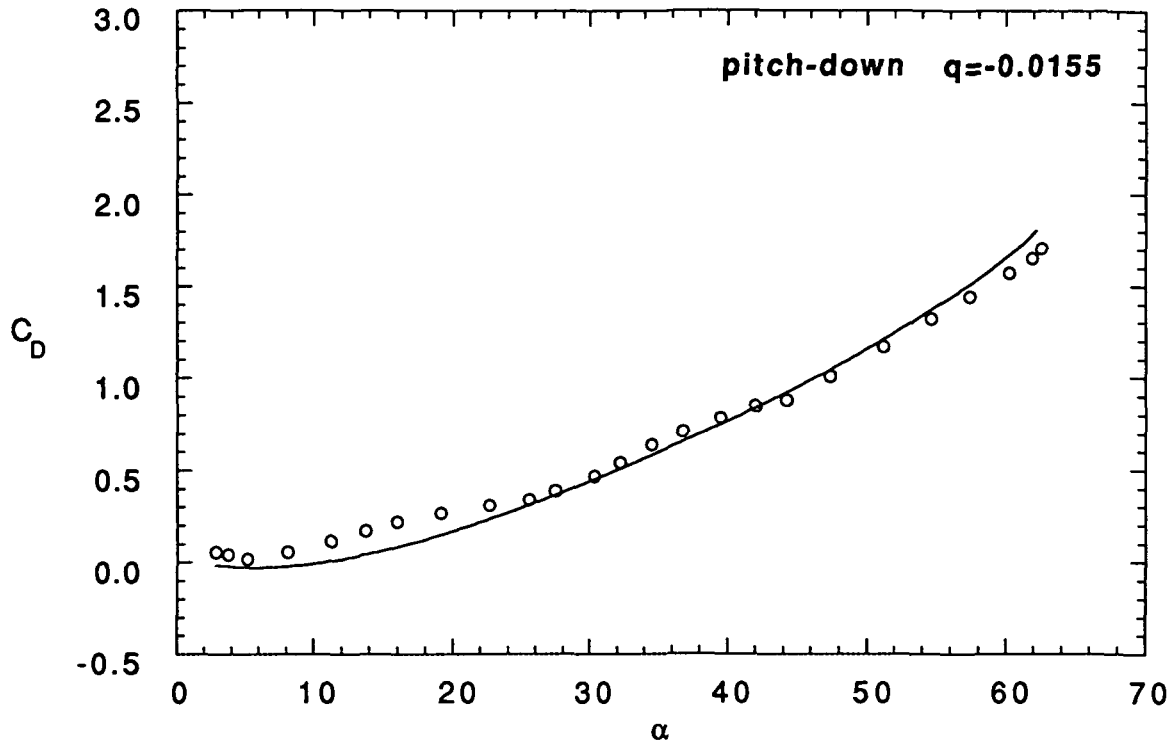

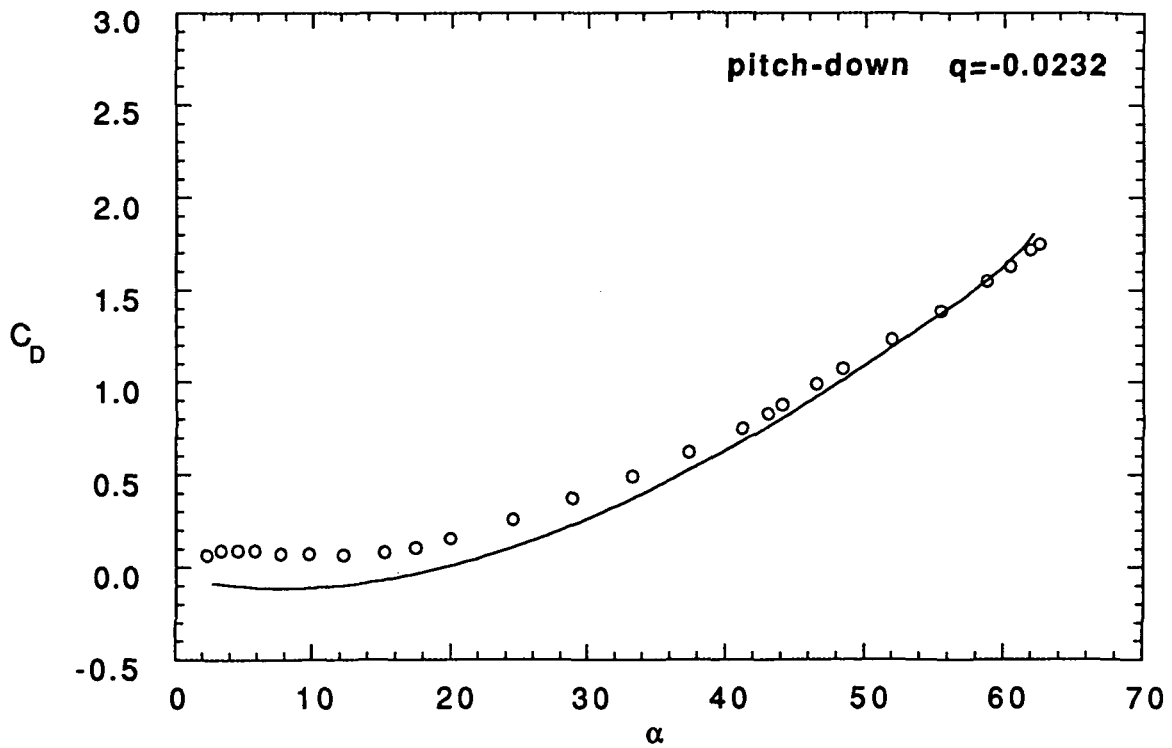

(b)Drag Data

Figure 6 Continued

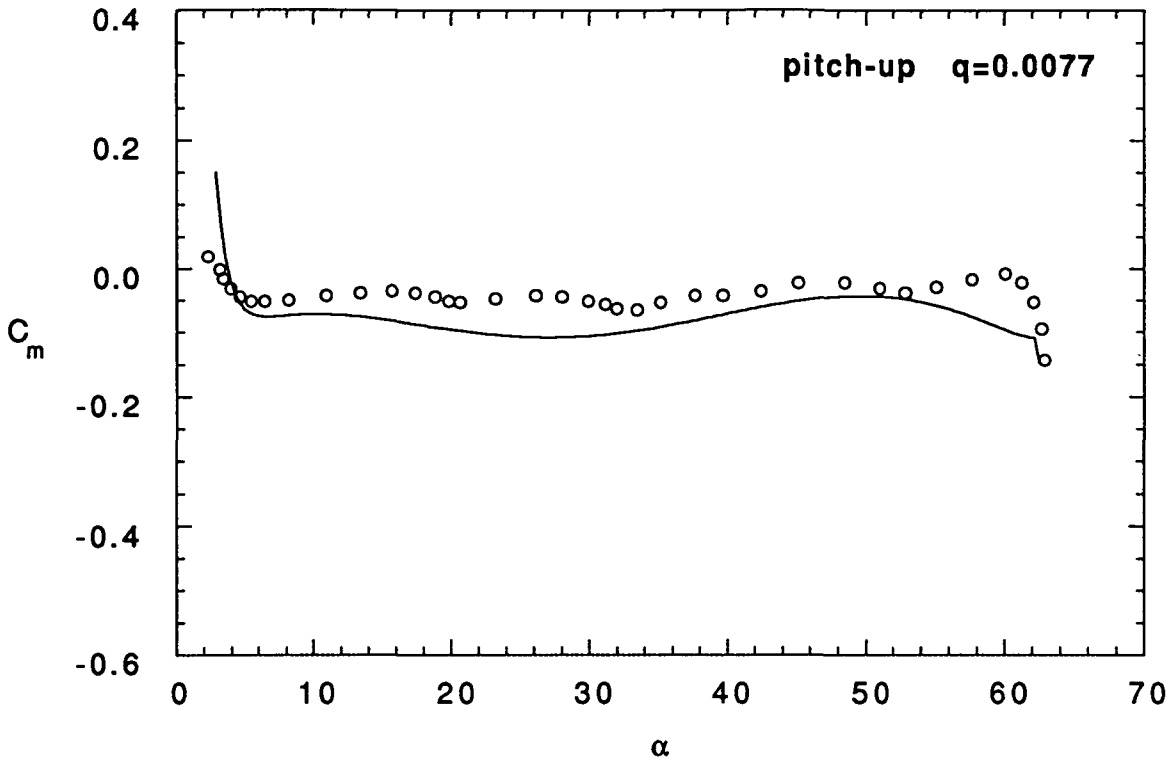

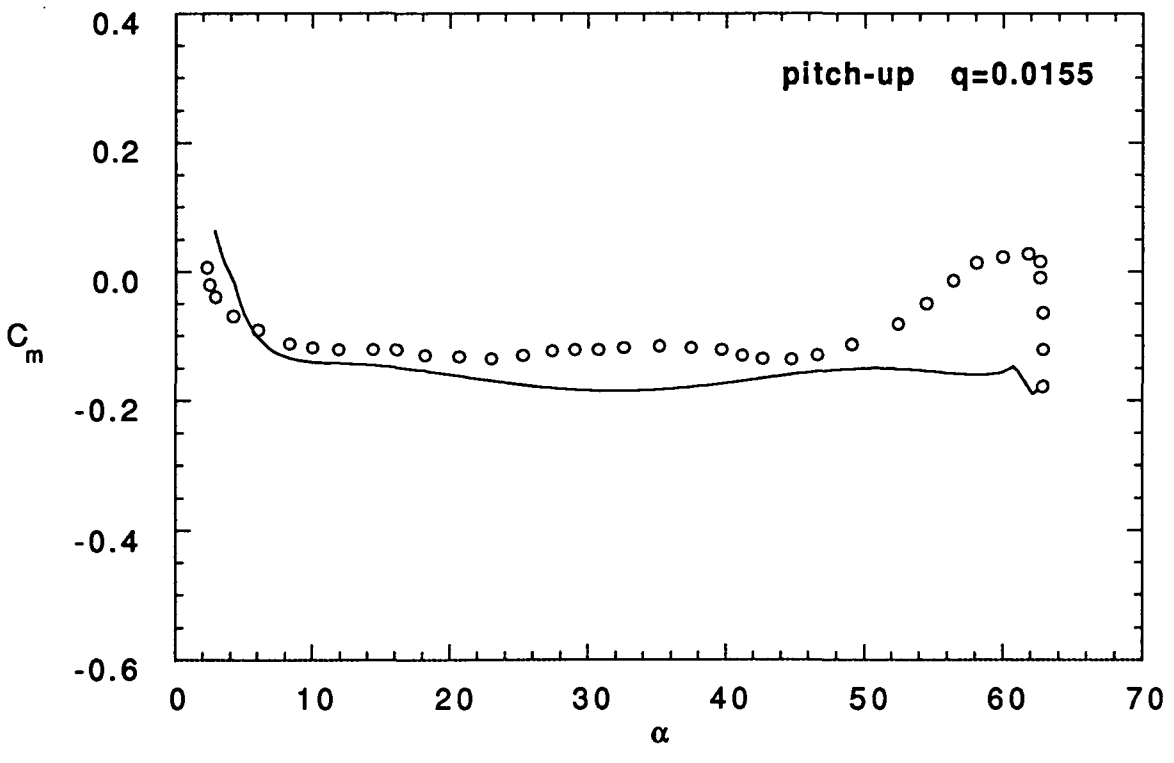

(c)Pitching Moment Data

Figure 6 Continued

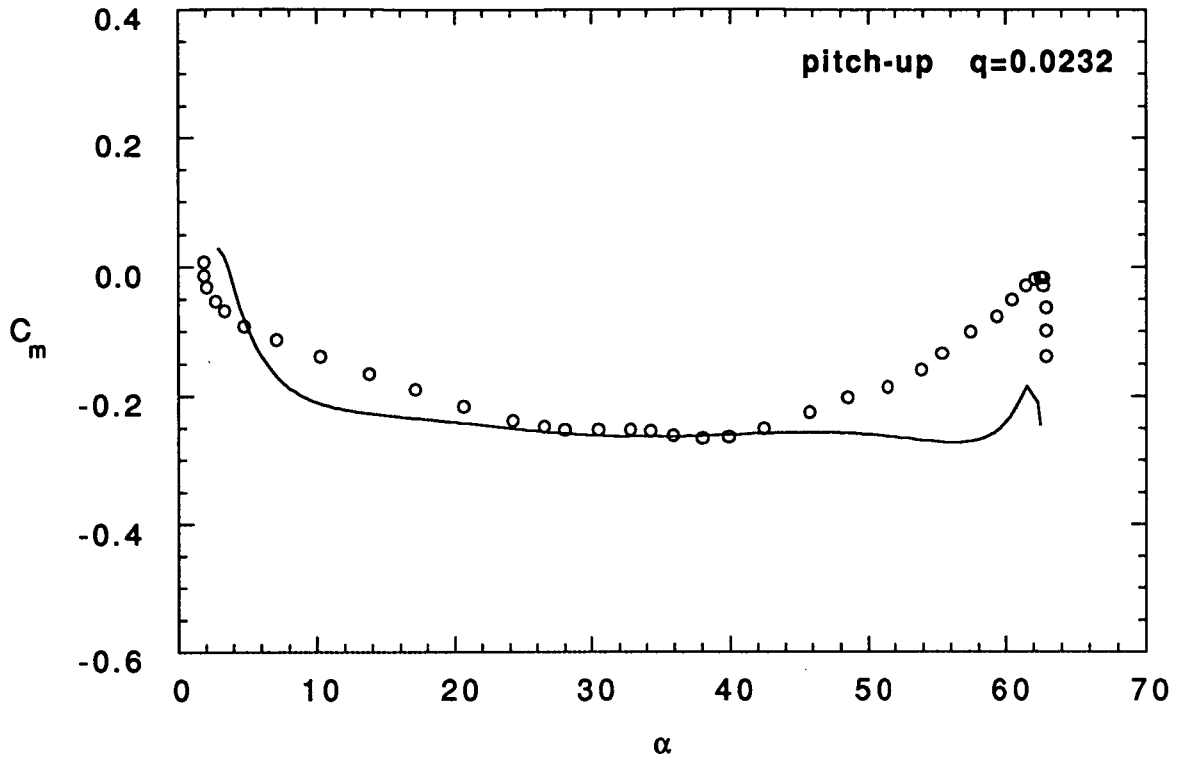

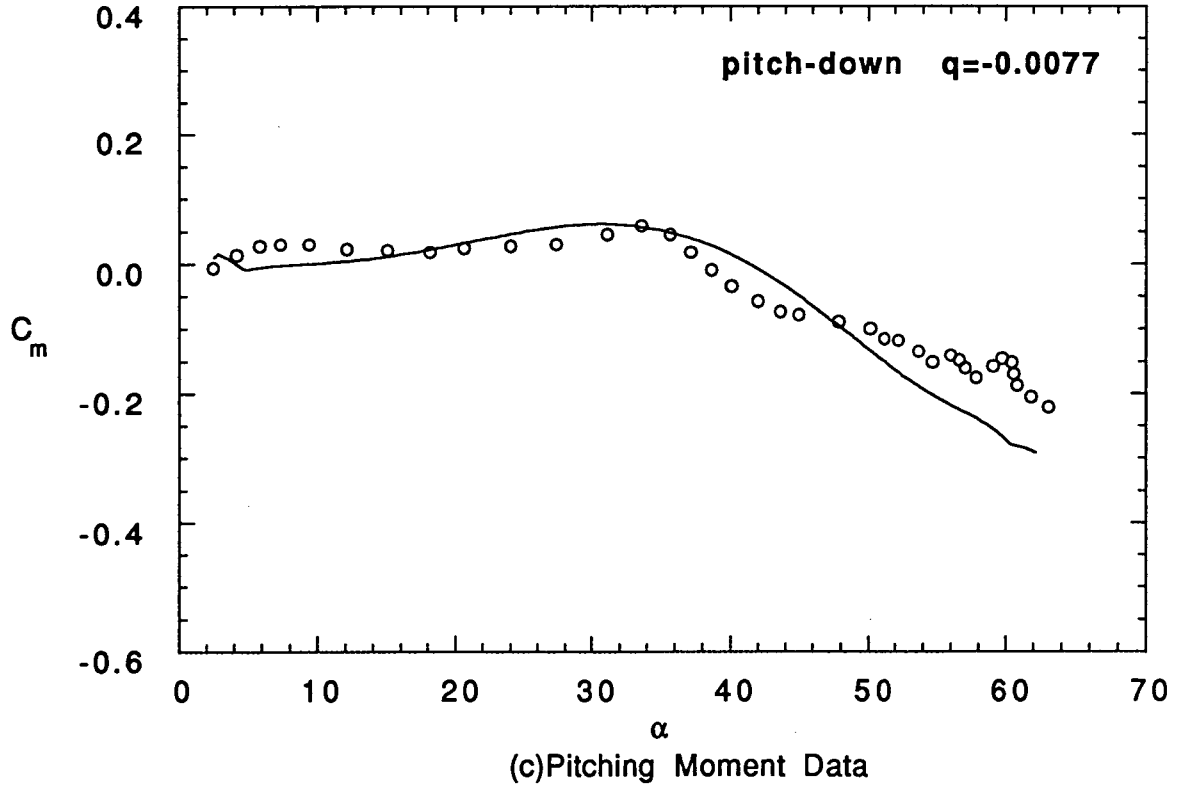

(c)Pitching Moment Data

Figure 6 Continued

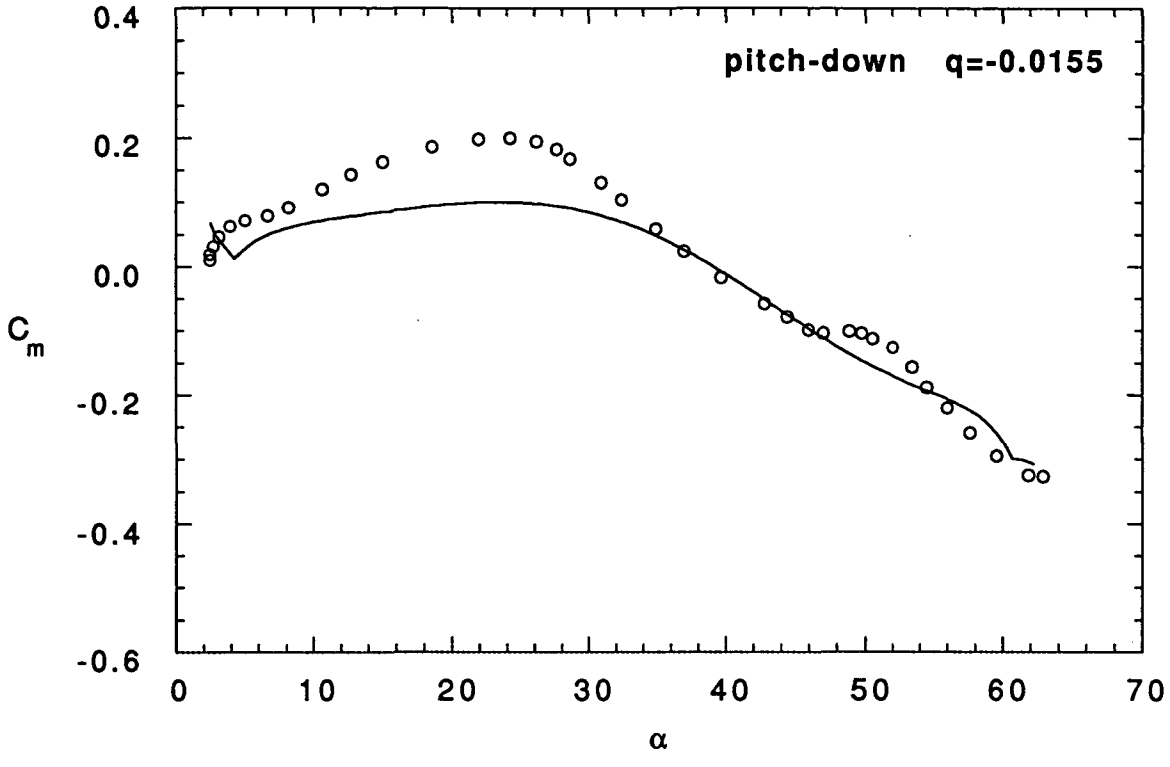

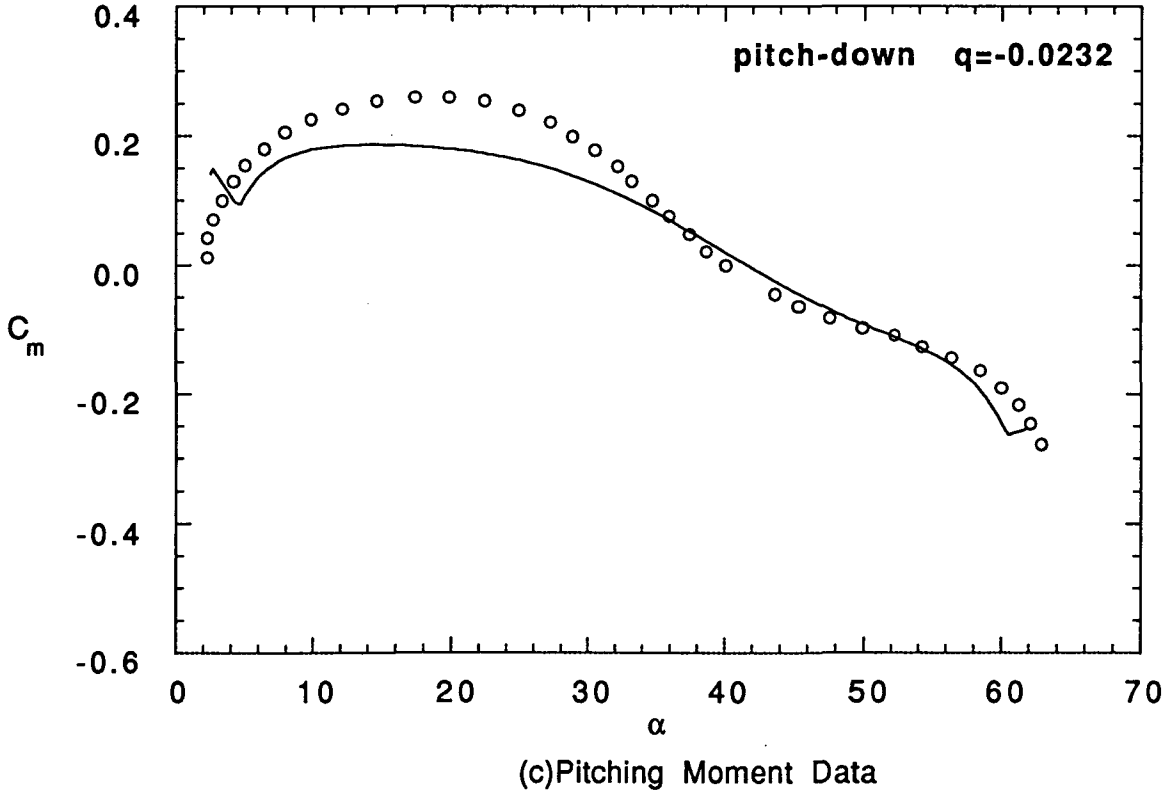

(c)Pitching Moment Data

Figure 6 Concluded

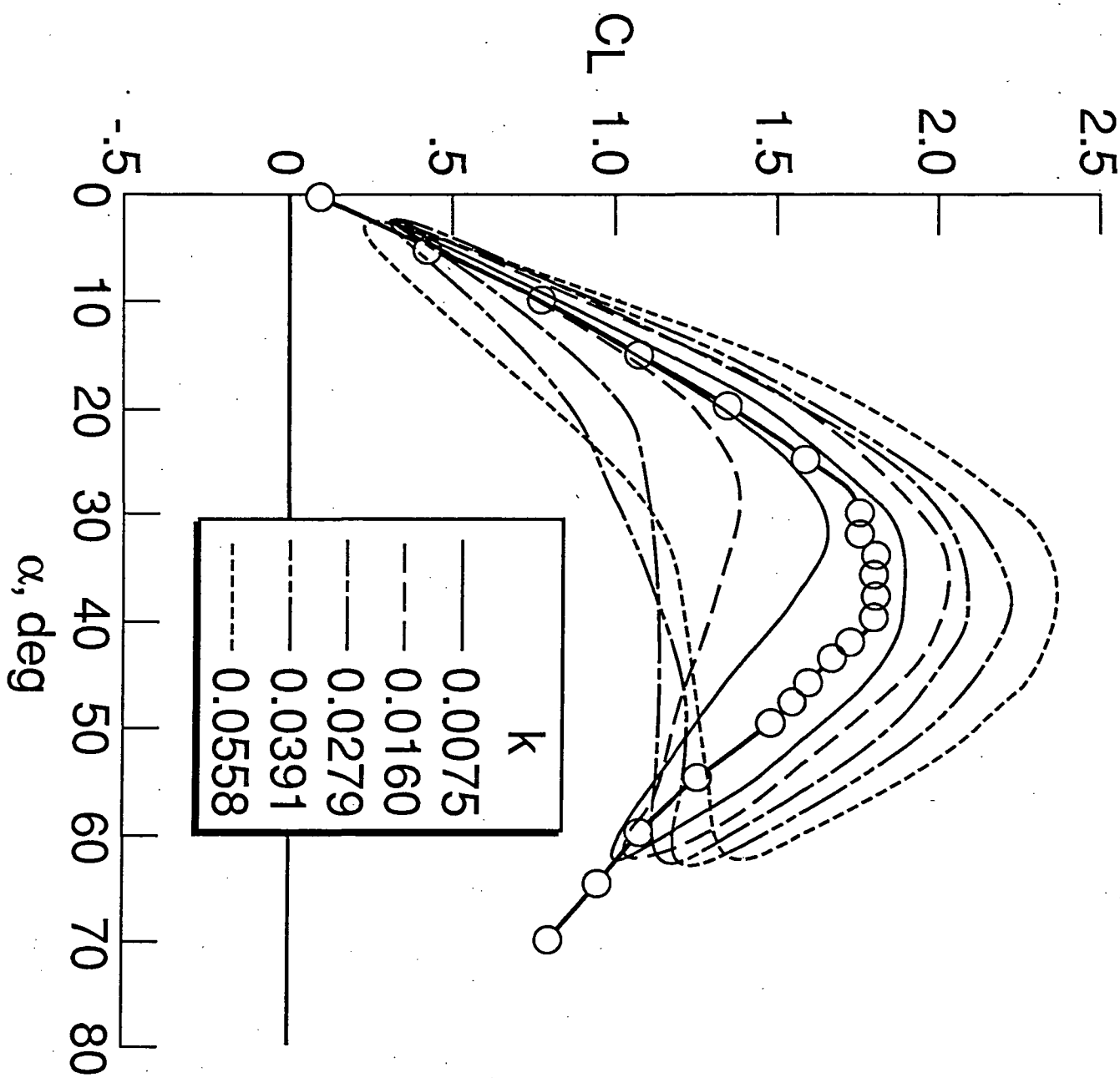

Figure 7 Test Data for the C_L Response of an F-18 Model

Fourier Functional Analysis

for

Unsteady Aerodynamic Modeling

Suei Chin* and C. Edward Lan**

The University of Kansas

Lawrence, Kansas 66045

Abstract

A method based on Fourier analysis is developed to analyze the force and moment data obtained in large-amplitude forced oscillation tests at high angles of attack. The aerodynamic models for lift, drag and pitching moment coefficients are built up from a set of aerodynamic responses to harmonic motions at different frequencies. The final expressions for the models involve time integrals of the indicial type. Results from linear two- and three-dimensional unsteady aerodynamic theories as well as test data for a 70-deg delta wing are used to verify the models. It is shown that the present modeling method is accurate in producing the aerodynamic responses to harmonic motions and the ramp-type motions.

Nomenclature

A_j coefficient of cosine Fourier series

B_j coefficient of sine Fourier series

C_{ave} average value of constant terms in the harmonic oscillation responses

C_D drag coefficient

---

*Graduate Research Assistant. Currently at Aeronautical Research Lab., Taichung, Taiwan.

**Professor, Aerospace Engineering and Center for Excellence in Computer Aided Systems Engineering. Associate Fellow AIAA.

c_ℓ 2-D lift coefficient.

C_L 3-D lift coefficient.

C_{L_α} variation of lift coefficient with respect to angle of attack

C_{L_q} variation of lift coefficient with respect to pitch rate

C_m pitching moment coefficient

E_{ij} constants associated with the zero-lag response

H_{ij} constants in amplitude functions

i imaginary part of a complex number

j index

k reduced frequency ($=\omega\ell/v_\infty$)

M Mach number

n index for reduced frequency. Also index for the coefficients in Padé approximants

N number of frequencies

PD_j Padé approximants

P_{ij} coefficients in Padé approximants

q pitch rate in rad/sec

t time

t' nondimensional time ($=tv_\infty/\ell$)

v_∞ free stream velocity

α variation in angle of attack ($=\alpha_0 \cos kt'$)

α_1 $= \alpha_m + \alpha$

α_o amplitude of angle-of-attack variation

α_m mean angle of attack

$\dot{\alpha}$ time rate of change in angle of attack

ℓ reference length

τ dummy time integration variable

ξ running variable in time

θ $= kt'$

Introduction

Due to the requirement of increased performance and maneuverability, the flight envelope of a modern fighter is frequently extended to the high angle-of-attack regime. Vehicles maneuvering in this regime are subjected to nonlinear aerodynamic loads. The nonlinearities are due mainly to three-dimensional separated flow and concentrated vortex flow that occur at large angles of attack. Accurate prediction of these nonlinear airloads is of great importance in the analysis of a vehicle's flight motion and in the design of its flight control system. As Tobak and Schiff mentioned in ref. 1, the main difficulty in determining the relationship between the instantaneous aerodynamic load on a maneuvering vehicle and the motion variables is that this relationship is determined not only by the instantaneous values of motion variables but also by all of the prior states of the motion up to the current state. With the advanced computing techniques, one straightforward way to solve this problem is to solve the flow-field and the flight dynamic equations simultaneously. However, this is obviously a very costly approach. In particular, at high angles of attack the aerodynamic loads depend nonlinearly on the motion variables. Under such conditions, even if the vehicles start from closely similar initial conditions, they may experience widely varying motion histories. Thus, a satisfactory evaluation of the performance envelope of an aircraft may require a large number of coupled computations, one for each change in initial conditions. Furthermore,

since the motion and the aerodynamic response are linked together in this approach, there can be no reutilization of the previously obtained aerodynamic reactions.

To avoid the disadvantage of solving the coupled flow- field equations and aircraft's motion equations, an alternate approach is to use a mathematical model to describe the steady and unsteady aerodynamics for the aircraft's equations of motion. Ideally, with a mathematical model, an evaluation of the aerodynamic terms specified by the model would be required only once. The specified model can be reutilized to solve the aircraft's equations of motion over a range of motion variables and flight conditions.

In the classical linear potential flow theory[2,3], researchers in the field of aeroelasticity used the Fourier transform to relate the aerodynamic response of step change in angle of attack of a wing to that of harmonic oscillatory motions. The transient aerodynamic reaction to a step change is called the "indicial function" and has been calculated for several classes of isolated wings[2-5]. By a suitable superposition[6] of these results, the aerodynamic forces and moments induced in any maneuvers can be studied[2,3]. Tobak applied the indicial function concept to analyze the motions of wings and wing-tail combinations[7]. Later, based on a consideration of functional, Tobak and his coworkers[1,8] extended the concept of indicial function into the nonlinear aerodynamic regimes, even with aerodynamic bifurcations[9]. The simplest nonlinear aerodynamic model proposed in ref. 1 has been applied by several authors[10-14] to perform the analysis. However, that simplest model is accurate only to the first order of frequency. It needs to be improved for a more general response.

Aerodynamic forces and moments acting on a rapidly maneuvering aircraft are, in general, nonlinear functions of motion variables, their time rate of change, and the history of maneuvering. How these unsteady aerodynamic forces and moments may be

represented in a form suitable for flight dynamic simulation becomes uncertain, in particular at high angles of attack. For a certain type of nonlinearities produced in an experiment with small-amplitude oscillation, the analysis has been accomplished by separating the time-history data into in-phase and out-phase components[15] . When large-amplitude forced oscillations are employed in the wind-tunnel testing at a large mean angle of attack, the aerodynamic phenomena may involve dynamic stall and/or strong vortex flow, with or without vortex breakdown. In this case, higher harmonic components in the aerodynamic response are expected to exist[16] and the phenomenon of aerodynamic lag would be important. Therefore, a more general modeling technique is needed.

In this paper, a numerical method will be developed to analyze the nonlinear and time-dependent aerodynamic response to establish the generalized indicial function in terms of motion variables and their time rates of change.

Theoretical Development

In existing flight simulation, two common ways are used to treat high-angle-of attack aerodynamics. One is to use tabulated quasi-steady data[17] and the other is to use a local linearized model which form a piecewise continuous fit of the nonlinear response[18]. In the present approach, a formula involving time integration will be developed.

Based on functional analysis, Tobak and Schiff[1] developed a fundamental formulation of aerodynamic response for arbitrary motion. Summing incremental responses to small step changes of α and $q\ell/v_\infty$ at time τ, an integral form for C_L at time t is obtained

$$C_L(t) - C_L(0) + \int_0^t C_{L_\alpha}[\alpha(\xi), q(\xi); t, \tau] \frac{d\alpha}{d\tau} d\tau + \frac{\ell}{v_\infty} \int_0^t C_{L_q}[\alpha(\xi), q(\xi); t, \tau] \frac{dq}{d\tau} d\tau \quad (1)$$

where ξ is a running variable in time over the interval 0 to τ, ℓ is a reference length and V_∞ is the freestream velocity.

To have practical applications, the functional integral form needs to be simplified. By assuming that α and q are analytical functions in the neighborhood of $\xi=\tau$, variables α and q can be expanded by their Taylor series at $\xi=\tau$. The indicial responses C_{L_α}, for example can be expressed as

$$C_{L_\alpha}[\alpha(\xi), q(\xi); t, \tau] = C_{L_\alpha}[t, \tau; \alpha(\tau), \dot{\alpha}(\tau),\cdots\cdots, q(\tau), \dot{q}(\tau),\cdots\cdots] \tag{2}$$

If only the first two coefficients are retained in the above Taylor series expansion, the integral form of eq. (1) becomes

$$C_L(t)=C_L(0)+\int_0^t C_{L_\alpha}[t,\tau;\alpha(\tau),\dot{\alpha}(\tau),q(\tau),\dot{q}(\tau)]\frac{d\alpha}{d\tau}d\tau + \frac{\ell}{v_\infty}\int_0^t C_{L_q}[t,\tau;\alpha(\tau),\dot{\alpha}(\tau),q(\tau),\dot{q}(\tau)]\frac{dq}{d\tau}d\tau \tag{3}$$

Eq. (3) is applicable to the study of rapidly varying maneuvers, where hysteresis phenomena are known to exist. However, it is difficult to implement eq. (3). By assuming a slowly varying motion, Tobak and Schiff neglected the dependence of the indicial response on $\dot{\alpha}$ and $\dot{q}$. By further assuming that the indicial response is a function of the elapsed time $t-\tau$ instead of t and τ separately, a simplified expression of eq. (1) can be written as

$$C_L(t)=C_L(0)+\int_0^t C_{L_\alpha}[t-\tau;\alpha(\tau),q(\tau)]\frac{d\alpha(\tau)}{d\tau}d\tau + \frac{\ell}{V_\infty}\int_0^t C_{L_q}[t-\tau;\alpha(\tau),q(\tau)]\frac{dq(\tau)}{d\tau}d\tau \tag{4}$$

Although the form of eq. (4) represents a great simplification over that of eq. (1), the equation still includes the full linear form as a special case.

Jenkins[19] applied a local Taylor expansion to indicial response C_{L_α} and used that Taylor expansion form to fit numerical indicial responses calculated from a program called

NLWAKE. By substituting C_{L_α} into eq. (4), Jenkins was able to predict the oscillating motion for airfoil at low frequencies.

In the present investigation, the hysteresis effect is included and the assumption of low frequencies will be removed. Therefore, a form between eq. (3) and eq. (4) is written as

$$C_L(t)-C_L(0)+\int_0^t C_{L_\alpha}[t-\tau;\ \alpha(\tau),\ \dot{\alpha}(\tau),\ q(\tau),\ \dot{q}(\tau)]\ \frac{d\alpha(\tau)}{d\tau}d\tau + \frac{\ell}{v_\infty}\int_0^t C_{L_q}[t-\tau;\ \alpha(\tau),\ \dot{\alpha}(\tau),\ q(\tau),\ \dot{q}(\tau)]\ \frac{dq(\tau)}{d\tau}d\tau \tag{5}$$

In wind-tunnel testing, the q effect cannot be separated from that of $\dot{\alpha}$. Since the method developed in this study will be used first to analyze the wind tunnel data, $\dot{\alpha}$ will be used instead of q in the following investigation . The effect of $\ddot{\alpha}$ (i.e. $\dot{q}$) is included in the response without aerodynamic lag, such as the virtual mass effect in incompressible flow. Since the zero-lag response does not involve the aerodynamic lag, it is removed out of the time integral. Then eq. (5) is rewritten for the present study as

$$C_L(t)-C_L(0)+\text{ zero-lag response} + \int_0^t C_{L_\alpha}[t-\tau;\ \alpha(\tau),\ \dot{\alpha}(\tau)]\ \frac{d\alpha(\tau)}{d\tau}d\tau + \frac{\ell}{v_\infty}\int_0^t C_{L_{\dot{\alpha}}}[t-\tau;\ \alpha(\tau),\ \dot{\alpha}(\tau)]\ \frac{d\dot{\alpha}(\tau)}{d\tau}d\tau \tag{6}$$

The main objective in the present investigation is to find a suitable form for the integrand of eq. (6). The basic building blocks of the present method are a set of aerodynamic responses to harmonic motions at different frequencies. These responses serve as a linearly independent set of functions upon which the response to an arbitrary motion can be built.

In the linear theory[2,3], the aerodynamic response can be separated into a product of an amplitude function and a phase function in harmonic motion. The amplitude

function depends on motion variables and their time rate of change. On the other hand, the phase function is a function of frequency and accounts for any phase lag between the response and the excitation. In a two-dimensional linear theory, the phase function is given by Theodorsen's circulation function[2,3]. After response is obtained at different frequencies with the same amplitude in harmonic oscillation, the phase function can be determined numerically. After use of reciprocal relations[20], the indicial function can be defined by numerical means. This approach has been used for numerical determination of indicial lift for plunging airfoils[5] and for plunging wings[21].

The method for the linear theory is generalized as follows. Instead of assuming that the aerodynamic response is a product of an amplitude function and a phase function, it is taken to be a sum of the products of amplitude functions and phase functions in harmonic motion; i.e.,

$$C_L - C_0 + \sum_j (\text{amplitude function})_j * (\text{phase function})_j \tag{7}$$

In the linear theory, j equals 1 in the equation. To determine the form of the amplitude functions as functions of $\alpha(t)$ and $\dot{\alpha}(t)$, and the phase functions, a functional analysis is needed. A practical method for this purpose is the Fourier analysis of forced oscillation data. The motion is assumed to be of the form:

$$\alpha_1 - \alpha_m + \alpha_0 \cos(kt') \tag{8a}$$

$$\alpha - \alpha_0 \cos(kt') \tag{8b}$$

$$\dot{\alpha} - (-\alpha_0 k)\sin(kt') \tag{8c}$$

where k is the reduced frequency, t' is the nondimensionalized time, α_m is the mean angle of attack and α_0 is the amplitude of angle-of-attack variation. The first step is to Fourier-analyze the response over one period. Let

$$C_L = A_0 + A_1\cos\theta + A_2\cos 2\theta + A_3\cos 3\theta + B_1\sin\theta + B_2\sin 2\theta + B_3\sin 3\theta + \ldots \tag{9}$$

From the past experience[21,22], it was found that Padé approximants provide an accurate approximation of the theoretical phase function. Therefore, Padé approximants will be used in the present model as phase functions. Following the classical airfoil theory, the analysis is best performed in complex algebra. For this purpose, eq. (9) (or the experimental oscillatory results) is rewritten in a complex form, as follows:

$$C_L = A_0 + (A_1 - iB_1)e^{ikt'} + (A_2 - iB_2)e^{i2kt'} + (A_3 - iB_3)e^{i3kt'} + \ldots \tag{10}$$

It should be kept in mind that only the real part of the response has a physical meaning. The reason to use the complex form is to benefit from the mathematical convenience of the $e^{ikt'}$ notation. If α is rewritten as

$$\alpha = \alpha_0 e^{ikt'}$$

and

$$\dot{\alpha} = (i\alpha_0 k) e^{ikt'}$$

then the classical airfoil theory suggests that the response can be put in the following form involving the products of amplitude functions and phase functions as

$$\begin{aligned} C_L \equiv\ & A_0(k) \\ & + E_{11}\dot{\alpha} + E_{21}\ddot{\alpha} + C_1 * (H_{11}\alpha + H_{21}\dot{\alpha}) * (1 - PD_1) \\ & + E_{12}\dot{\alpha}_2 + E_{22}\ddot{\alpha}_2 + C_2 * (H_{12}\alpha^2 + H_{22}\alpha\dot{\alpha} + H_{32}\dot{\alpha}^2) \\ & \qquad * (1 - PD_2) \\ & + E_{13}\dot{\alpha}_3 + E_{23}\ddot{\alpha}_3 + C_3 * (H_{13}\alpha^3 + H_{23}\alpha^2\dot{\alpha} + H_{33}\alpha\dot{\alpha}^2 + H_{43}\dot{\alpha}^3) \\ & \qquad * (1 - PD_3) \\ & \qquad + \ldots \end{aligned} \tag{11}$$

where PD's are Padé approximants of order 2 and are defined as

$$PD_j = \frac{P_{1j}\,(ik)^2 + P_{2j}\,(ik)}{P_{3j}\,(ik)^2 + (ik) + P_{4j}} \tag{12}$$

$E_{11}\,\dot{\alpha}_j + E_{21}\,\ddot{\alpha}_j$ etc. are the zero-lag response. The variables $\dot{\alpha}_j$ and $\ddot{\alpha}_j$ are defined as

$$\dot{\alpha}_j = ik\,\alpha_0{}^j\,e^{ijkt'}$$

and

$$\ddot{\alpha}_j = -k^2\,\alpha_0{}^j\,e^{ijkt'}$$

to be consistent with higher order terms. When j=1 in the above equations, $\dot{\alpha}_1 = \dot{\alpha}$ and $\ddot{\alpha}_1 = \ddot{\alpha}$. In addition, H_{21}, H_{22}, H_{23}, etc., are related to the pitch-rate effect. It should be noted that those terms inside the parentheses following C_1, C_2, C_3, such as $(H_{11}\alpha + H_{21}\dot{\alpha})$, represent the magnitude (or amplitude) and $(1 - PD_j)$ represents the unsteady aerodynamic lag (or phase) in response. Therefore, the present assumed form for aerodynamic modeling encompasses the classical linear theory and is capable of representing a complete set of harmonic-oscillatory data with different frequencies in one expression. It should be noted that in eq. (11), the contribution to each mode is summed in complex form. The response in time domain is given by the real part, similar to obtaining eq. (9) from eq. (10).

C_j are the reference values used to normalize the lift given by $A_j - i\,B_j$ in the least squared-error method. j is the index consistent with the exponent of the exponential terms in eq. (10). For example if the j's term in eq. (11) represents the coefficient of $e^{ikt'}$, then j is 1. If the j's term in eq. (11) represents the coefficient of $e^{i2kt'}$ then j is 2, etc. The first term, $A_0(k)$, in eq. (11) is a constant term, supposedly a function of frequency. From available experimental data for a delta wing[22], $A_0(k)$ can be assumed to be constant approximately. The unknown coefficients P_{1j}, P_{2j}, P_{3j} and P_{4j} are calculated from the

least squared-error method. E_{11}, E_{21}, H_{11}, H_{12}, etc., are obtained separately by minimizing the sum of squares of errors. This is equivalent to a two-level optimization method to determine the unknowns in eq. (11). That is, E, H, etc., are assumed first. Then P_{1j}, etc., are determined by minimizing the sum of squared errors. The values of E_{11}, H_{11}, etc., are varied next so that the sum of squared errors is minimized based on a gradient method. It was found that this approach is more effective in determining a global minimum solution for the unknowns than a straightforward optimization (one level) method because of nonlinearity in the unknowns in this optimization problem. It should be noted that in the literature the phase function has been typically determined by the response to plunging motions, not pitching motions. Therefore, those terms associated with $\dot{\alpha}$ in eq. (11) do not appear. This would very much simplify the mathematics of determining the Padé approximants. The details of the present method are discussed in the following.

Least-Square Method

By choosing proper values of E_{11}, H_{11}, H_{12}, etc., in eq. (11), the corresponding A_j - i B_j term in eq. (10) is then divided by the amplitude function. The result will appear as

$$V_j + iW_j \equiv 1 - \frac{A_j - iB_j - E_{1j}\, ik - E_{2j}\,(-k^2)}{(\text{amplitude function})_j} - \frac{P_{1j}\,(ik)^2 + P_{2j}\,(ik)}{P_{3j}\,(ik)^2 + (ik) + P_{4j}} \tag{13}$$

If both sides of eq. (13) are multiplied by the denominator of the Padé approximant and separated into real and imaginary parts, then

$$Re \equiv P_{1j}k^2 - P_{3j}V_jk^2 + P_{4j}\,V_j - W_j\,k = 0 \tag{14a}$$

and

$$Im \equiv P_{2j}k + P_{3j}W_jk^2 - P_{4j}W_j - V_jk = 0 \tag{14b}$$

The sum of squared errors is defined as

$$Err \equiv \Sigma\, Re(k_i)^2 + \Sigma\, Im(k_i)^2 \tag{15}$$

By equating the first derivatives of squared errors (eq. 15) with respect to variables P_{1j}, P_{2j}, P_{3j} and P_{4j} to zero, the unknown coefficients P_{1j}, P_{2j}, P_{3j} and P_{4j} can be determined from

$$\begin{bmatrix} \Sigma k_i^4 & 0 & -\Sigma V_i k_i^4 & \Sigma V_i k_i^2 \\ 0 & \Sigma k_i^2 & \Sigma W_i k_i^3 & -\Sigma W_i k_i \\ -\Sigma V_i k_i^4 & \Sigma W_i k_i^3 & \Sigma(V_i^2 k_i^4 + W_i^2 k_i^4) & -\Sigma(V_i^2 k_i^2 + W_i^2 k_i^2) \\ \Sigma V_i k_i^2 & -\Sigma W_i k_i & \Sigma(V_i^2 k_i^2 + W_i^2 k_i^2) & \Sigma(V_i^2 + W_i^2) \end{bmatrix} \begin{bmatrix} P_{1j} \\ P_{2j} \\ P_{3j} \\ P_{4j} \end{bmatrix} = \begin{bmatrix} \Sigma W_i k_i^3 \\ \Sigma V_i k_i^2 \\ 0 \\ 0 \end{bmatrix} \tag{16}$$

where i varies over the range of input frequencies, and the mode subscript j on V and W has been omitted.

Gradient Method

After the unknown coefficients P_{1j}, P_{2j}, P_{3j} and P_{4j} have been found, a one-dimensional gradient method is used to find E and H values which will make the sum of the squared errors minimum. The E or H value is perturbed first by a small amount ΔE or ΔH to find the gradient of the sum of squared errors. If the gradient tends to reduce the error, then the E or H value is perturbed further until several iterations has been reached (it is set to be 5 iterations in the current program). After that, the same procedure is applied to other E or H. Then the whole procedure is repeated again for several iterations.

Indicial Formulation

To express the aerodynamic response in time domain (eq. 6), the phase function, as represented by the Padé approximants, is inverted from frequency to time domains by inverse Fourier transform. The Padé approximants are first factored as follows:

$$1 - \frac{P_{1j}\,(ik)^2 + P_{2j}\,(ik)}{P_{3j}\,(ik)^2 + ik + P_{4j}} = 1 - \frac{ik\,a_{1j}}{ik + a_{3j}} - \frac{ik\,a_{2j}}{ik + a_{4j}} \tag{17}$$

and then it is inverted based on a step input[2] to be

$$\frac{1}{2\pi\,ik}\int_{-\infty}^{\infty}\left[1 - \frac{P_{1j}(ik)^2 + P_{2j}(ik)}{P_{3j}(ik)^2 + ik + P_{4j}}\right] e^{ikt'} d\,(jk) \tag{18}$$

$$= 1 - a_{1j}\,e^{-a_{3j}t'} - a_{2j}\,e^{-a_{4j}t'}$$

The final form for the aerodynamic response in time domain for arbitrary motion is therefore given by

$$C_L(t') = C_{L_{indicial}}[t'-\tau,\ \alpha(\tau),\ \dot{\alpha}(\tau)]_{\tau=0} + C_{ave} + \sum_{j=1}^{m}(E_{1j}\dot{\alpha}_j + E_{2j}\ddot{\alpha}_j)$$

$$+ \sum_{j=1}^{m}\int_0^{t'} \frac{d\,(a.f.)_j}{d\alpha}*(1-a_{1j}e^{-a_{3j}(t'-\tau)}-a_{2j}e^{-a_{4j}(t'-\tau)})\,\frac{d\alpha(\tau)}{d\tau}\,d\tau \tag{19}$$

$$+ \frac{\ell}{v_\infty}\sum_{j=1}^{m}\int_0^{t'} \frac{d\,(a.f.)_j}{d\,\alpha}*(1-a_{1j}e^{-a_{3j}(t'-\tau)}-a_{2j}e^{-a_{4j}(t'-\tau)})\,\frac{d\dot{\alpha}(\tau)}{d\tau}\,d\tau$$

where the amplitude functions (a.f.) are given by those H-terms in eq. (11) and C_{ave} is the average of A_0 and is a function of α_m. It should be noted that α in eq. (19) denotes a perturbation from α_m. The first term in eq. (19) is the amplitude of C_L (eq. 11) when α is abruptly changed to $\alpha(0)$ at $\tau = 0$ and represents an initial value in the indicial lift formulation (see eqs. 5.370 and 5.382 of Ref. 2). Again, each mode is evaluated in complex form and the real part of the result is taken as the response in time domain.

To perform the time integration in eq. (19), the 3-point Simpson rule is used in the present method. Since the amplitude functions are determined in the frequency domain using complex algebra, for an arbitrary motion an equivalent frequency k and phase angle ϕ at τ must be obtained by matching the given α_1 and $\dot{\alpha}_1$ as follows:

$$\alpha_1(\tau) = \alpha_m + \alpha_0 \cos(k\tau + \phi) \tag{20a}$$

$$\dot{\alpha}_1 = -\alpha_0 k \sin(k\tau + \phi) \tag{20b}$$

Eqs. (20) are solved by Newton's method. It should be noted that k and ϕ are needed merely to simulate an equivalent harmonic motion in the present formulation. The resulting k and ϕ are then used to determine the magnitude of the amplitude function using complex algebra.

Results and Discussions

Because appropriate high-alpha experimental data to apply the present modeling method are limited, the present method will first be tested with linear theoretical results.

Linear Results

Several cases in the two-dimensional and three-dimensional linear flow at different Mach numbers have been studied to verify the present method of aerodynamic modeling. The oscillatory 2-D results are computed from a 2-D unsteady quasi-vortex-lattice method (QVLM)[24] as input data for the current model. Through numerical experimentation, it is found that six frequencies are needed to have accurate results. In the present model (eq. 11), only the coefficients E_{11}, E_{21}, H_{11}, H_{21} and P_{i1} are not zero. Three Mach numbers, 0, 0.2 and 0.4 are employed. The results at M=0.4 are presented in Fig. 1. It is seen that the present modeling method is very accurate for harmonic motion. The modeling method is further verified with a 70-degree delta wing which oscillates from 0 to 20 deg. in angle of attack about the mid-root chord:

$\alpha_1 = 0.17453 + 0.17453 \cos kt'$ (in radian)

This means that the mean angle of attack is 10 deg. (0.17453 radian) and the amplitude of the oscillation is also 10 deg. (0.17453 radian). The aerodynamic responses are calculated from a 3-D unsteady QVLM code[25]. Through numerical experimentation, it is

found that the responses at low frequencies do not change significantly, so that accuracy in modeling would be reduced. To have more accurate approximation, high frequencies' responses are needed. Seven reduced frequencies (k = 0.01, 0.1, 0.2, 0.6, 1.0, 2.0, 2.5) are used in this 3-D attached flow case. The results for C_L at M=0.4 from modeling are plotted in Fig. 2 and show very good agreement again with results from the 3-D unsteady QVLM program.

Nonlinear Results

The forced-oscillation test data[23] for a 70-deg delta wing in pitching oscillation are used to validate the present nonlinear aerodynamic model. The angle of attack which describes the pitching motion is given as

$$\alpha_1 = 27.5 - 27.5 \cos kt' \text{ (in degree)}$$

which means the delta wing oscillates from 0 to 55 deg. in angle of attack and then back to 0 deg. for one cycle. The pitching center is at 57 % of the root chord. The reduced frequency k is nondimensionalized based on wing's root chord. Five sets of data corresponding to 5 different frequencies are available and they are used as the input data to calculate the coefficients for the current aerodynamic model with 5 Fourier terms. The lift coefficients obtained from the aerodynamic model (eq. 11) are compared with the original test data in Fig. 3 with good agreement. Expressions for C_D and C_m similar to eq. (11) are obtained with the same procedures as those used for C_L. The modeled harmonic results are compared with data in Figs. 4 and 5 for C_D and C_m, respectively. Again, the good agreement indicates that the present aerodynamic model is accurate in representing the experimental harmonic data. The coefficients for C_L are tabulated in Table 1.

To check the validity of indicial formulation (eq. 19) for the present nonlinear

response, two oscillatory cases in Fig. 3 will be used. That is, by assuming oscillatory motion in eq. (19), the time-integrated lift response should agree with the forced-oscillation results. The lift coefficient by integrating eq. (19) for the same 70-deg. oscillating delta wing with k=0.098 is plotted in Fig. 6. Compared with the results from aerodynamic modeling, the integrated lift shows good agreement.

To verify the aerodynamic models further, aerodynamic responses to harmonic ramp motions for a 70-deg delta wing reported in ref. 26 will be employed. The ramp motions start from α = 0 to 35, 45 and 55 deg. In the present calculation based on eq. (19), the same harmonic data shown in Figs. 3 - 5 and reported in ref. 23 are used. That is, the data are based on harmonic motions from α = 0 to 55 deg. The results for C_L are presented in Fig. 7 for a reduced frequency of 0.0714. It is seen that the present aerodynamic model is fairly accurate if the harmonic ramp motion is from α = 0 to 55 deg. However, the final C_L is overpredicted if the ramp motion stops at an α less than 55 deg, even though the peak C_L is still well predicted. A possible reason for this is that the harmonic data based on α = 0 - 55 deg. contain dynamic effect on vortex-breakdown characteristics at α < 55 deg. Therefore, the results for C_L at a final steady α = 35 or 45 deg. should be higher.

The corresponding drag and pitching moment coefficients at one reduced frequency are presented in Figs. 8 and 9, respectively. The drag coefficient is not as well predicted in ramp motions as in harmonic motions (see Fig. 4). It is not known whether this is caused by differences in the test models and test Reynolds numbers. The test model for the harmonic motions (ref. 23) has two-sided chamfered leading edges with a thickness of 0.5 inch at a Reynolds number of 1.64×10^6 based on the root chord. The model for the ramp motions (ref. 26) is chamfered only on the lower surface of the leading edge and has

a thickness of 0.25 inch, and tested at a Reynolds number of 1.54×10^6. The pitching moment coefficient appears to be well predicted except at small time.

To illustrate the present aerodynamic model (eq. 19) for arbitrary motions, a linear ramp motion is assumed in the integration. The results are compared with those in a harmonic ramp motion in Fig. 10. It is seen that the linear ramp motion tends to produce higher C_L beyond the peak value because it has a higher value in α .

Although verification of the present model was presented only with one set of α_o and α_m, some preliminary results with different α_o and α_m indicate that eq. (19) could still produce good results if a new α-range is within the test range used in setting up the model.

Table 1 Model Coefficients for C_L for the 70-deg Delta Wing

C_{ave} = 0.6451

j	C_j	E_{1j}	E_{2j}	H_{1j}	H_{2j}	H_{3j}	H_{4j}	H_{5j}	H_{6j}
1	1.0	-0.389	1.062	0.700	0.463				
2	1.0	0.212	0.250	-0.700	0.500	0.600			
3	1.0	-0.368	0.118	-0.970	0.534	0.995	-1.019		
4	5.0	0.025	-0.063	-0.100	0.400	0.400	1.000	0.000	
5	30.0	0.186	0.039	0.096	0.588	-0.015	-0.020	.0009	.0007
j	P_{1j}	P_{2j}	P_{3j}	P_{4j}	a_{1j}	a_{2j}	a_{3j}	a_{4j}	
1	-5.788	-0.453	5.520	0.030	-0.402	-0.646	-0.037	-0.144	
2	4.947	-1.387	15.243	0.001	-1.437	1.761	-0.001	-0.065	
3	3.561	0.653	4.383	0.041	0.866	-0.054	-0.053	-0.175	
4	24.424	3.412	21.343	0.001	3.541	-2.396	-0.001	-0.046	
5	6.127	1.604	1.244	0.025	1.545	3.379	-0.026	-0.778	

Conclusions

A Fourier analysis method was developed to analyze harmonic forced-oscillation data at high angles of attack as functions of the angle of attack and its time rate of change. The resulting aerodynamic responses at different frequencies are used to build up the aerodynamic models involving time integrals of the indicial type. An efficient numerical method was also developed to evaluate these time integrals for arbitrary motions based on a concept of equivalent harmonic motion. The method was verified by first using results from two-dimensional and three-dimensional linear theories. The developed models for C_L, C_D and C_m based on high-alpha data for a 70-deg delta wing in harmonic motions showed accurate results in reproducing hysteresis. The aerodynamic models are further verified by comparing with test data using ramp-type motions.

References

[1] Tobak, M.; and Schiff, L. B. "Aerodynamic Mathematical Modeling-Basic Concepts.", in Dynamic Stability Parameters, AGARD-LS-114, 1981.

[2] Bisplinghoff, R. L.; Ashley, H.; and Halfman, R. L., Aeroelasticity. Addison-Wesly Publishing Company, Cambridge, Mass., 1955.

[3] Dowell, E. H. (editor)., A Modern Course in Aeroelasticity. Sijthoff & Noordhoft International Publishers, Rockville, Maryland, 1980.

[4] Heaslet, M. A.; and Lomax, H. "Two-Dimensional Unsteady Lift Problems in Supersonic Flight." NACA Rep. 945, 1949.

[5] Mazelsky, B. "Numerical Determination of Indicial Lift of a Two-Dimensional Sinking Airfoil at Subsonic Mach Numbers from Oscillatory Lift Coefficients with Calculations for Mach Number 0.7." NACA TN 2562, December, 1951.

[6] Hildebrand, F. B., Advanced Calculus for Application. Prentice-Hall, Inc., Englewood

Cliff, New Jersey, 1976.

[7] Tobak, M. "On the Use of the Indicial Function Concept in the Analysis of Unsteady Motions of Wings and Wing-Tail Combination." NASA Rep. 1188, 1954.

[8] Tobak, M.; and Pearson, W. E. "A Study of Nonlinear Logitudinal Dynamic Stability." NASA TR R-209, September, 1964.

[9] Tobak, M. and Chapman, G. T. "Nonlinear Problems in Flight Dynamics Involving Aerodynamic Bifurcations," AGARD CP-386, Paper 25, May 1985.

[10] Katz, J.; and Schiff, L. B. "Modeling Aerodynamic Responses to Aircraft Maneuvers--A Numerical Validation." Journal of Aircraft, Vol. 23, No. 1, January, 1986, pp. 19-25.

[11] Chyu, W. J.; and Schiff, L. B. "Nonlinear Aerodynamic Modeling of Flap Oscillation in Transonic Flow--A Numerical Validation." AIAA Journal, Vol. 21, Jan. 1983, pp. 106-113.

[12] Levy, L. L.; and Tobak, M. "Nonlinear Aerodynamics of Bodies of Revolution in Free Flight." AIAA Journal, Vol. 8, Dec. 1970, pp. 2168-2171.

[13] Tobak, M.; and Schiff, L. B. "Generalized Formulation of Nonlinear Pitch-Yaw-Roll Coupling, Part 1: Nonlinear Coning-Rate Dependence." AIAA Journal, Vol. 13, March, 1975, pp. 323-326.

[14] Tobak, M.; and Schiff, L. B. "Generalized Formulation of Nonlinear Pitch-Yaw-Roll Coupling, Part 2: Nonlinear Coning-Rate Dependence." AIAA Journal, Vol. 13, March, 1975, pp. 327-332.

[15] Chambers, J. R.; and Grafton, S. B. "Static and Dynamic Longitudinal Stability Derivatives of a Powered 1/9-Scale Model of a Tilt-Wing V/Stol Transport." NASA TN D-3591, September 1966.

[16] Hanff, E. S. "Determination of Non-linear Loads on Oscillating Models in Wind Tunnels." IEEE 10th International Congress on Instrumentation in Aerospace Simulation

Facilities, September 1983.

[17] Nguyen, L. T.; Ogburn, M. E.; Gilbert W. P.; Kibler K. S.; Brown, P. W.; and Deal, P. L. "Simulator Study of Stall/Post-Stall Characteristics of a Fighter Airplane With Relaxed Longitudinal Static Stability." NASA TP 1538, December 1979.

[18] Linse, D. J. "The Design and Analysis of A High Angle of Attack Fighter Control System." University of Kansas Flight Research Laboratory, Report No. KU-FRL-776-1, 1987.

[19] Jenkins, J. E. "Simplification of Nonlinear Indicial Response Models: Assessment for the Two-Dimensional Airfoil Case," Journal of Aircraft, Vol. 28, Feb. 1991, pp.131-138.

[20] Garrick, I. E. "Nonsteady Wing Characteristics." High Speed Aerodynamics and Jet Propulsion, Vol. 7, Princeton, New Jersey, 1957.

[21] Chao, C. D.; and Lan, C. E. "Calculation of Wing Response to Gusts and Blast Waves with Vortex Lift Effect." NASA CR-172232, October 1983.

[22] Vepa, R. "Finite State Modeling of Aeroelastic Systems." NASA CR 2779, Feb. 1977.

[23] Soltani, M. R.; Bragg, M. B.; and Brandon, J. M. "Experimental Measurements on an Oscillating 70-Degree Delta Wing in Subsonic Flow." AIAA Paper No. 88-2576, 1988.

[24] Lan, C. E. "The Induced Drag of Oscillating Airfoils in Linear Subsonic Compressible Flow." University of Kansas Flight Research Laboratory, Report No. KU-FRL-400, 1975.

[25] Lan, C. E. "The Unsteady Suction Analogy and Applications." AIAA Journal, Vol. 20, No. 12 Dec. 1982, pp. 1647-1656.

[26] Bragg, M. B. and Soltani, M. R. "Measured Forces and Moments on a Delta Wing during Pitch-Up," Journal of Aircraft, vol. 27, March 1990, pp. 262 - 267.

Acknowledgement

This research was supported by NASA Grant NAG 1-1087. Mr. Luat T. Nguyen of

NASA Langley was the technical monitor.

Figure 1 Unsteady Lift Coefficient for a 2-D Flat Plate Pitching about Midchord at M = 0.4

Figure 2 Unsteady Lift Coefficient for a 70-deg Delta Wing Pitching about Mid-root Chord at M = 0.4

Figure 3 Unsteady Lift Coefficient for a 70-deg Delta Wing Pitching about 57% of Root Chord at Low Speed and Various Frequencies. Re = 1.64×10^6

Figure 4 Unsteady Drag Coefficient for a 70-deg Delta Wing Pitching about 57% of Root Chord at Low Speed and Various Frequencies. Re = 1.64×10^6

Figure 5 Unsteady Pitching Moment Coefficient for a 70-deg Delta Wing Pitching about 57% of Root Chord at Low Speed and Various Frequencies. Moment Center at 25% of Root Chord. Re = 1.64×10^6

Figure 6 Unsteady Lift Coefficient from Numerical Modeling and Indicial Time Integration for a 70-deg Delta Wing in Harmonic Pitching Oscillation about 57% of Root Chord at Low Speed. Re = 1.64×10^6 and k = 0.098

Figure 7 Unsteady Lift Coefficient from Indicial Lift Model and Experiment for a 70-deg Delta Wing in Harmonic Ramp Motion at Low Speed. Re = 1.54×10^6 and k = 0.0714

Figure 8 Unsteady Drag Coefficient from Indicial Drag Model and Experiment for a 70-deg Delta Wing in Harmonic Ramp Motion at Low Speed. Re = 1.54×10^6 and k = 0.0714

Figure 9 Unsteady Pitching Moment Coefficient from Indicial Pitching Model and Experiment for a 70-deg Delta Wing in Harmonic Ramp Motion at Low Speed. Moment Center at 25% of Root Chord. Re = 1.54×10^6 and k = 0.0714

Figure 10 Unsteady Lift Coefficient from Indicial Lift Model in Harmonic and Linear Ramp Motions for a 70-deg Delta Wing at Low Speed. Re = 1.54×10^6 and k = 0.0926

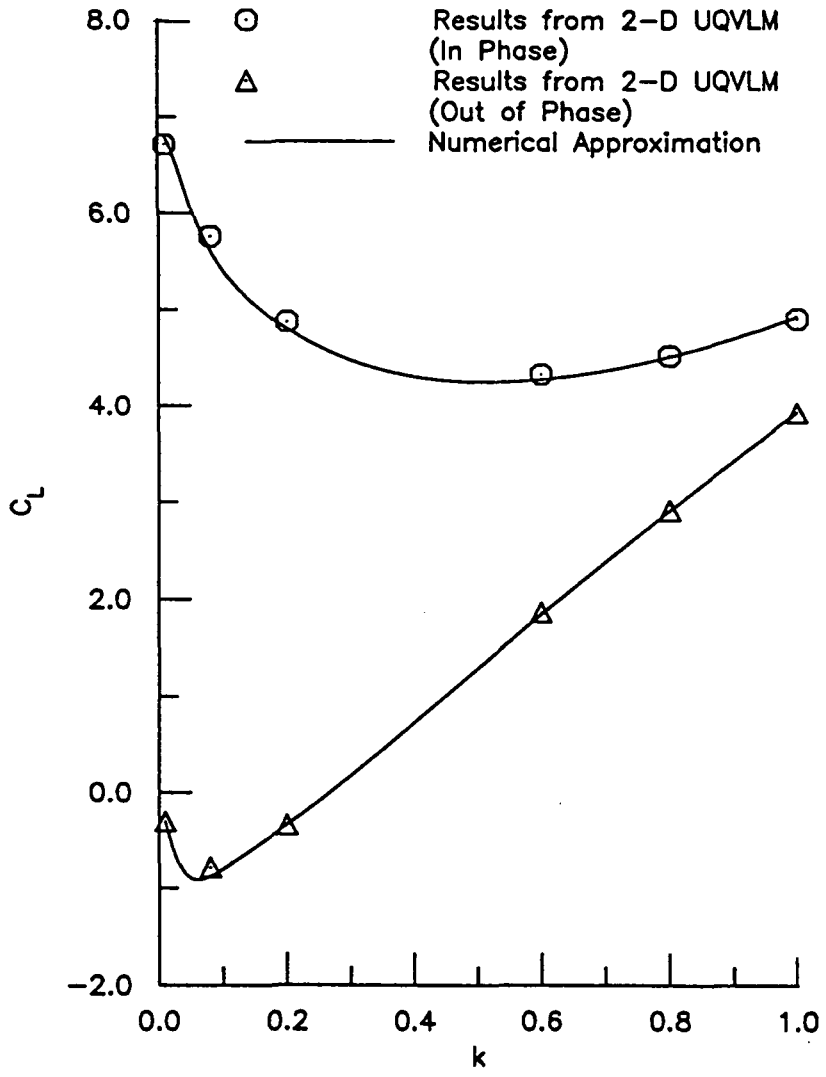
8.0
6.0
4.0
2.0
0.0
−2.0
C_L
0.0
0.2
0.4
0.6
0.8
1.0
k
Results from 2−D UQVLM (In Phase)
Results from 2−D UQVLM (Out of Phase)
Numerical Approximation

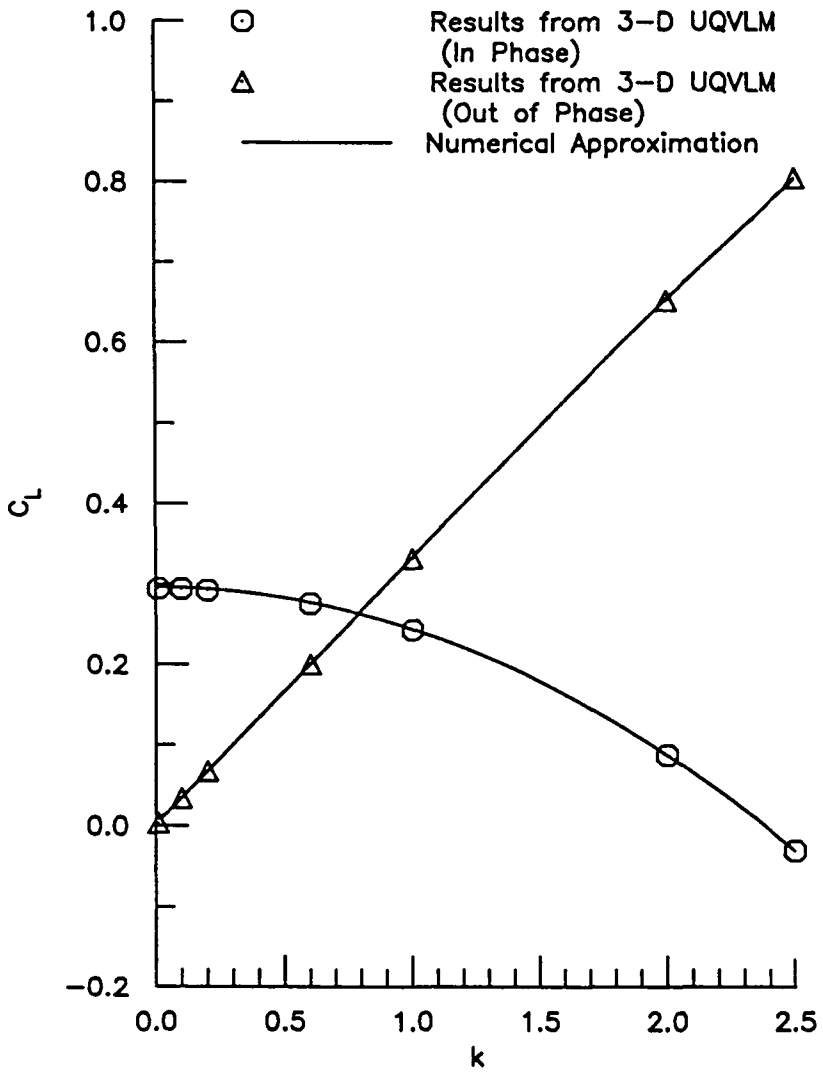
Results from 3-D UQVLM
(In Phase)
Results from 3-D UQVLM
(Out of Phase)
Numerical Approximation
1.0
0.8
0.6
0.4
0.2
0.0
-0.2
C_L
0.0
0.5
1.0
1.5
2.0
2.5
k

Fig 3

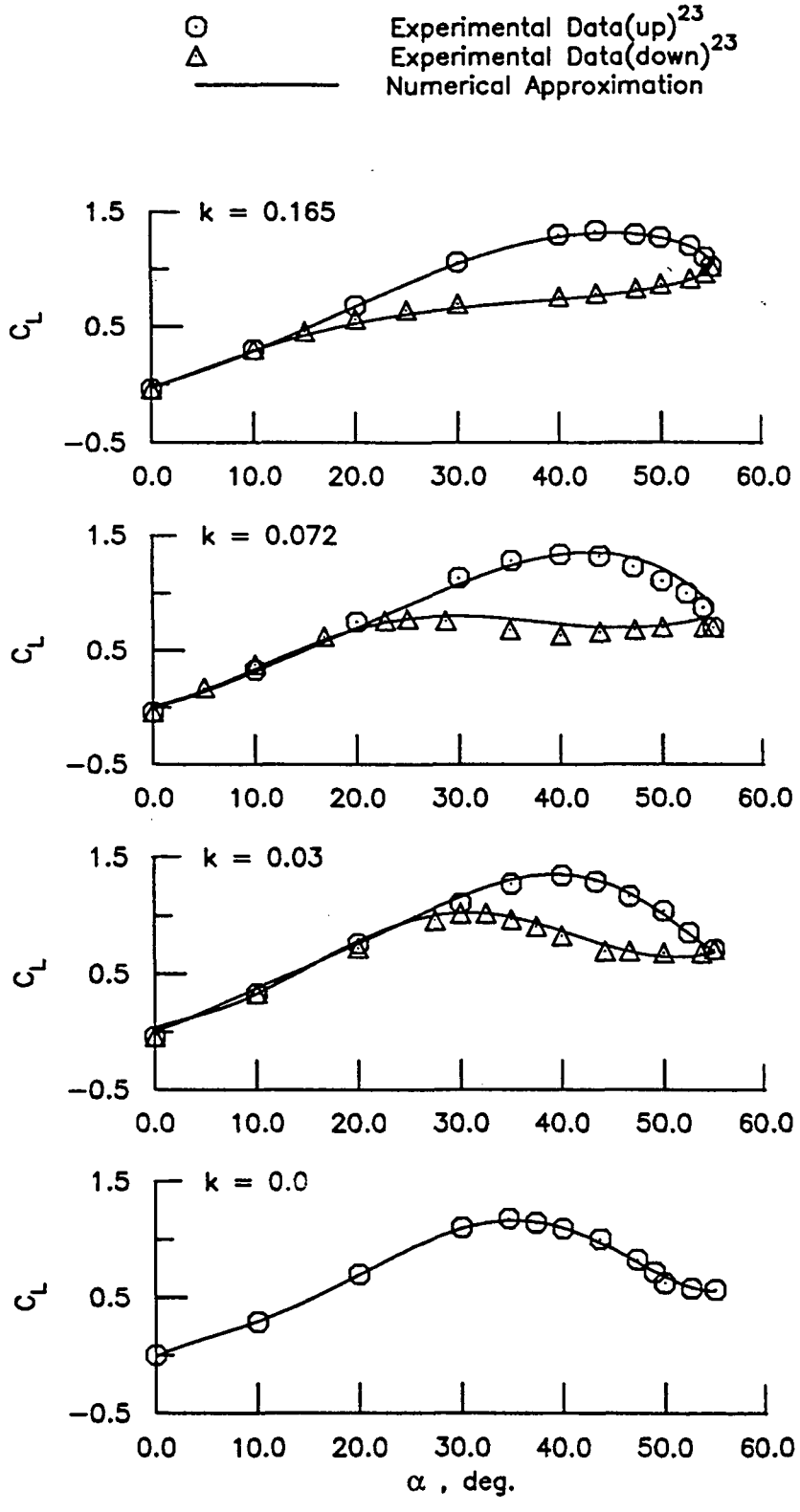
Experimental Data(up)[23]
Experimental Data(down)[23]
Numerical Approximation
k = 0.165
k = 0.072
k = 0.03
k = 0.0
C_L
1.5
0.5
−0.5
0.0
10.0
20.0
30.0
40.0
50.0
60.0
α , deg.

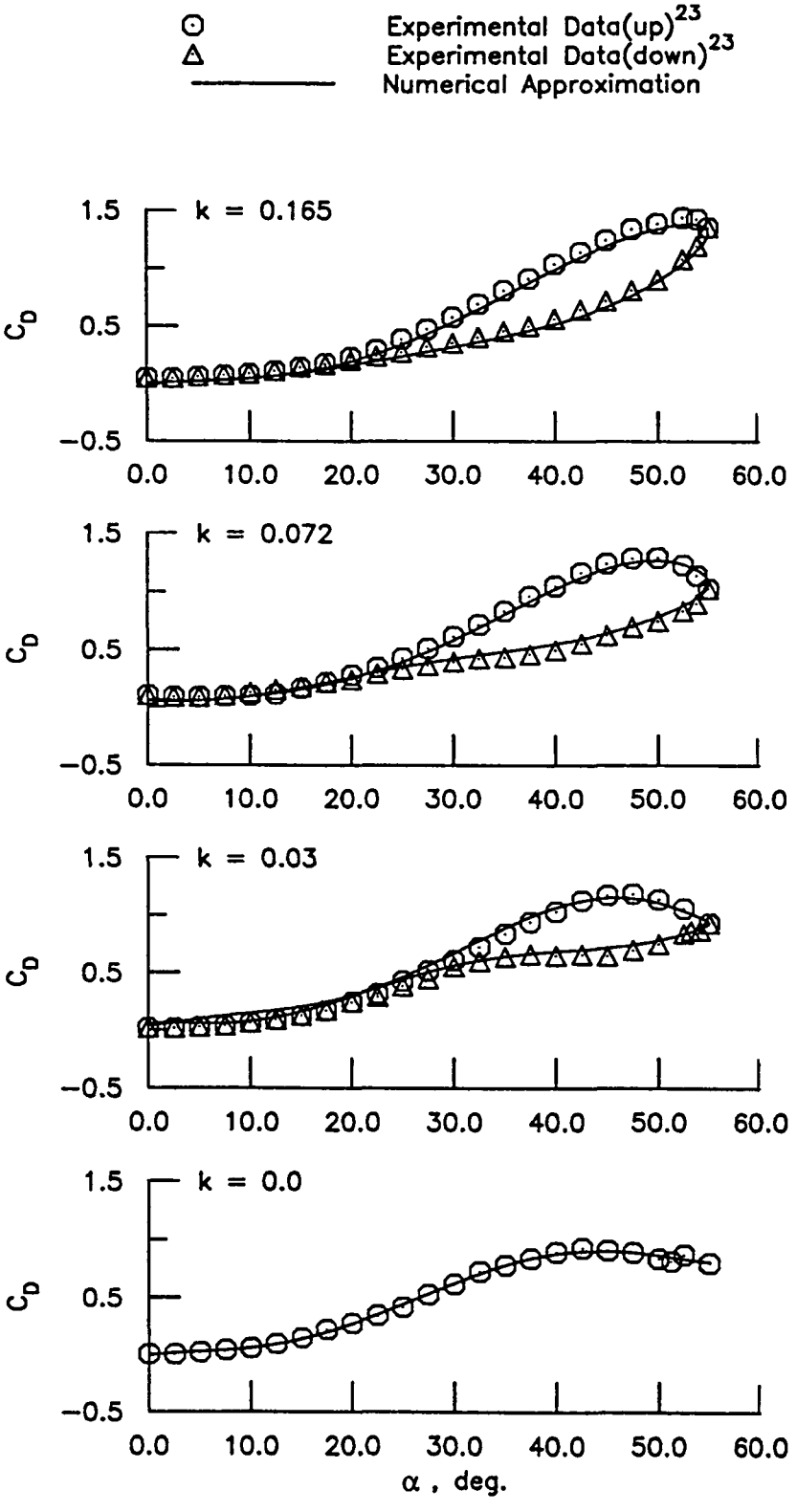
Experimental Data(up)[23]
Experimental Data(down)[23]
Numerical Approximation
k = 0.165
k = 0.072
k = 0.03
k = 0.0
C_D
1.5
0.5
−0.5
0.0
10.0
20.0
30.0
40.0
50.0
60.0
α , deg.

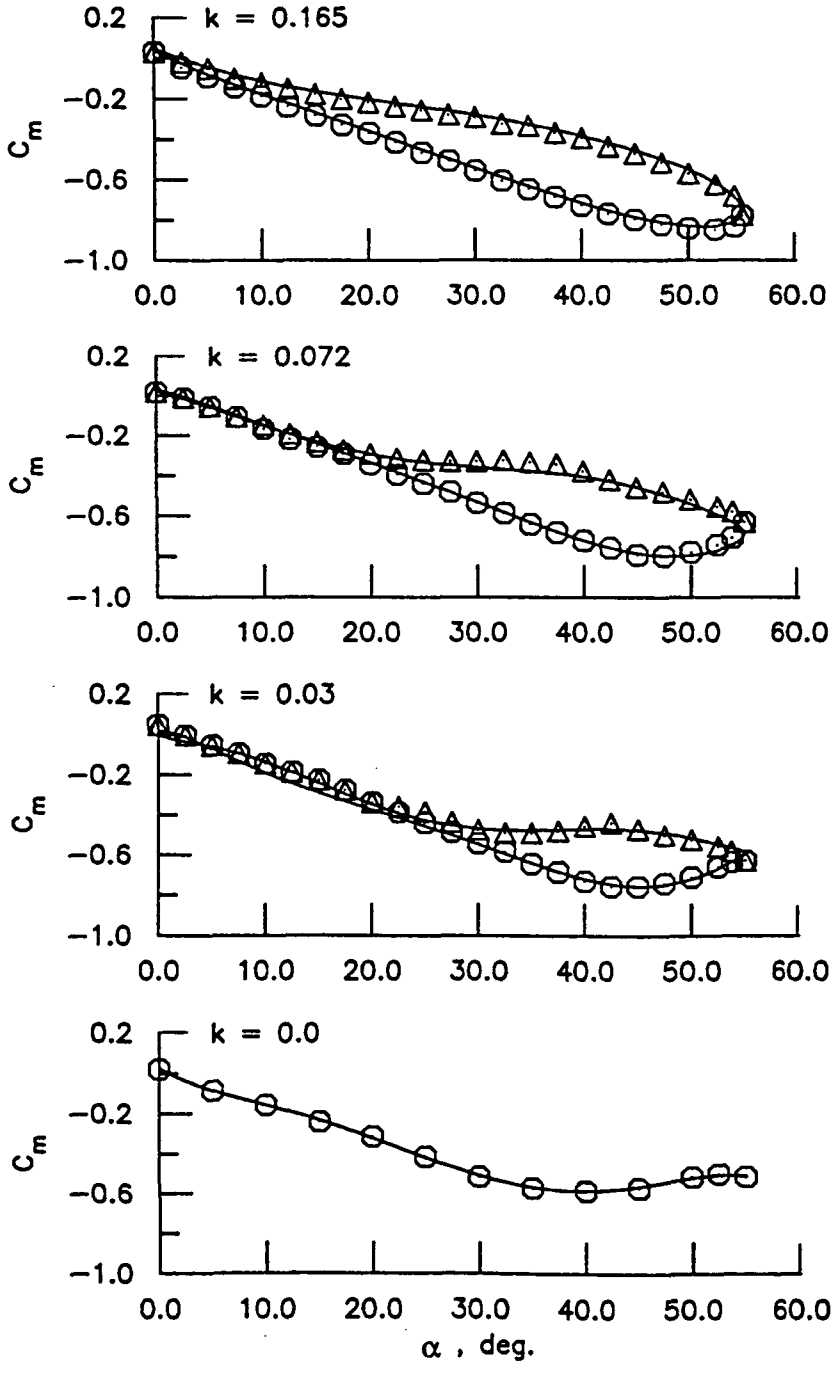
Experimental Data(up)[23]
Experimental Data(down)[23]
Numerical Approximation
k = 0.165
k = 0.072
k = 0.03
k = 0.0
C_m
0.2
−0.2
−0.6
−1.0
0.0
10.0
20.0
30.0
40.0
50.0
60.0
α , deg.

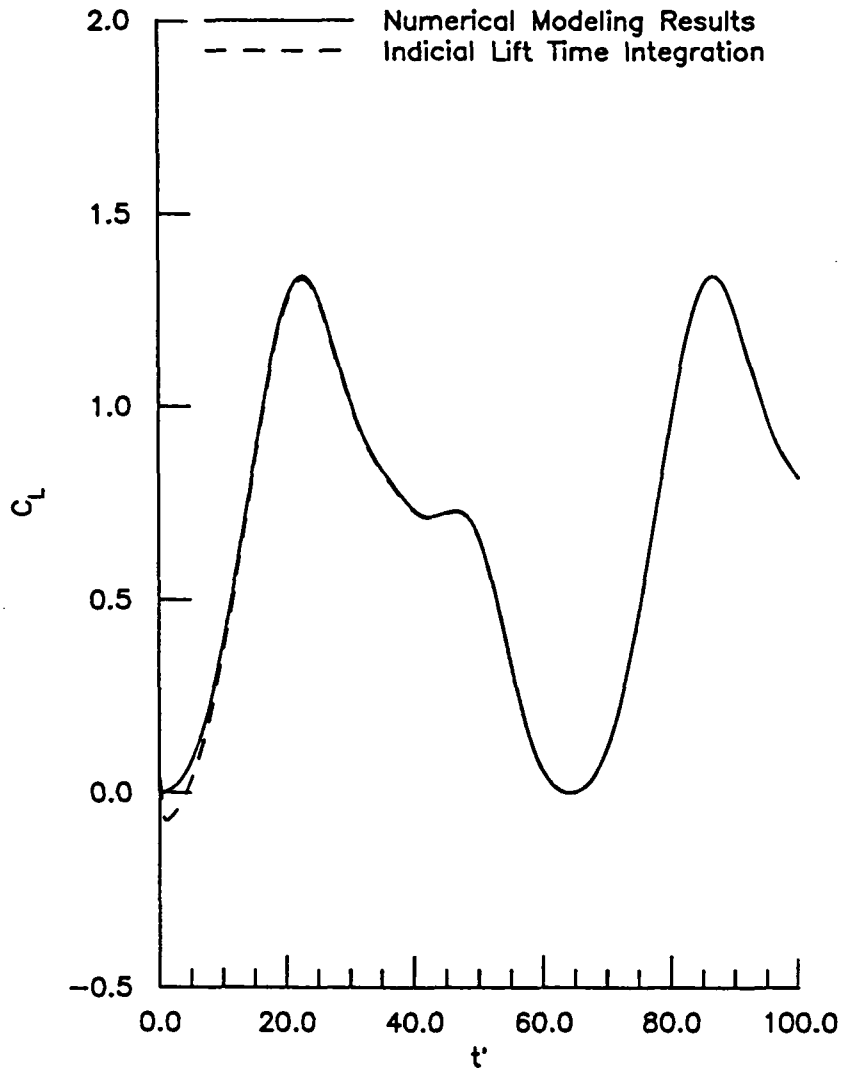
Numerical Modeling Results
Indicial Lift Time Integration
2.0
1.5
1.0
0.5
0.0
-0.5
C_L
0.0
20.0
40.0
60.0
80.0
100.0
t'

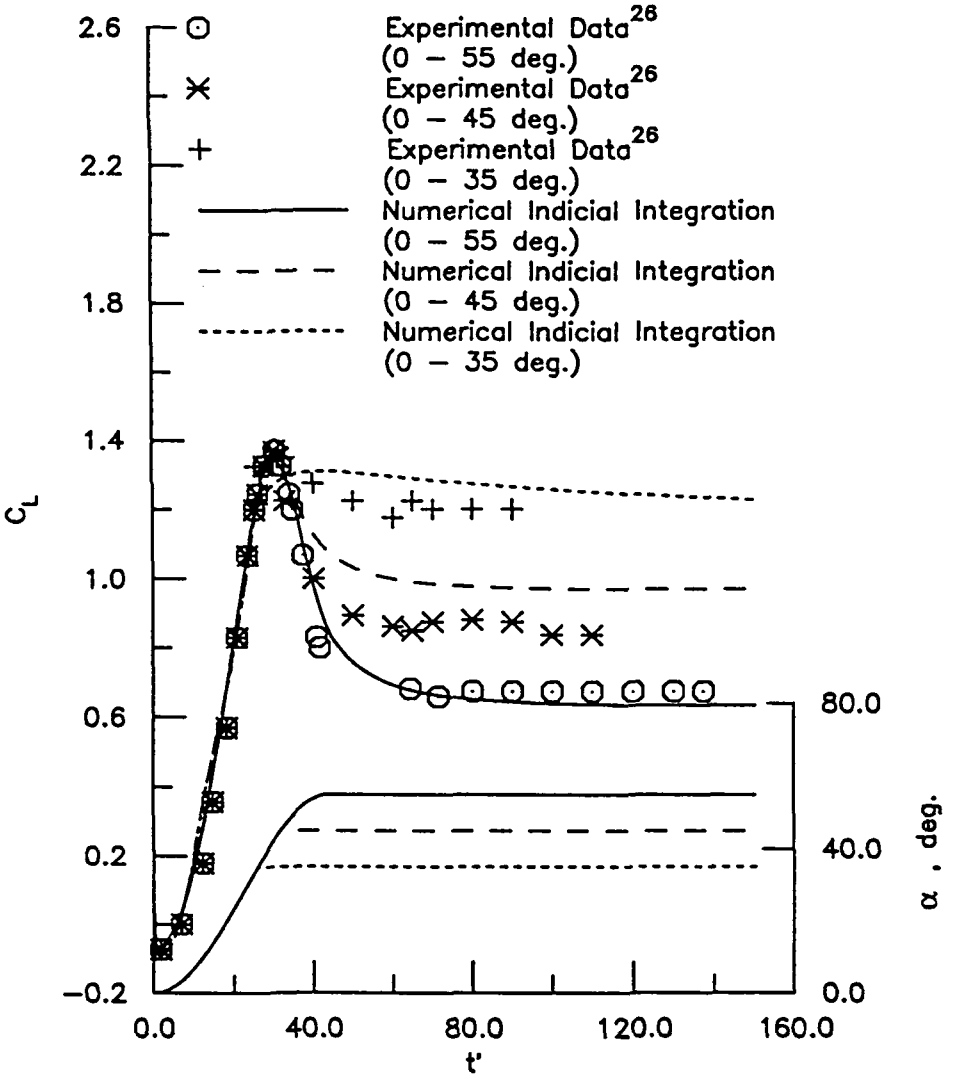
Experimental Data[26]
(0 – 55 deg.)
Experimental Data[26]
(0 – 45 deg.)
Experimental Data[26]
(0 – 35 deg.)
Numerical Indicial Integration
(0 – 55 deg.)
Numerical Indicial Integration
(0 – 45 deg.)
Numerical Indicial Integration
(0 – 35 deg.)
2.6
2.2
1.8
1.4
1.0
0.6
0.2
−0.2
C_L
0.0
40.0
80.0
120.0
160.0
t'
80.0
40.0
0.0
α , deg.

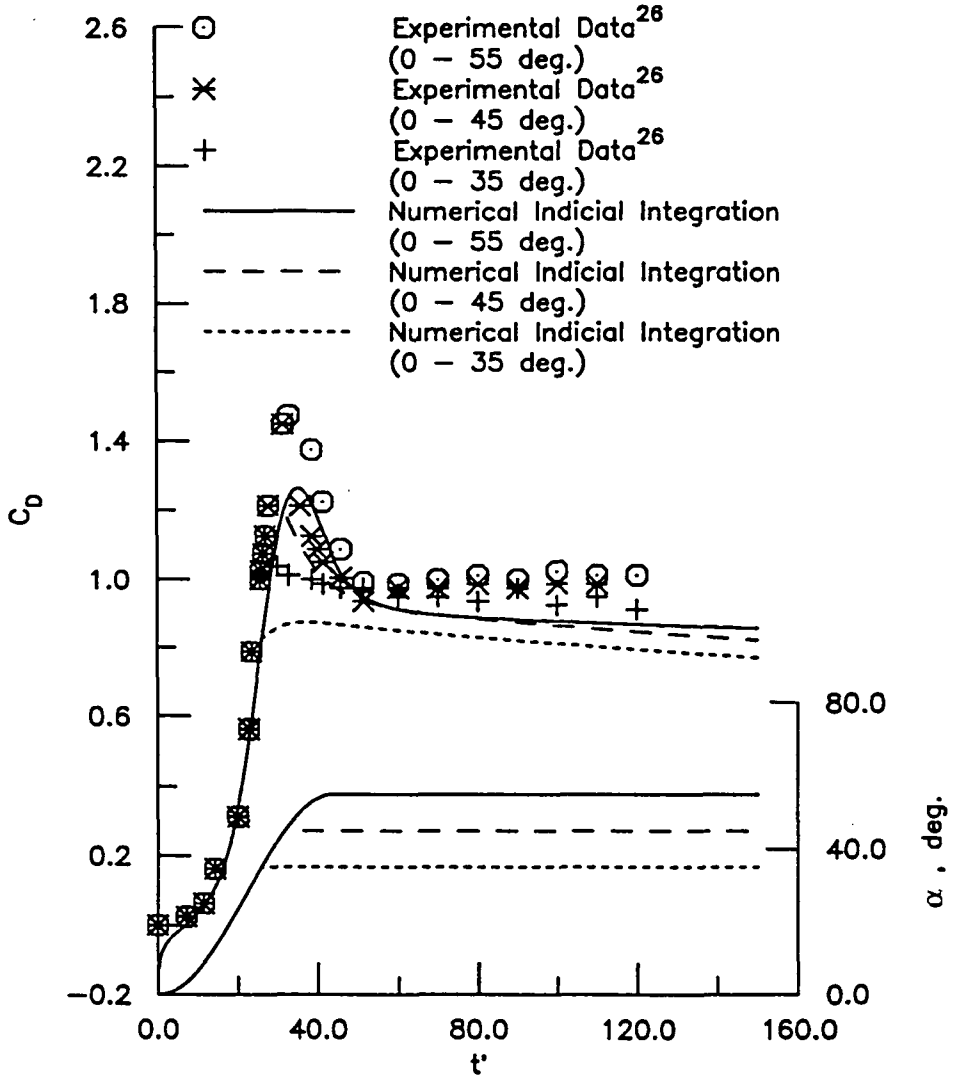
Experimental Data[26]
(0 – 55 deg.)
Experimental Data[26]
(0 – 45 deg.)
Experimental Data[26]
(0 – 35 deg.)
Numerical Indicial Integration
(0 – 55 deg.)
Numerical Indicial Integration
(0 – 45 deg.)
Numerical Indicial Integration
(0 – 35 deg.)
C_D
2.6
2.2
1.8
1.4
1.0
0.6
0.2
−0.2
0.0
40.0
80.0
120.0
160.0
t'
80.0
40.0
0.0
α , deg.

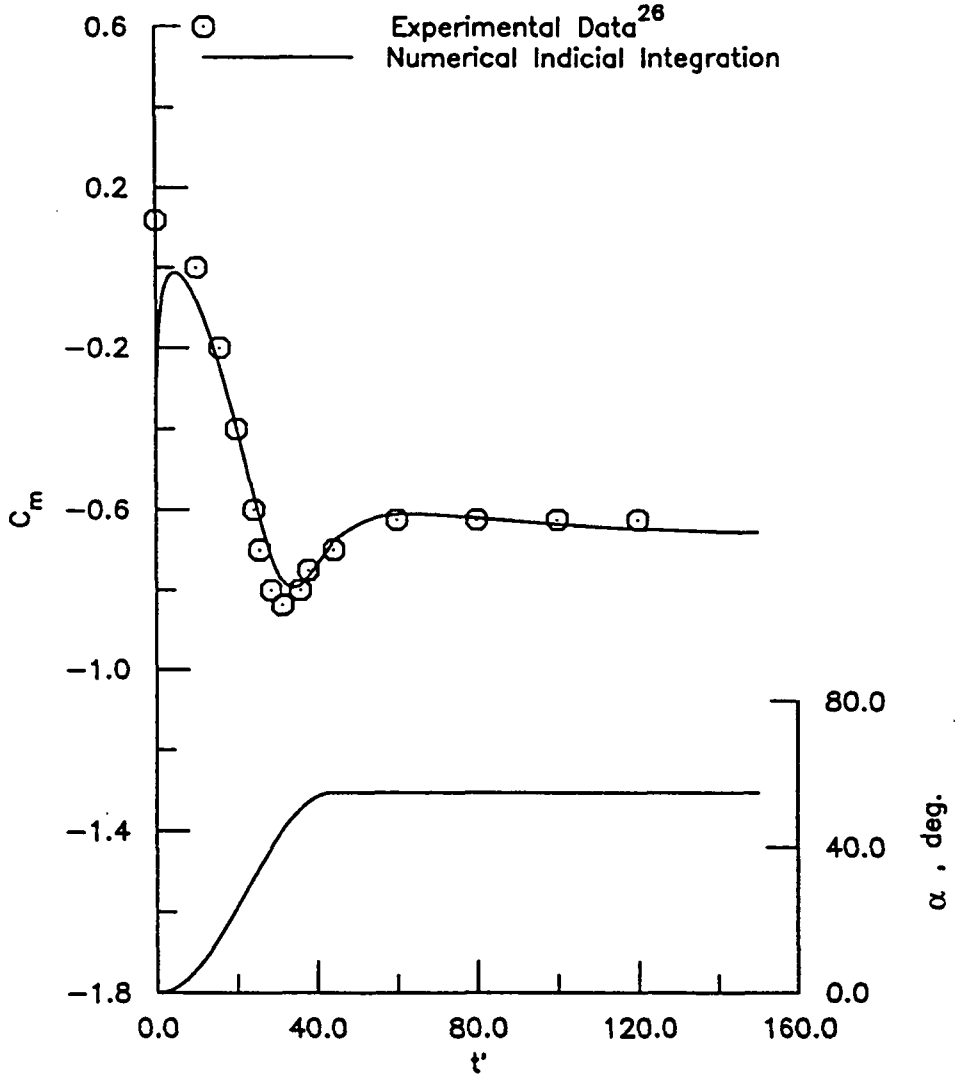
Experimental Data[26]
Numerical Indicial Integration
0.6
0.2
−0.2
−0.6
−1.0
−1.4
−1.8
C_m
80.0
40.0
0.0
α , deg.
0.0
40.0
80.0
120.0
160.0
t'

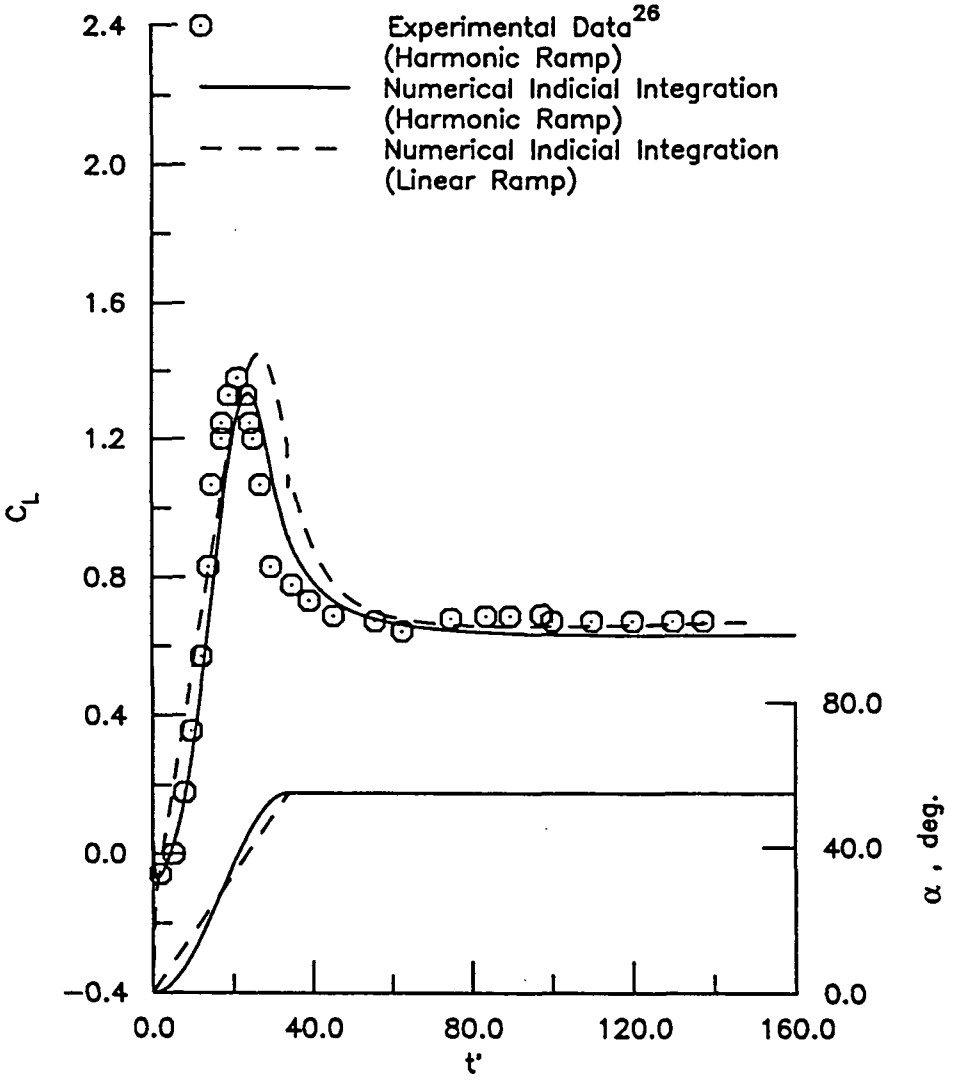
Experimental Data[26]
(Harmonic Ramp)
Numerical Indicial Integration
(Harmonic Ramp)
Numerical Indicial Integration
(Linear Ramp)
2.4
2.0
1.6
1.2
0.8
0.4
0.0
−0.4
C_L
80.0
40.0
0.0
α , deg.
0.0
40.0
80.0
120.0
160.0
t'